University of Milano-Bicocca
School of Medicine and Faculty of Science

PhD
PROGRAM IN TRANSLATIONAL AND MOLECULAR MEDICINE - DIMET

Multi-functionalized nanoparticles for therapy and diagnosis of Alzheimer's disease

Coordinator: Prof. Andrea Biondi
Tutor: Dr. Ilaria Rivolta
Co-Tutor: Prof. Massimo Masserini

Dr. Elisa Salvati
Matr. No. 063716

XXV Cycle
Academic Year
2011-2012

TABLE OF CONTENTS

CHAPTER 1

General Introduction

1.1 Alzheimer's Disease (AD)

1.1.1 Overview of the pathology

Alzheimer's disease (AD) is one of the most common neurodegenerative disorders, comprising 50–70% of all reported cases of dementia [Gotz, 2011] and affecting the middle- to old-aged individuals, approximately one in four individuals over the age of 85 [Feng, 2012]. Dementia is characterized by a progressive cognitive decline leading to social or occupational disability. Symptoms of AD usually develop slowly and gradually worsen over time, progressing from mild forgetfulness to widespread brain impairment. Chemical and structural changes in the brain slowly destroy the ability to create, remember, learn, reason, and relate to others. As critical cells die, drastic personality loss occurs and body systems fail.

The pathophysiological hallmarks of AD include extracellular β-amyloid protein (Aβ) deposition in the forms of senile plaques and intracellular deposits of the microtubule-associated protein tau as neurofibrillary tangles (NFTs) in the brain (Fig. 1).

AD has either an early-onset familial form (<60 years), that represents less then 5% of cases, with a genetic origin involving mutations in the amyloid precursor protein (APP) and presenilin 1 and 2 (PS1 and PS2) genes, and an age-associated late onset sporadic form (>60 years), for which the etiogenesis still be largely unclear [Quetfurth, 2010; Minati, 2009]. Several competing hypotheses have been proposed. The current pathophysiologic approach is based on a number of common mechanisms of neurodegeneration, including accumulation of

abnormal proteins (tau and Aβ), mitochondrial dysfunction, oxidative stress, impaired insulin signaling, calcium homeostasis dysregulation, imbalance of neurotransmitters (glutamate, acetylcholine, dopamine, and serotonin), early synaptic disconnection, and late apoptotic cell death [Chen, 2011; Popescu, 2009; Querfurth, 2010].

The presence of ε4 allele of apolipoprotein E (ApoE) has been identified as an important genetic risk factor for the sporadic late-onset form of AD. Nevertheless, possessing the ε4 allele is neither necessary nor sufficient for the development of AD [Ertekin-Taner, 2007]. Aging is the most important known nongenetic risk factor for late-onset AD. Potential environmental risk factors for late-onset AD include head injury, hyperlipidemia, hypertension, homocysteinemia, diabetes mellitus, and obesity [Barnes, 2011; Rosendorff, 2007; Van Den Heuvel, 2007]. However, several of these associations remain controversial [Daviglus et al., 2010].

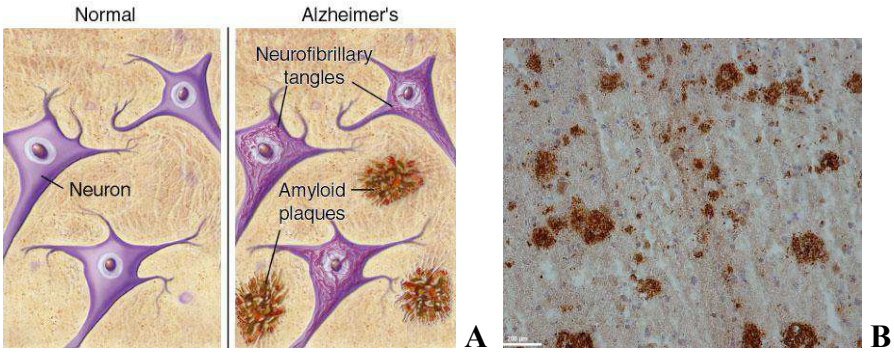

Fig.1 A. Illustration of normal and AD brain with plaques and tangles. **B.** Immunohistochemistry of post-mortem section of AD human brain stained for the visualization of amyloid plaques (A. Lazar-E. Salvati, Lab. Prof. C. Duyckaerts).

1.1.2 The amyloid cascade hypothesis

Despite the remarkable improvements in understanding of the pathogenesis of the disease have been made over last several decades, the accurate mechanism of AD remains unclear [Dong, 2012].

Several independent hypotheses have been proposed, among them the amyloid metabolic cascade and the post-translational modification of tau protein are considered to be the most important, although none of them or other theories alone is sufficient to explain the diversity of biochemical and pathological abnormalities of AD [Bachman, 1993]. The most widely-accepted amyloid cascade hypothesis (Fig. 2) revolves around an imbalance in Aβ peptide metabolism (production and clearance) followed by its aggregation in monomers, oligomers and fibrils ending in the formation of plaques, commonly known as the main actors in the pathology of AD [Verdile, 2004].

Aβ originates from an aberrant cleavage of APP, a transmembrane glycoprotein proposed to be implicated in the neurogenesis and to have neurotrophic functions [Vassar, 2004]. Physiologically, APP is cleaved by α- and β-secretase to produce a soluble APP (sAPPα) through a non-amyloidogenic pathway [Thornton, 2006]. On the contrary, sequential proteolytic effects of β-secretase (BACE) and β- secretase, cutting APP at N-terminus and C-terminus of Aβ sequence respectively, results in production of Aβ peptides, through the amyloidogenic pathway. Depending on the β-secretase cleavage site, different Aβspecies are generated. The two most common variants have a number of 40 (Aβ40) or 42 (Aβ42) aminoacids. Both type of peptides could be found in amyloid plaque but Aβ 42 is more hydrophobic and shows an higher aggregation propensity then Aβ 40 and is believed to be the primary toxic

amyloid-β peptide [Citron, 2010]. Accumulation and aggregation lead to amyloidogenesis process, through which the toxic amyloid species are formed.

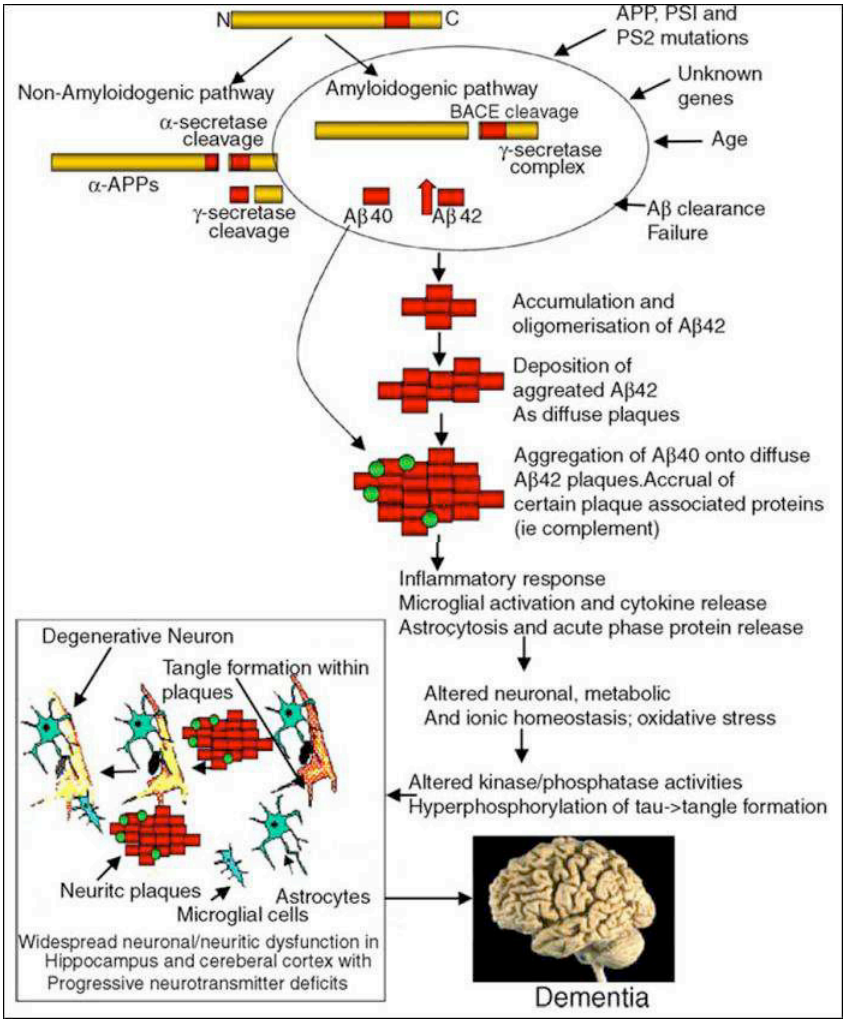

Fig. 2. The amyloid cascade hypothesis [Verdile, 2004].

1.1.3 Current diagnosis and treatment

Presently, a definitive diagnosis of AD is possible only after death, when the presence of plaques and neurofibrillary tangles in the brain parenchyma can be revealed after pathological examination [Van der Zee, 2008]. Current diagnostic practices can be used to screen patients for ‘‘probable’’ AD, including behavioural history assessments, physical examinations, neuropsychiatric tests (i.e., the Mini-Mental State Examination, MMSE), laboratory tests and neuroimaging techniques. To date, the best established measurements for the detection and tracking of AD include cerebrospinal fluid (CSF) measures of Aβ and tau, structural magnetic resonance imaging (MRI) of hippocampal atrophy, fluorodeoxyglucose positron emission tomography (FDG-PET) measurements of decline in the metabolic rate of glucose, PET measurements of brain Aβ by Pittsburgh Compound B (PIB) [Apostolova, 2010; Reiman, 2012]. None of these methods by themselves or in combination provide for early detection or yield high accuracy. There has been a great deal of research emphasis on the search for blood-borne biomarkers indicative of AD pathology, but most attempts have found only limited success [Nagele, 2011].

There are still no effective treatments to prevent, halt, or reverse AD [Huang, 2012]. Common medications are only symptomatic and aim to restore the disrupted neurotransmission between the degenerated neurons [Nazem, 2008]. Current therapies for AD include the acetylcholinesterase inhibitors (donepezil, galantamine and rivastigmine), and a low-affinity NMDA (N-methyl-d-aspartate)

receptor antagonist (memantine) for moderate to severe AD. The acetylcholinesterase inhibitors mediate their effects by remediating, in part, the cholinergic deficit in AD, whereas the precise mechanism of action of memantine remains to be elucidated. Overall, the effects of these drugs are limited as they modestly improve some of the symptoms but do not treat the underlying causes of the disease [Karran, 2011]. With further research, mechanistic therapeutic approaches could gradually complement the abovementioned medications. Various molecular therapeutic approaches are currently under investigation: (i) inhibition of Aβ production; (ii) inhibition of Aβaggregation, (iii) anti-inflammation, (iv) cholesterol homeostasis modulation; and (v) metal chelation [Nazem, 2008].

1.1.4 The blood-brain barrier: a common obstacle in treating CNS diseases

The blood–brain barrier (BBB) is a highly regulated interface that separates the peripheral circulation and central nervous system (CNS). It is a dynamic and functional neurovascular unit comprised of the capillary endothelium, astrocytes, pericytes, and extracellular matrix. The tight junctions between the endothelial cells serve to restrict blood-borne substances from entering the brain [Sandoval, 2008]. Only some small molecules with appropriate lipophilicity, molecular weight and charge will diffuse from blood into the CNS [Gabathuler, 2010]. It has been reported that approximately 98% of the small molecules and nearly all large molecules do not cross the BBB [Pardridge, 2007]. This almost impenetrable barrier, enables a

protection of the brain from the peripheral circulation and toxic substances but restricts the transport of many diagnostic molecules and therapeutically important drugs from the blood into the brain [Pardridge, 1997], including anticancer drugs, antibiotics, and a wide variety of CNS-active drugs. Because the BBB represents such an insurmountable obstacle for most drugs and contrast agents, an effective treatment or diagnosis of many brain diseases is difficult or not possible. Therefore, a number of different strategies have been employed during the past years to overcome this barrier. These strategies included the osmotic opening of the tight junctions, the direct surgical administration of molecules into the brain, and the use of prodrugs or carrier systems interacting with specific transporters and/or receptors expressed at the luminal (blood) side of the endothelial cells [Begley, 2004; Pardridge, 1997]. Among these, nanotechnology based strategies have gained tremendous importance as some of them are capable of overcoming the limitations inherent to BBB passage. These include various types of lipidic, polymeric, inorganic and other types of nanoparticles (NPs) for controlled drug delivery and release pertinent to various CNS conditions [Patel, 2009; Silva, 2010; Wong, 2012].

1.2 Nanomedicine

1.2.1 Nanoparticles for medical purposes

Nanotechnology is an area of science devoted to the manipulation of atoms and molecules leading to the construction of structures in the nanometer scale (~ 100 nm), which retain unique properties (surface area to volume ratio, electrical, chemical, optical properties) [Moghimi, 2005; Albanese, 2012].

Applications of nanotechnology for treatment, diagnosis, monitoring, and control of biological systems has been referred to as ‘‘nanomedicine’’ by the National Institutes of Health. Over the last few decades a great variety of nanotechnology based platforms have been synthesized to improve the delivery of active compounds to a disease site [Godin, 2011].

NPs currently used in the clinic and the majority of nanotherapeutics/nanodiagnostics under investigation, accommodate single- or multiple- functionalities on the same entity. The reason why these NPs are attractive for medical purposes is based on their important and unique features. The following are among the most important advantages of NPs as carriers [Gelperina, 2005; Tassa, 2010]:

1. NPs can be made using biocompatible and biodegradable materials such as polymers, either natural (e.g., gelatin, albumin) or synthetic (e.g., polylactides, polyalkylcyanoacrylates), or lipids;
2. they can be multi-functionalized by attaching various targeting ligands to the external surface;

3. multivalent interactions may strikingly increase the affinity of functionalized NPs for their targets, with respect to the ligand itself;
4. high stability and long circulating time after administration can be achieved by modulating the NPs components;
5. many drugs/contrast agents molecules can be loaded in/on the particles, protected from rapid degradation into the bloodstream, thus increasing their efficacy and reducing side effects;
6. the system can be used for various routes of administration including oral, nasal, parenteral, intra-ocular etc.

Liposomes, nanosomes, polymeric nanoparticles, nanobubbles are some examples of this targeted delivery systems.

As already mentioned above, NPs exert some very special properties and to date, there is no consensus on the long term consequences of NPs, particularly those which are not bio-compatible, such as carbon nanotube [Conti, 2006; Fond, 2012]. In general, NPs, may cause the same effects as 'traditional' particles (e.g., inflammation, lung cancer) but they could also cause new types of effects not previously seen with larger particles (e.g., mitochondrial damage, uptake through olfactory epithelium, platelet aggregation, cardiovascular effects) [De Jong 2008].

In conclusion, the versatility of the NPs platform could enabling the creation of personalized solutions with broad clinical implications within the so called field of ''theranostics'' (therapy and diagnostic). Anyway, additional work is still required to fully understand the fate and possible toxicity of internalized NPs on health.

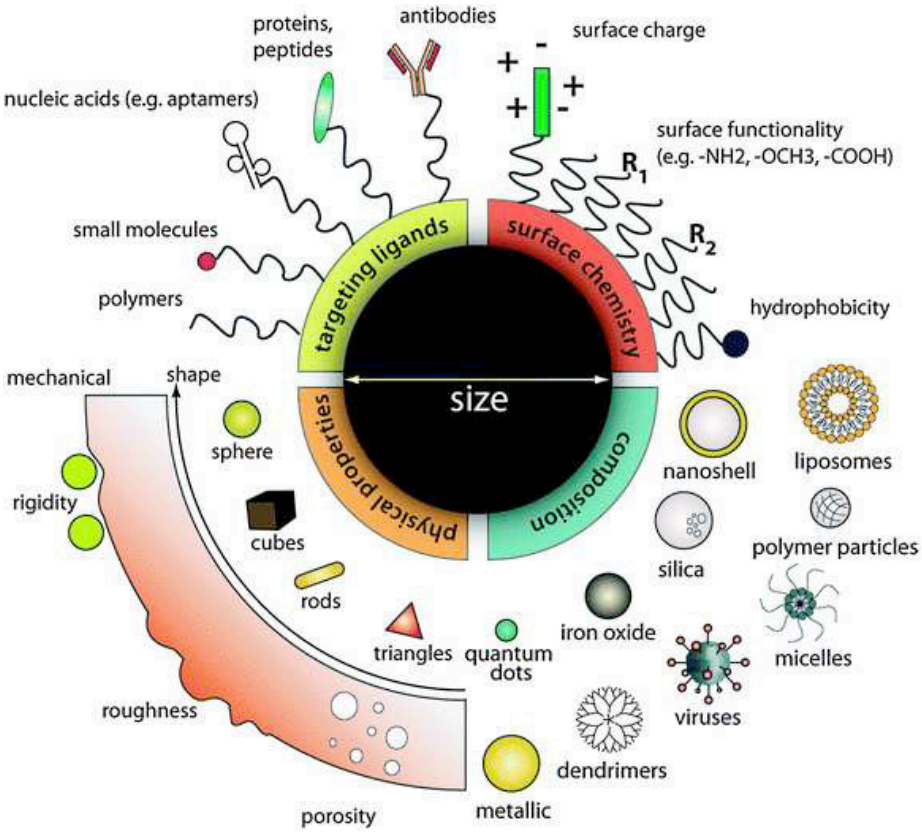

Fig. 3 Nanoparticles. NPs can be modularly assembled from different materials composition with different physical and chemical properties and functionalized with a myriad of ligands for biological targeting. Such flexibility in design freedom enables researchers to tailor NP for specific intracellular applications as contrast agents, drug delivery vehicles, and therapeutics [Chou, 2010].

1.2.2 Strategies for binding the amyloid beta peptide

The abnormal deposition and aggregation of Aβ on brain tissues are considered one of the characteristic neuropathological features of AD [Small, 2001]. Therefore, ligands selectively targeting Aβ in the living brain are promising candidates of therapeutics and early diagnosis tools for AD. Monomers, oligomers and fibrils are excellent targets to reduce neurotoxic brain damages for prevention of the disease progression or to develop reliable imaging probes [Kim, 2009]. NPs carrying molecules that can act as inhibitor of Aβaggregation or as disaggregant agents, or that can promote the clearance of Aβ by forming complexes recognizable by the immune system, could be employed as novel therapy of AD.

A number of molecules have been described to interact with Aù, to stabilize the soluble Aβ conformation, to destabilize the altered amyloidogenic conformer, and to prevent the required conformational transition [Airoldi 2011; Re, 2010].

The sequence of Aβ42 is the following:

N-EAFRHDSGYEVHHQKLVFFAEDVGSNKGAIIGLMVGGVVIA-C.

Natural or synthetic compounds that have been found to bind Aβ and eventually to interfere with its aggregation, are for example curcumin, tannic acid, wine-related polyphenols, vitamin A and β-carotene [Ono, 2004], tetracyclins [Forloni, 2001], melatonin [Bazoti, 2005], Congo red, thioflavin T and their derivatives [Maezawa, 2008]. Numerous new agents for use in molecular imaging of the amyloid deposits have been developed on the bases of the above mentioned compounds, and successfully introduced as tracer for PET imaging [Svedberg, 2012].

It has been claimed that fibrillogenesis can be inhibited by short synthetic peptides partially homologous to Aβ. In particular, the short fragment of AβQKLVFF was shown to bind specifically to the full-length peptide [Tjernberg, 1996]. Other studies have shown also that LVFFA and its derivatives [Findeis, 1999] and LPFFD [Soto, 1998] are all potent inhibitors of amyloid formation.

Aβpeptides have been reported to bind to anionic lipids, cholesterol and gangliosides that were also shown to be involved at various stages of Aβ aggregation [Ariga, 2001; Avdulov, 1997; Curtain, 2003; Kakio, 2002; McLaurin, 2000].

The decoration of NPs with the above described natural or synthetic compounds, peptides or lipids, represents a strategy to target Aβ and a way to increase their affinity thanks to the multivalent effects. In fact, when NPs are used for the attachment of ligands, simultaneous binding between the multiple ligands presents on the NPs surface and their target can occur. This multivalent interactions, sometimes termed as avidity effects, increases the affinity between the two partners resulting in a very strong binding that can be beneficial for improved specificity of targeting [Tassa, 2010; Simnick, 2010]. Recently, various types of NPs, such as liposomes, Solid Lipid NPs (SLN) and polymeric NPs, have been functionalized with Aβ-ligands. For example, a curcumin-derivative have been used to decorate liposomes and it has been described to bind Aβ with very high affinity and also inhibiting its aggregation in vitro [Mourtas, 2011; Taylor, 2011]. Liposomes and SLN containing anionic lipids (phosphatidic acid or cardiolipin) have been developed and have been showed to be highly affine for Aβand to reduce its toxicity in vitro [Gobbi, 2010]. Canovi

et al., synthesized liposomes decorated with an anti-Aβ monoclonal antibody, with high affinity for Aβ either in vitro or ex vivo on post-mortem AD brain samples [Canovi, 2011].

1.2.3 Strategies for overcoming the blood-brain barrier

To date, strategies for the delivery of drugs or contrast agents that do not have an appreciable BBB permeability have included both invasive and non-invasive approaches.

The various strategies that have been explored to increase drug delivery into the brain include (i) chemical delivery systems, such as lipid-mediated transport, the prodrug approach and the lock-in system; (ii) biological delivery systems, in which pharmaceuticals are re-engineered to cross the BBB via specific endogenous transporters localized within the brain capillary endothelium; (iii) disruption of the BBB, for example by modification of tight junctions, which causes a controlled and transient increase in the permeability of brain capillaries; (iv) the use of molecular Trojan horses, such as peptidomimetic monoclonal antibodies to transport large molecules (e.g. antibodies, recombinant proteins, nonviral gene medicines or RNA interference drugs) across the BBB [Patel, 2009].

One promising strategy to reach the brain could arise from the decoration of NPs surface with ligands that can enhance the cells internalization and the BBB crossing, for example by exploiting the transport systems present at the barrier. Receptor-mediated transport (RMT) systems exist for certain endogenous peptides, such as insulin and transferrin, enabling these molecules to cross the BBB in vivo.

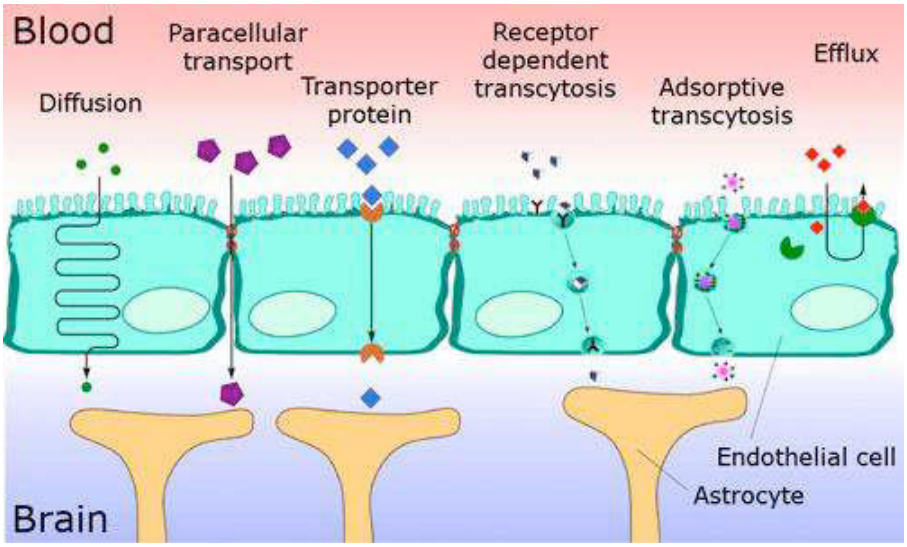

Fig. 4. Mechanisms to overcome the blood brain barrier: representation of the main physiological transport mechanisms across the endothelial cells that form the BBB: paracellular aqueous passage of small hydrophilic molecules, transcellular passage of lipophilic molecules and mediated transcytosis.

The transferrin receptor (TfR), perhaps the most studied receptor known to undergo RMT, is highly expressed by brain capillaries to mediate the delivery of iron to the brain [Jefferies, 1984]. The natural ligand for the TfR is the iron binding protein, transferrin (Tf) [Pardridge, 1987]. Tf is likely not an ideal brain delivery vector since the endogenous Tf persists in the bloodstream at high concentrations, meaning that a Tf-targeted drug would have to compete with the natural ligand [Qian, 2002]. As an alternative, there has been much proof-of-concept success in using antibodies against the TfR, that bind to an extracellular epitope of the receptor. Examples of monoclonal antibodies against TfR studied for NPs decoration are OX26, 8D3 and RI7217 [Van Rooy, 2011].

The insulin receptor, like the TfR, is found on the luminal membrane of brain capillary endothelial cells as well as at the plasma membrane of other brain cells, and it can undergo RMT across the BBB endothelium [Duffy, 1987]. Using the endogenous ligand, insulin, as a vector has not been attempted, likely it is rapidly degraded in the bloodstream and secondly, interfering with the natural insulin balance could cause hypoglycemia. However, like the TfR, there are antibodies recognizing the insulin receptor that have been used as BBB-targeting vectors [Jones, 2007].

Other receptors expressed in many tissues and in the CNS have been used for drug delivery to the brain included the low density lipoprotein receptor (LDLR) and the LDLR-related protein (LRP). These receptors can bind multiple ligands, such as low-density lipoprotein (LDL), receptor associated protein (RAP), lactoferrin, melanotransferrin (P97), and apolipoproteins (ApoE) [Gabathuler 2010; Van Rooy, 2011].

Enhanced delivery across the BBB can also be achieved by application of so-called cell-penetrating peptides (CPP). These are typical amino acid sequences that are capable of enhancing the delivery of large molecules into cells. The internalization mechanism of CPPs remains to be fully elucidated. However, these peptides are typically basic molecules, and therefore cations, that might be able to enhance protein uptake by cells mainly by increased adsorptive mediated endocytosis [De Boer, 2007]. The most commonly studied CPP for NPs functionalization is the HIV-1 trans-activating transcriptional activator peptide (TAT) [Hillaireau, 2009].

1.3 Liposomes design and functionalization

1.3.1 Liposomes general features

Among several promising new delivery systems, liposomes represent an advanced technology to deliver active molecules to the site of action, and at present, several formulations are in clinical use (Doxil (Sequus), DaunoXome (Gilead, Nexstar), Myocet (Zeneus)).

Liposomes are artificial phospholipid vesicles that vary in size from 30 nm to several micrometers that consist of an aqueous core entrapped by one or more bilayers composed of natural or synthetic lipids. Liposomes are attractive tools in biomedical applications thanks to their biocompatibility, non-immunogenicity, non-toxicity, biodegradability, high physical stability, versatility in surface functionalization. They can be loaded with a variety of hydrophilic molecules into the inner aqueous compartment, and with hydrophobic molecules into the phospholipid bilayer.

Different approaches exist for the production of finely dispersed liposomes. They can be prepared using handshaking method, re-hydration methods and reverse phase evaporation, followed by sonication, freeze thawing or extrusion to downsize the particles produced [Wagner, 2011].

Research on liposome technology has progressed from conventional vesicles (‘‘first-generation liposomes’’) to ‘‘second-generation liposomes’’, in which long-circulating liposomes are obtained by modulating the lipid composition, size, and charge of the vesicle [Immordino, 2006].

A significant step in the development of liposomes came with inclusion of the synthetic polymer poly- (ethylene glycol) (PEG) in

their composition. The presence of PEG on the surface of the liposomal carrier has been shown to avoid the vesicle aggregation, increasing the stability of formulations [Needham, 1992], and also to extend blood-circulation time while reducing mononuclear phagocyte system uptake [Maruyama, 1992]. These liposomes are known as ‘‘stealth’’ liposomes. Further, by synthetic modification of the terminal PEG molecule, liposomes can be actively targeted with ligands.

Moreover, liposomes can be chemically modified with negatively/positively charged groups, fluorescent probes, contrast agents, and biologically active targeting moieties including antibodies, peptides, aptamers, and phage [Godin, 2011].

In clinical studies, liposomes show improved pharmacokinetics and biodistribution of therapeutic agents and thus minimize toxicity by their accumulation at the target tissue [Immordino, 2006].

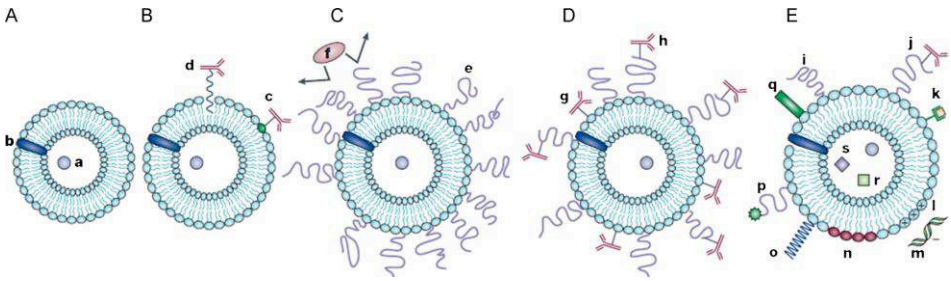

Fig. 5. Evolution of liposomes as drug delivery systems: (A) Early traditional phospholipids 'plain' liposomes with water soluble drug (a) entrapped into the aqueous liposome interior, and water-insoluble drug (b) incorporated into the liposomal membrane. (B) Antibody-targeted immunoliposome with antibody covalently coupled (c) to the reactive phospholipids in the membrane, or hydrophobically anchored (d) into the liposomal membrane after preliminary modification with a hydrophobic moiety. (C) Long-circulating liposome grafted with a protective polymer (e) such as PEG, which shields the liposome surface from the interaction with opsonizing proteins (f). (D) Long-circulating immunoliposome simultaneously bearing both protective polymer and antibody, which can be attached to the liposome surface (g) or, preferably, to the distal end of the grafted polymeric chain (h). (E) New-generation liposome, the surface of which can be modified (separately or simultaneously) in different ways. Among these modifications are: the attachment of protective polymer (i) or protective polymer and targeting ligand, such as antibody (j); the attachment/incorporation of the diagnostic label (k); the incorporation of positively charged lipids (l) allowing for the complexation with DNA (m); the incorporation of stimuli-sensitive lipids (n); the attachment of stimuli-sensitive polymer (o); the attachment of cell-penetrating peptide (p); the incorporation of viral components (q). In addition to a drug, liposomes can be loaded with magnetic particles (r) for magnetic targeting and/or with colloidal gold or silver particles (s) for electron microscopy [Torchilin, 2005].

1.3.2 Conjugation of targeting ligands to liposome surface

Several well-established methods for conjugation of antibodies, peptides, proteins and drugs to the external surface of liposomes have been developed [Anabousi, 2005; Ansell, 2000; Béduneau, 2007; Loughrey, 1987; Markoutsa, 2011; Schnyder, 2004].

Numerous modified lipids exist for the covalent or non-covalent attachment of ligands to the liposome surface. Most of these lipids fall into three major classes of functionality: conjugation through amide bond formation, disulfide or thioether formation, or biotin/streptavidin binding.

Targeting ligands are usually coupled to the terminal groups of the PEG polymer that is incorporated into the liposomes bilayer via a lipid moiety (usually, 1,2-distearoyl-sn-glycero-3-phosphoethanolamine, DSPE) and it is easily accessible by targeting ligands for conjugation [Wang, 2012].

A possible methods involve the formation of an amide bound between 1,2-distearoyl-sn-glycero-3-phosphoethanolamine -N-[carboxy(polyethylene glycol) 2000] (DSPE-PEG_{2000}-COOH), as linker lipid, and the peptide/antibody. The bond between free amino groups of the ligand and carboxylic groups of the linker is formed by mixing sulpho-N-hydroxysuccinimide (S-NHS) with a carboxyl containing molecule and a dehydrating agent, N-(3-dimethylaminopropyl)-N′-ethylcarbodiimide hydrochloride (EDC), which reacts with the carboxyl group first and forms an amine-reactive intermediate, an O-acylisourea [Anabousi, 2005].

The second method, relies on the formation of thioether-bonds between the ligand and the liposome containing 1,2-Distearoyl-sn-glycero-3-phosphocholine-(polyethylene glycol) 2000-maleimide (DSPE-PEG_{2000}-MAL) as linker lipid. Sulfhydryl groups are introduced into the ligand via modification of —NH_2, -S-S or COOH groups with reagents such as EDC, dithriotreitol (DTT), 2-iminothiolane (Traut's reagent) [Weber, 2000]. The most commonly used methods for thiolation is the reaction between Traut's reagent and amine groups of the ligands to form sulfhydryls that react with the maleimide on the PEG-terminus [Huwyler, 1996; Béduneau, 2007].

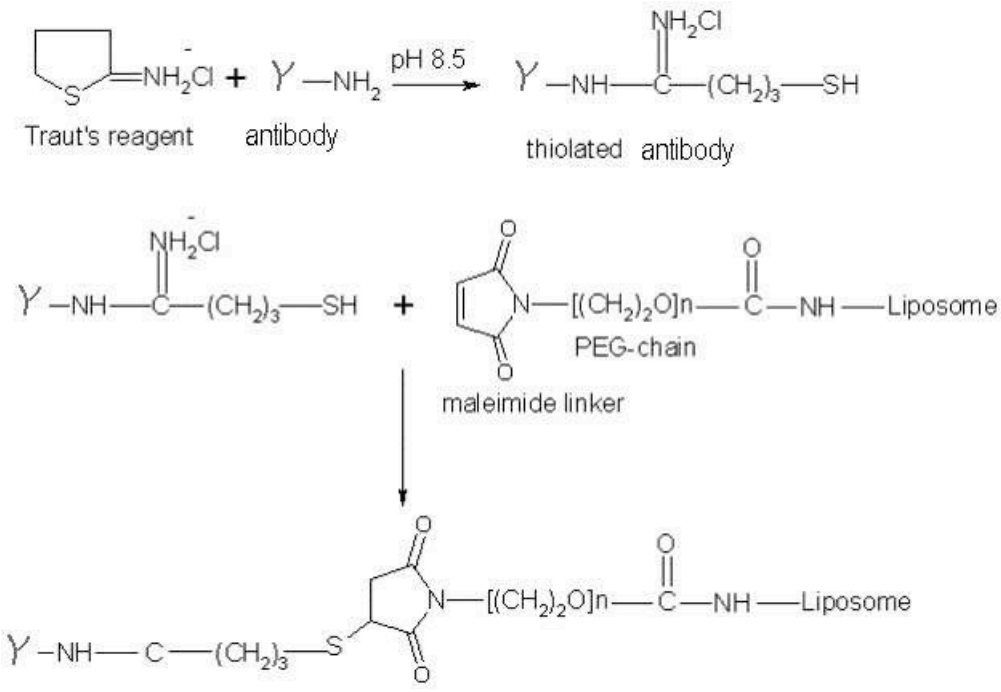

Fig. 6 Coupling reaction of antibody to the surface of liposomes using DSPE-PEG_{2000}-MAL as linker lipid [Adapted from Anabousi 2005].

The non-covalent streptavidin-biotin linkage is also a widely used method to functionalize liposomes. The biotin-avidin interaction is among the strongest non-covalent binding known and the related tetrameric protein streptavidin conserved the high biotin binding affinity [Pähler, 1987]. Biotinylated linker lipid, e.g. biotinylated-PEG-DSPE, are commercially available and they can be easily introduced into the liposome bilayer during fabrication. Preformed biotin-PEG-liposomes can be simply mixed with an excess of free streptavidin and then with the biotinylated ligand or they can be mixed to a streptavidin-conjugated ligands resulting in an immediate quantitative coupling.

Besides the most popular reactions, there are alternative coupling chemistry that are used for nanocarriers functionalization. Among these the 1,3-dipolar cycloaddition [Huisgen, 1989] between azides and terminal alkynes has recently emerged as a highly useful chemical handle for conjugation in both a non copper-mediated [Bernardin, 2010] and a copper-catalyzed manner [Rostovtsev, 2002, Woo, 2012], also known as ‘‘click’’ chemistry [Lallana, β01β]. For example, curcumin-liposomes have been developed by incorporating into the outer bilayer a lipid-PEG carrying an azido group during the preparation and a curcumin-derivative, carrying an alkyne group, have been successfully linked as targeting ligand [Mourtas, 2011].

Despite the wide range of methodologies currently available for NPs funtionalization, the investigation on simple, highly efficient and broadly applicable conjugation chemistries is still ongoing.

1.4 Surface Plasmon Resonance (SPR)

1.4.1 SPR principles and applications

Surface plasmon resonance (SPR) is a phenomenon occuring at metal surfaces (typically gold and silver) when an incident light beam strikes the surface at a particular angle at the interface (sensor surface) between two media of different refractive index: the glass of a sensor surface (high refractive index) and a buffer (low refractive index) [Torreri, 2005]. Depending on the thickness of a molecular layer at the metal surface, the SPR phenomenon results in a graded reduction in intensity of the reflected light. Biomedical applications take advantage of the exquisite sensitivity of SPR to the refractive index of the medium next to the metal surface, which makes it possible to measure accurately the adsorption of molecules on the metal surface and their eventual interactions with specific ligands [Englebienne, 2003].

The experimental procedure involves immobilizing one reactant (ligand) on a surface and monitoring its interaction with a second component (analyte) in solution. Essentially, SPR detects changes in mass in the aqueous layer close to the sensor chip surface by measuring changes in the refractive index.

An SPR instrument comprises an SPR detector, a sensor chip and an integrated liquid handling system for the exact transport of the sample to the adsorption and detection spot. The sensor chip consists of a glass coated with a thin layer of gold, usually modified with a carboxymethylated dextran layer, which forms a hydrophilic environment for the attached molecules, preserving them in a non-

denaturated state. The integrated microfluid system allows the molecules in the test solution - the analyte - to pass over the sensor surface in a continuous, pulse-free and controlled flow that maintains constant analyte concentrations at the sensor chip surface. When the analyte binds to a target molecule bound to sensor chip, the mass increases and when it dissociates the mass falls. This produces changes in the refractive index close to the surface, which are detected as changes in the SPR signals expressed in arbitrary or resonance units (RUs). A sensorgram is obtained by plotting the changes of RU as a function of time [Torreri, 2005].

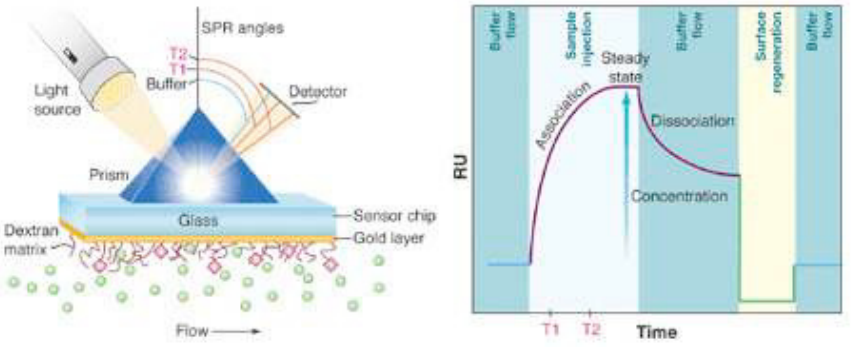

Wilson, W. Science 295, 2103 (2002)

Fig. 7 Representation of an SPR sensor surface and a typical real-time response signal as RU versus time.

SPR biosensors have been used to study a wide range of biomolecular interactions, providing both qualitative (identification, site specificity, epitope mapping) and quantitative (kinetics, affinity and concentration analysis) information [Karlsson, 2004; Lee, 2003]. Recently, this

instrument has been widely used to detect the interaction between different types of NPs and biomaterials such as peptides, protein, antibodies or drugs [Efremova, 2000; Jule, 2003; Patel, 2012; Gobbi 2010; Brambilla, 2012].

Within this PhD project, SPR was used as principle technique for detecting the interactions of differently functionalized NPs towards their target. This study especially concerned liposomes or polymeric nanoparticles binding Aβ and liposomes functionalized to enhance the BBB crossing through a specific receptor. Aβ or the receptor were covalently immobilized on a dextran-coated sensor surface and different concentrations of nanoparticles were flowed over the sensor in solution. The resulting sensorgrams (RU vs time) were then analyzed to obtain the kinetic parameters of the binding. SPR is also a useful and rapid technique to analyze the binding properties of ligands after chemical modification, needed for their linkage to the NPs surface.

1.4.2 Analyses of binding responses

A biomolecular interaction between a soluble analyte (A) and an immobilized ligand (B) can be interpreted in terms of pseudo-first-order kinetics [Liu, 2003; Karlsson, 1991], where the rate of formation of complex is described by the following differential equation:

$$dAB/dt = ka.A.B - kd.AB \qquad [1]$$

where

AB = Molar concentration of complex at the interaction surface.

A = Molar concentration of analyte at the interaction surface at time t.

B = Molar concentration of immobilized ligand.

$B = AB_{tot} - AB$

where

B = Molar concentration of available immobilized ligand.

When employing flow cell-based analysis, the analyte concentration at the interaction surface can be approximated by the injected analyte concentration at any time assuming mass transport of analyte to the surface is not limiting.

$$A_0 = A$$

where

A_0 = Molar concentration of injected analyte sample.

A = Molar concentration of analyte at the interaction surface at time t.

SPR monitors these surface binding events, producing 'real-time' interaction curves where the rate of change of response (dR/dt) is directly related to the formation of complex AB. Hence, equation [1] can be rewritten and integrated to give the following integrated association rate equation for a 1:1 pseudo-first-order interaction:

$$R_t = \frac{k_a . A. R_{max}.(1 - \exp [- k_a.A + k_d] t}{k_a.A + k_d} \qquad [2]$$

where

R_{max} = Maximal response if all available ligand binding sites are occupied.

R_t = Biosensor response at time t.

The pseudo-first-order dissociation phase is described by the following expression:

$$R_t = R_0 \exp(- k_d t) \qquad [3]$$

where

R_0 is the sensor response at time to (i.e. time at the onset of the dissociation phase).

From the ratio k_d/k_a the value of the dissociation constant k_D is obtained. This parameter gives an indication of the binding affinity between the ligand and the analyte [Schuck, 1997].

1.5 Scope of the thesis

This PhD thesis has been developed within the European project NAD - Nanoparticles for therapy and diagnosis of Alzheimer's Disease - founded by the European Union's 7th Framework Program. The project started in 2008 and includes nineteen European research Institutes with Prof. Massimo Masserini as scientific coordinator.

The principal intent was to develop a platform of NPs able to cross the BBB and to target the Aβ, that aggregates into the brain leading to the neurodegeneration process typical of AD.

Chapter 1 is dedicated to a general introduction on AD pathology, with an overview on the current diagnosis and therapies, and it contains a paragraph on the BBB as obstacle in treating CNS diseases. This Chapter also includes a section on nanomedicine and its application for AD; a section on liposomes and a section on SPR technique. This work of thesis is focused on the preparation and characterization of liposomes functionalized with ligands able to bind Aβ (Chapter 2) or multi-functionalized with ligands able to bind Aβand molecules stimulating the BBB crossing (Chapter 3 and 4). The ability of this NPs to bind the peptide was assessed in vitro by using the SPR technology as principal technique and the ability to cross the BBB was studied on a cellular model of barrier (hCMEC/D3).

Within this PhD project, other NPs (polymeric NPs) provided by the NAD Consortium have been tested for their binding towards Aβ peptide (Chapter 5). Chapter 6 is dedicated to the summary, the discussion on results and the future outlook about the use of these NPs for diagnosis and treatment of AD.

References

Airoldi C, Cardona F, Sironi E, Colombo L, Salmona M, Silva A, Nicotra F, La Ferla B. cis-Glyco-fused benzopyran compounds as new amyloid-βpeptide ligands. Chem Commun (Camb). 2011. 47(37):10266-8.

Albanese A, Tang PS, Chan WC, The effect of nanoparticle size, shape, and surface chemistry on biological systems. Annu Rev Biomed Eng. 2012. 14:1-16.

Anabousi S, Laue M, Lehr CM, Bakowsky U, Ehrhardt C. Assessing transferrin modification of liposomes by AFM and transmission electron microscopy. Eur J Pharm Biopharm.2005.60(2):295-303.

Ansell SM, Harasym TO, Tardi PG, Buchkowsky SS, Bally MB, Cullis PR. Antibody conjugation methods for active targeting of liposomes. Methods Mol Med. 2000. 25:51-68.

Apostolova LG, Hwang KS, Andrawis JP, Green AE, Babakchanian S, Morra JH, Cummings JL, Toga AW, Trojanowski JQ, Shaw LM, Jack CR Jr, Petersen RC, Aisen PS, Jagust WJ, Koeppe RA, Mathis CA, Weiner MW, Thompson PM; Alzheimer's Disease Neuroimaging Initiative. 3D PIB and CSF biomarker associations with hippocampal atrophy in ADNI subjects. Neurobiol Aging. 2010. 31(8):1284-303.

Ariga T, Kobayashi K, Hasegawa A, Kiso M, Ishida H, Miyatake T. Characterization of high-affinity binding between gangliosides and amyloid beta-protein. Arch Biochem Biophys. 2001. 388(2):225-30.

Avdulov NA, Chochina SV, Igbavboa U, Warden CS, Vassiliev AV, Wood WG. Lipid binding to amyloid beta-peptide aggregates: preferential binding of cholesterol as compared with phosphatidylcholine and fatty acids. J Neurochem. 1997. 69(4):1746-52.

Bachman DL, Wolf PA, Linn RT, Knoefel JE, Cobb JL, Belanger AJ, White LR, D'Agostino RB: Incidence of dementia and probable Alzheimer's disease in a general population: the Framingham Study. Neurology 1993. 43:515–519.

Bangham, A. D.; Standish, M. M.; Watkins, J. C. Diffusion of univalent ions across the lamellae of swollen phospholipids Journal of Molecular Biology. 1965. 13(1), 238-52.

Barnes, D.E., and Yaffe, K. The projected effect of risk factor reduction on Alzheimer's disease prevalence. Lancet Neurol. β011. 10, 819–828.

Bazoti FN, Tsarbopoulos A, Markides KE, Bergquist J. Study of the non-covalent interaction between amyloid-beta-peptide and melatonin using electrospray ionization mass spectrometry. J Mass Spectrom. 2005. 40(2):182-92.

Béduneau A, Saulnier P, Hindré F, Clavreul A, Leroux JC, Benoit JP. Design of targeted lipid nanocapsules by conjugation of whole antibodies and antibody Fab' fragments. Biomaterials. 2007. 28(33):4978-90.

Begley DJ. Delivery of therapeutic agents to the central nervous system: the problems and the possibilities. Pharmacol Ther. 2004. 104: 29–45.

Bernardin A, Cazet A, Guyon L, Delannoy P, Vinet F, Bonnaffé D, Texier I.Copper-free click chemistry for highly luminescent quantum dot conjugates: application to in vivo metabolic imaging. Bioconjug Chem. 2010. 21(4):583-8.

Brambilla D, Verpillot R, Le Droumaguet B, Nicolas J, Taverna M, Kóňa J, Lettiero B, Hashemi SH, De Kimpe L, Canovi M, Gobbi M, Nicolas V, Scheper W, Moghimi SM, Tvaroška I, Couvreur P, Andrieux K. PEGylated nanoparticles bind to and alter amyloid-beta peptide conformation: toward engineering of functional nanomedicines for Alzheimer's disease. ACS Nano. 2012. 6(7):5897-908.

Canovi M, Markoutsa E, Lazar AN, Pampalakis G, Clemente C, Re F, Sesana S, Masserini M, Salmona M, Duyckaerts C, Flores O, Gobbi M, Antimisiaris SG. The binding affinity of anti-Aù1-42 MAb-decorated nanoliposomes to Aù1-42 peptides in vitro and to amyloid deposits in post-mortem tissue. Biomaterials. 2011 Aug;32(23):5489-97.

Castellani R. J., Raj K. Rolston,2 and Mark A. Smith, Alzheimer Disease Dis Mon. 2010. 56(9): 484–546.

Chen KH, Reese EA, Kim HW, Rapoport SI, Rao JS. Disturbed neurotransmitter transporter expression in Alzheimer's disease brain. J Alzheimers Dis. 2011;26(4):755-66.

Conti M, Tazzari V, Baccini C, Pertici G, Serino LP, De Giorgi U. Anticancer drug delivery with nanoparticles. In Vivo. 2006. 20(6A):697-701.

Curtain, C. C., Ali, F. E., Smith, D. G., Bush, A. I., Masters, C. L. & Barnham, K. J. Metal ions, pH, and cholesterol regulate the interactions of Alzheimer's disease amyloid-b peptide with membrane lipid. J. Biol. Chem. 2003. 278: 2977–2982.

Daviglus, M.L., Bell, C.C., Berrettini, W., Bowen, P.E., Connolly, E.S., Jr., Cox, N.J., Dunbar-Jacob, J.M., Granieri, E.C., Hunt, G., McGarry, K., et al. National Institutes of Health State-of-the-Science Conference statement: preventing alzheimer disease and cognitive decline. Ann. Intern. Med. 2010. 153, 176–181.

De Boer AG, Gaillard PJ. Drug targeting to the brain. Annu Rev Pharmacol Toxicol. 2007. 47:323-55. Review.

De Jong W. H., Borm P. J. A., Drug delivery and nanoparticles: Applications and hazards, Int J Nanomedicine. 2008. 3(2): 133–149.

Dong S, Duan Y, Hu Y, Zhao Z. Advances in the pathogenesis of Alzheimer's disease: a re-evaluation of amyloid cascade hypothesis, Translational Neurodegeneration, 2012. 1 (1):18.

Duffy KR, Pardridge WM. Blood-brain barrier transcytosis of insulin in developing rabbits. Brain Res. 1987. 420:32–38.

Efremova NV, Bondurant B, O'Brien DF, Leckband DE. Measurements of interbilayer forces and protein adsorption on uncharged lipid bilayers displaying poly(ethylene glycol) chains. Biochemistry.2000.39(12):3441-51.

Englebienne P., Van Hoonacker A. and Verhas M. Surface plasmon resonance: principles, methods and applications in biomedical sciences. Spectroscopy 2003. 17: 255–273.

Ertekin-Taner N. Genetics of Alzheimer's disease: a centennial review. Neurol Clin. 2007. 25(3):611-67.

Feng Y, Wang X Antioxidant therapies for Alzheimer's disease. Oxid Med Cell Longev. 2012;2012:472932.

Findeis M.A., Musso G.M., Arico–Muendel C.C., Benjamin H.W., Hundal, A.M., Le J–J., Chin, J., Kelley M., Wakefiel J., Hayward N.J., Molineaux S.M. Modified-peptide inhibitors of amyloid beta-peptide polymerization. Biochemistry. 1999. 38: 6791-6800.

Fond G, Macgregor A, Miot S. Nanopsychiatry-The potential role of nanotechnologies in the future of psychiatry: A systematic review. Eur Neuropsychopharmacol. 2012.

Forloni G, Colombo L, Girola L, Tagliavini F, Salmona M. Anti-amyloidogenic activity of tetracyclines: studies in vitro. FEBS Lett. 2001. 487(3):404-7.

Frisch B, Hassane FS, Schuber F. Conjugation of ligands to the surface of preformed liposomes by click chemistry. Methods Mol Biol. 2010, 605:267-77.

Gabathuler R., Approaches to transport therapeutic drugs across the blood–brain barrier to treat brain diseases, Neurobiol Dis. 2010.37(1):48-57.

Gelperina S., Kisich K, Iseman M. D, Heifets L., The Potential Advantages of Nanoparticle Drug Delivery Systems in Chemotherapy of Tuberculosis. Am J Respir Crit Care Med. 2005. 172(12): 1487–1490.

Gobbi M, Re F, Canovi M, Beeg M, Gregori M, Sesana S, Sonnino S, Brogioli D, Musicanti C, Gasco P, Salmona M, Masserini ME. Lipid-based nanoparticles with high binding affinity for amyloid-beta1-42 peptide. Biomaterials. 2010.31(25):6519-29.

Godin B, Tasciotti E, Liu X, Serda RE, Ferrari M. Multistage nanovectors: from concept to novel imaging contrast agents and therapeutics. Acc Chem Res. 2011 Oct 18;44(10):979-89.

Götz J., Eckert A., Matamales M., Ittner L. M., Liu X., Modes of Aβtoxicity in Alzheimer's disease, Cell Mol Life Sci. β011.68(β0): γγ59–3375.

Hillaireau H., Couvreur P., Nanocarriers' entry into the cell: relevance to drug delivery, Cell. Mol. Life Sci. 2009. 66:2873–2896.

Huang Y, Mucke L. Alzheimer mechanisms and therapeutic strategies. Cell. 2012 Mar 16;148(6):1204-22.

Huisgen, R. In 1,3-Dipolar Cycloaddition Chemistry; Padwa, A., Ed.; Wiley: New York. 1984.(1):1-176.

Huwyler J, Wu D, Pardridge WM. Brain drug delivery of small molecules using immunoliposomes. Proc Natl Acad Sci U S A. 1996. 93(24):14164-9.

Immordino ML, Dosio F, Cattel L. Stealth liposomes: review of the basic science, rationale, and clinical applications, existing and potential. Int J Nanomedicine. 2006;1(3):297-315. Review.

Jefferies WA, Brandon MR, Hunt SV, Williams AF, Gatter KC, Mason DY. Transferrin receptor on endothelium of brain capillaries. Nature. 1984;312:162–163.

Jones AR, Shusta EV.Blood-brain barrier transport of therapeutics via receptor-mediation. Pharm Res. 2007. 24(9):1759-71.

Jule E, Nagasaki Y, Kataoka K. Lactose-installed poly(ethylene glycol)-poly(d,l-lactide) block copolymer micelles exhibit fast-rate binding and high affinity toward a protein bed simulating a cell surface. A surface plasmon resonance study. Bioconjug Chem. 2003. 14(1):177-86

Kakio A, Nishimoto S, Yanagisawa K, Kozutsumi Y, Matsuzaki K. Interactions of amyloid beta-protein with various gangliosides in raft-like membranes: importance of GM1 ganglioside-bound form as an endogenous seed for Alzheimer amyloid. Biochemistry. 2002. 41(23):7385-90.

Karlsson R, Michaelsson A, Mattsson L. Kinetic analysis of monoclonal antibody-antigen interactions with a new biosensor based analytical system. J Immunol Methods. 1991. 145(1-2):229-40.

Karlsson R. SPR for molecular interaction analysis: a review of emerging application areas. J Mol Recognit. 2004. 17(3):151-61.

Karran E, Mercken M, De Strooper B. The amyloid cascade hypothesis for Alzheimer's disease: an appraisal for the development of therapeutics. Nat Rev Drug Discov. 2011.10(9):698-712.

Kim Y, Lee JH, Ryu J, Kim DJ. Multivalent & multifunctional ligands to beta-amyloid. Curr Pharm Des. 2009.15(6):637-58.

Lallana E, Sousa-Herves A, Fernandez-Trillo F, Riguera R, Fernandez-Megia E. Click chemistry for drug delivery nanosystems. Pharm Res. 2012. 29(1):1-34.

Lee HJ, Yan Y, Marriott G, Corn RM. Quantitative functional analysis of protein complexes on surfaces. J Physiol 2005. 563(1):61-71.

Liu X, Wei J, Song D, Zhang Z, Zhang H, Luo G. Determination of affinities and antigenic epitopes of bovine cardiac troponin I (cTnI) with monoclonal antibodies by surface plasmon resonance biosensor. Anal Biochem. 2003. 314(2):301-9.

Loughrey H., Bally M.B., Cullis P.R. A non-covalent method of attaching antibodies to liposomes Biochim. Biophys. Acta, 1987. (910):157–160.

Maezawa I, Hong HS, Liu R, Wu CY, Cheng RH, Kung MP, Kung HF, Lam KS, Oddo S, Laferla FM, Jin LW. Congo red and thioflavin-T analogs detect Abeta oligomers. J Neurochem. 2008. 104(2):457-68.

Markoutsa E, Pampalakis G, Niarakis A, Romero IA, Weksler B, Couraud PO, Antimisiaris SG.Uptake and permeability studies of BBB-targeting immunoliposomes using the hCMEC/D3 cell line. Eur J Pharm Biopharm. 2011. 77(2):265-74.

Maruyama K, Yuda T, Okamoto A, Kojima S, Suginaka A, Iwatsuru M. Prolonged circulation time in vivo of large unilamellar liposomes composed of distearoyl phosphatidylcholine and cholesterol containing amphipathic poly(ethylene glycol). Biochim Biophys Acta. 1992. 1128(1):44-9.

McLaurin, J., Yang, D.-S., Yip, C. M. & Fraser, P. E. Review: modulating factors in amyloid-b fibril formation. J. Struct. Biol. 2000. 130 (2-3): 259–270.

Minati L., Edginton T., Bruzzone M. G., Giaccone G. MD Current Concepts in Alzheimer's Disease: A multidisciplinary Review. Am J Alzheimers Dis Other Demen. 2009. 24(2):95-121.

Moghimi, S. M., Hunter, A. C. and Murray, J. C. Nanomedicine: current status and future prospects. FASEB J. 2005.19: 311–330.

Mourtas S, Canovi M, Zona C, Aurilia D, Niarakis A, La Ferla B, Salmona M, Nicotra F, Gobbi M, Antimisiaris SG. Curcumin-decorated nanoliposomes with very high affinity for amyloid-ù1-42 peptide. Biomaterials. 2011. 32(6):1635-45.

Nagele E, Han M, Demarshall C, Belinka B, Nagele R. Diagnosis of Alzheimer's disease based on disease-specific autoantibody profiles in human sera. PLoS One. 2011;6(8):e23112.

Nazem A, Mansoori GA. Nanotechnology solutions for Alzheimer's disease: advances in research tools, diagnostic methods and therapeutic agents. J Alzheimers Dis. 2008.13(2):199-223.

Needham D, McIntosh TJ, Lasic DD. Repulsive interactions and mechanical stability of polymer-grafted lipid membranes. Biochim Biophys Acta. 1992. 1108(1):40-8.

Ono K, Hasegawa K, Naiki H, Yamada M. Curcumin has potent anti-amyloidogenic effects for Alzheimer's beta-amyloid fibrils in vitro. J Neurosci Res. 2004.75(6):742-50.

Pähler A, Hendrickson WA, Kolks MA, Argaraña CE, Cantor CR. Characterization and crystallization of core streptavidin. J Biol Chem. 1987. 262(29):13933–13937.

Pardridge WM, Eisenberg J, Yang J. Human blood-brain barrier transferrin receptor. Metabolism. 1987;36:892–895.

Pardridge WM Drug delivery to the brain. J Cereb Blood Flow Metab. 1997. 17(7):713–731.

Pardridge WM. Brain drug development and brain drug targeting. Pharm Res. 2007. 24(9):1729-32.

Patel MM, Goyal BR, Bhadada SV, Bhatt JS, Amin AF.Getting into the brain: approaches to enhance brain drug delivery. CNS Drugs. 2009. 23(1):35-58.

Patel A. M., Ashish J. Modi, Patel G. N., Intelligent Polymeric Micelles as Novel Carrier for Delivery of Most Anticancer Drugs and Nucleic Acids. Pharmacologia, 2012. 3(9) : 362-370

Pauwels K, Williams TL, Morris KL, Jonckheere W, Vandersteen A, Kelly G, Schymkowitz J, Rousseau F, Pastore A, Serpell LC, Broersen K. Structural basis for increased toxicity of pathological aù4β:aù40 ratios in Alzheimer disease. J Biol Chem. 2012. 287(8):5650-60.

Popescu BO, Toescu EC, Popescu LM, Bajenaru O, Muresanu DF, Schultzberg M, Bogdanovic N. Blood-brain barrier alterations in ageing and dementia. J Neurol Sci. 2009. 283(1-2):99-106.

Qian ZM, Li HY, Sun HZ, Ho K. Targeted drug delivery via the transferrin receptor-mediated endocytosis pathway. Pharmacol Rev. 2002. 54:561–587.

Querfurth HW, LaFerla FM. Alzheimer's disease. N Engl J Med. 2010. 362(4):329-44.

Re F, Airoldi C, Zona C, Masserini M, La Ferla B, Quattrocchi N, Nicotra F. Beta amyloid aggregation inhibitors: small molecules as candidate drugs for therapy of Alzheimer's disease. Curr Med Chem. 2010.17(27):2990-3006. Reiman EM, Jagust WJ. Brain imaging in the study of Alzheimer's disease. Neuroimage. 2012. 61(2):505-16.

Rosendorff, C., Beeri, M.S., and Silverman, J.M. Cardiovascular risk factors for Alzheimer's disease. Am. J. Geriatr. Cardiol. β007. 16:14γ–149.

Rostovtsev VV, Green LG, Fokin VV, Sharpless KB. A stepwise huisgen cycloaddition process: copper(I)-catalyzed regioselective "ligation" of azides and terminal alkynes. Angew Chem Int Ed Engl. 2002. 41(14):2596-9.

Sandoval KE, Witt KA.Blood-brain barrier tight junction permeability and ischemic stroke. Neurobiol Dis. 2008. 32(2):200-19.

Schnyder A., Krahenbuhl S., Torok M., Drewe J., Huwyler J. Targeting of skeletal muscle in vitro using biotinylated immunoliposomes Biochem. J., 2004. 377:61–67.

Schuck P. Use of surface plasmon resonance to probe the equilibrium and dynamic aspects of interactions between biological macromolecules. Annu Rev Biophys Biomol Struct. 1997. 26:541-66.

Sharma A., Sharma U. S., Liposomes in drug delivery: progress and limitations, International Journal of Pharmaceutics. 1997.154:123-140.

Silva GA. Nanotechnology applications and approaches for neuroregeneration and drug delivery to the central nervous system. Ann N Y Acad Sci 2010. 1199: 221-30.

Small DH, Mok SS, Bornstein JC. Alzheimer's disease and Aβtoxicity: from top to bottom. Nat Rev Neurosci. 2001. 2:595-598.

Simnick AJ, Valencia CA, Liu R, Chilkoti A. Morphing low-affinity ligands into high-avidity nanoparticles by thermally triggered self-assembly of a genetically encoded polymer. ACS Nano. 2010. 4(4):2217-27.

Soto, C.; Sigurdsson, E.; Morelli, L.; Kumar, R.; Castano, E.; Frangione, B. Beta-sheet breaker peptides inhibit fibrillogenesis in a rat brain model of amyloidosis: implications for Alzheimer's therapy. Nat. Med. 1998.4(7):822-826.
Stains CI, Mondal K, Ghosh I.Molecules that target beta-amyloid. ChemMedChem. 2007. 2(12):1674-92.

Svedberg MM, Rahman O, Hall H. Preclinical studies of potential amyloid binding PET/SPECT ligands in Alzheimer's disease. Nucl Med Biol. 2012. 39(4):484-501.

Tassa C, Duffner J. L., Lewis T. A. Weissleder R., Schreiber S. L., Koehler A.N., Shaw S. Y., Binding affinity and kinetic analysis of targeted small molecule-modified nanoparticles Bioconjug Chem. Bioconjug Chem. 2010. 21(1):14-9.

Taylor M, Moore S, Mayes J, Parkin E, Beeg M, Canovi M, Gobbi M, Mann DM, Allsop D. Development of a proteolytically stable retro-inverso peptide inhibitor of beta-amyloid oligomerization as a potential novel treatment for Alzheimer's disease. Biochemistry. 2010. 49(15):3261-72.

Taylor M, Moore S, Mourtas S, Niarakis A, Re F, Zona C, LaFerla B, Nicotra F, Masserini M, Antimisiaris SG, Gregori M, Allsop D. Effect of curcumin-associated and lipid ligand-functionalized nanoliposomes on aggregation of the Alzheimer's Aβpeptide. Nanomedicine.β011.7(5):541-50.

Thornton E., Vink R., Blumbergs P. C., Van Den Heuvel C., "Soluble amyloid precursor protein α reduces neuronal injury and improves functional outcome following diffuse traumatic brain injury in rats," Brain Research, 2006. 1094(1): 38-46.

Tjernberg L.O., Näslund J., Lindqvist F., Johansson J., Karlström A.R., Thyberg J., Terenius L., Nordstedt C. Arrest of ù-Amyloid Fibril Formation by a Pentapeptide Ligand. J. Biol. Chem.. 1996. 271: 8545-8548.

Torreri P, Ceccarini M, Macioce P, Petrucci TC. Biomolecular interactions by Surface Plasmon Resonance technology. Ann Ist Super Sanita. 2005.41(4):437-41.

Torchilin VP, Recent advances with liposomes as pharmaceutical carriers, Nature Reviews Drug Discovery. 2005. 4: 145-160.

Van der Zee J., K. Sleegers, C. Van Broeckhoven, The Alzheimer disease-frontotemporal lobar degeneration spectrum, Neurology. 2008. 71(15):1191-1197.

Van Den Heuvel, C., Thornton, E., and Vink, R. Traumatic brain injuryand Alzheimer's disease: a review. Prog. Brain Res. β007. 161, 303–316.

Van Rooy I, Mastrobattista E, Storm G, Hennink WE, Schiffelers RM.Comparison of five different targeting ligands to enhance accumulation of liposomes into the brain. J Control Release. 2011. 150(1):30-6.

Vassar R., "BACE1: the ù-secreiase enzyme in Alzheimer's disease," Journal of Molecular Neuroscience. 2004. 23(1-2): 105–113.

Verdile G, Fuller S, Atwood CS, Laws SM, Gandy SE, Martins RN. The role of beta amyloid in Alzheimer's disease: still a cause of everything or the only one who got caught? Pharmacol Res. 2004. 50(4):397-409.

Wagner A, Vorauer-Uhl K Liposome technology for industrial purposes. J. Drug Deliv. 2011. 2011:591325.

Wagner S, Zensi A, Wien SL, Tschickardt SE, Maier W, Vogel T, Worek F, Pietrzik CU, Kreuter J, von Briesen H. Uptake mechanism of ApoE-modified nanoparticles on brain capillary endothelial cells as a blood-brain barrier model. PLoS One. 2012. 7(3):e32568.

Wang R, Xiao R, Zeng Z, Xu L, Wang J. Application of poly(ethylene glycol)-distearoylphosphatidylethanolamine (PEG-DSPE) block copolymers and their derivatives as nanomaterials in drug delivery. Int J Nanomedicine. 2012. 7:4185-98.

Weber C, Reiss S, Langer K. Preparation of surface modified protein nanoparticles by introduction of sulfhydryl groups. Int J Pharm. 2000. 211(1-2):67-78.

Woo H, Kang H, Kim A, Jang S, Park JC, Park S, Kim BS, Song H, Park KH Azide-Alkyne Huisgen [3+2] Cycloaddition Using CuO Nanoparticles. Molecules. 2012.17(11):13235-53

Wong HL, Wu XY, Bendayan R. Nanotechnological advances for the delivery of CNS therapeutics. Adv Drug Deliv Rev. 2012. 64(7):686-700.

CHAPTER 2

Liposomes Functionalized with GT1b Ganglioside with High Affinity for Amyloid β-peptide.

Journal of Alzheimer Disease, 2012, 29 Suppl. 1, 33-36

Elisa Salvati, Massimo Masserini, Silvia Sesana, Sandro Sonnino, Francesca Re, Maria Gregori

ABSTRACT

Alzheimer's Disease (AD) is a neurodegenerative disorder that affects millions of individuals worldwide. Accumulation of amyloid-β peptide (Aβ) in the brain, and its aggregation into oligomers, fibrils and plaques, plays a central role in the onset and development of AD. Starting from this observation, the E.C. FP7 project "NAD" (Nanoparticles for therapy and diagnosis of Alzheimer's disease) is involved in the design of nanoparticles that recognize and remove brain Aβ. Previous investigations by NAD Consortium have already produced nanoparticles containing anionic phospholipids or curcumin-analogues able to bind Aβ with very high affi nity, to inhibit fibril formation and to reduce Aβ toxicity in-vitro. Starting from the observation that ganglioside GT1b binds Aβ in vitro, we have synthesized liposomes, composed of sphingomyelin and cholesterol and containing GT1b ganglioside, and investigated their affi nity towards Aβ peptide. Surface Plasmon Resonance experiments showed a good interaction of liposomes with Aβ fibrils, displaying Kd values between 125 and 150 nM. Moreover, Aβ aggregation into fi brils, measured by Thioflavin T and Congo Red binding assays, was reduced of about 50%, after two weeks of monomeric peptide incubation in the presence of GT1b-containing liposomes. The ability of GT1b-containing liposomes, and the other liposomes previously described by NAD research, to bind Aβ and to reduce fibrils formation, increases the interest in studying them as possible future diagnostic and therapeutic tools for the treatment of Alzheimer Disease.

INTRODUCTION

Alzheimer's Disease (AD) is a neurodegenerative disorder affecting millions of individuals worldwide. The figures are expected to increase, as the elderly population proportionately increases [1]. The production band accumulation of amyloid-β peptide 1-42 (Aβ) plays a central role in the onset and development of AD. Aβ aggregates in the brain, forming oligomers, fibrils and plaques and inducing a progressive neurodegeneration [2]. Since treatment and diagnosis of the pathology are still a challenge,

nanotechnology has been proposed as a promising approach to investigate this problem [3, 4]. The present study is part of the EC FP7 project "NAD" Nanoparticles for therapy and diagnosis of Alzheimer's disease), involving 19 European partners and aimed to create nanoparticles (NPs) able to recognize and remove Aβ from the brain. A number of NPs have already been developed within the NAD Consortium, e.g. liposomes and solid-lipid NPs functionalized with anionic lipids or curcumin analogues, binding Aβ with very high affinity [6, 7], thanks to multivalency effect [8]. These NPs showed the ability to reduce Aβ fibril formation [9] and peptide toxicity in vitro [10]. Moreover, studies with NPs double-functionalized with Aβ ligands and molecules potentially enhancing the blood-brain barrier crossing gave promising results on an in vitro model [11, 12]. In the present investigation we started from the observation that gangliosides, and in particular trisialoganglioside GT1b, bind Aβ in vitro. Therefore, we synthesized liposomes functionalized with the ganglioside (GT1b-liposomes) and investigated their affinity for Aβ peptide, using Surface Plasmon Resonance. Moreover, we investigated the ability of NPs to inhibit the aggregation of Aβ using Thioflavin T and Congo Red assays.

MATERIALS

Sphingomyelin (Sm), cholesterol (Chol) Thiofl avinT (ThT), Congo Red (CR), recombinant human Aβ1–42, HFIP and DMSO were purchased from Sigma Aldrich (Milano, Italy). Trisialoganglioside (GT1b) was extracted and purified from bovine brain as described in [13]. Mouse monoclonal anti-Aβ antibody mAb 6E10 was purchased from Signet (Dedham, MA). All other chemicals were reagent grade.

METHODS

TLC immunostaining analysis of Aβ binding to gangliosides The Thin Layer Chromatography (TLC) immunostaining technique previously described was utilized [6]. With this technique, equal amounts (0.5 nmoles) of different gangliosides are separated on a TLC plate. After fixation with

polyisobutylmethacrylate, the plate is incubated with Aβ, then with the mAb 6E10 and finally with HRP-conjugated IgG anti-mouse followed by ECL detection.

Liposome preparation. Liposomes composed of Sm/Chol (1:1, mol/mol) and containing 5% molar GT1b were prepared by extrusion (Lipex Biomembranes extruder) through a 100-nm pore polycarbonate fi lter (Millipore). Lipid recovery, size, polydispersity and ζ-potential were determined as described [6].

Monomeric and fi brillar Aβ preparation. Different aggregation forms of the peptide were prepared and checked by Atomic Force Microscopy as previously described [6].

Aβ aggregation assay Monomeric Aβ (25 μM) was incubated for 14 days in the dark at 37°C in TBS (pH 7.4) with or without GT1b-liposomes (50 μM or 250 μM total lipids). Aggregated Aβ was quantified after 4 and 14 days using CR and ThT binding assays. Each sample was assayed in triplicate, and values were expressed as a mean of three individual results. CR binding assay was performed following the procedure described [14]. Relative fibril content was calculated as the ratio of fi bril concentration in the sample (liposomes plus Aβ) and in control (pure Aβ). For ThT binding assay, fluorescence was measured after mixing 15 μL of 100 μM ThT, 50 μL of 100 mM glycine pH 8.5, 20 μL of samples and 65 μL water. Measurements were performed at excitation and emission wavelengths of 450 nm and 485 nm, respectively. Fluorescence intensity of GT1b-liposomes was subtracted from the intensity of samples.

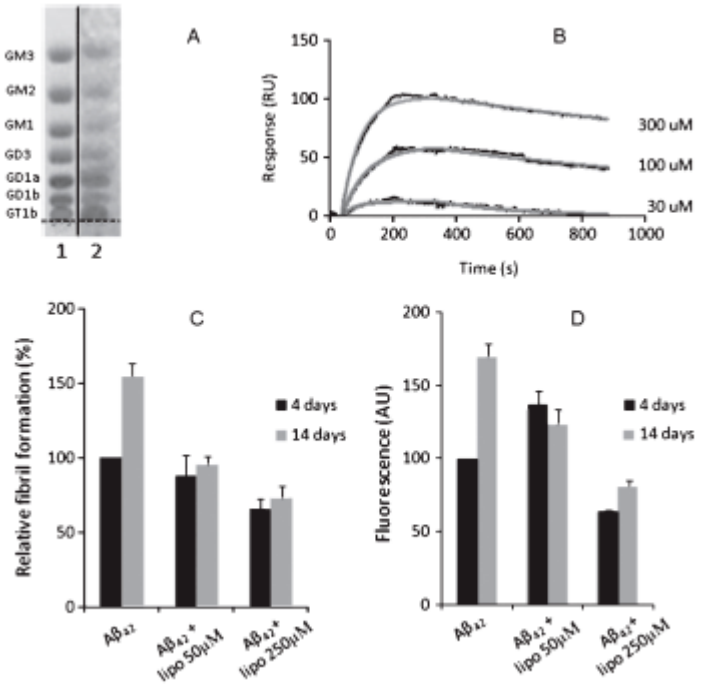

Fig. 1. (A) TLC immunostaining analysis of Aβ binding to gangliosides. 0.5 nmoles of different gangliosides were separated by TLC and revealed by iodine vapors (lane 1), or submitted to immunostaining with Aβ, followed by blotting with anti-Aβ antibody and ECL detection (lane 2). B) Liposomes composed of sphingomyelin/cholesterol (1:1, mol/mol) and containing 5% molar GT1b ganglioside, studied by SPR. Sensorgrams of GT1b-functionalized liposomes fl owed at various concentrations of total lipids (30, 100, 300 μM) for 5 minutes onto Aβ fibrils immobilized on sensor surface. C–D) Effect of liposomes composed of sphingomyelin/cholesterol (1:1, mol/mol) and containing 5% molar GT1b ganglioside, on Aβ aggregation. Aβ fibril formation was evaluated after 4 and 14 days of incubation at 37°C in the presence or absence of GT1b-functionalized liposomes, as estimated from Congo Red (CR) (panel C) and Thioflavin T (ThT) (panel D) binding assay. For CR binding assay, values were calculated as the percent ratio of fibril concentration in the presence of GT1b liposomes to fibril concentration in the absence of liposomes, after 4 days. For ThT binding assay, fibril formation is estimated from fluorescence values expressed as arbitrary units. The graph represents the mean ± standard deviation of at least three

independent experiments.

Binding of GT1b-liposomes to Aβ studied by Surface Plasmon Resonance (SPR) SensiQ semi-automatic apparatus with two parallel flow channels and a COOH5 sensor chip were employed (ICX Technologies). Fibrils were immobilized on one channel, while the other one was used as reference. After surface activation, the peptide (10 μM in acetate buffer pH 4.0) was injected for 5 min at a flow rate of 30 μL.min–1 and the remaining activated groups were blocked with ethanolamine, pH 8.0. The final immobilization levels were about 4000 Resonance Units (1 RU = 1 pg protein.mm–2). The reference surface was prepared in parallel using the same immobilization procedure but without addition of the peptide. Preliminary injections with anti-Aβ antibody 6E10 were performed. Liposomes were injected at 30, 100, 300 μM in parallel in the channels, for 5 min at a flow rate of 30 μL min–1 at 25°C. Control liposomes (without GT1b) signal was subtracted from the fi nal sensorgram. The fitted data were obtained using the Qdat Analysis Software (ICX Technologies).

RESULTS AND DISCUSSION

As first, the ability of GT1b to interact with Aβ was studied by a TLC-immunostaining technique previously utilized [6]. The results (Fig. 1A) suggest the ability of Aβ to preferentially bind GT1b, in comparison with other gangliosides, at least in this in vitro system, confirming previous data [6].

Succesively, GT1b-liposomes were synthesized. Liposomes have numerous advantages, such as biodegradability, low immunogenicity, lack of toxicity, high biocompatibility and high stability. Moreover, they offer the possibility of multi-functionalization, e.g. with contrast agents for diagnostic purposes and with ligands able to enhance the crossing of the blood brain barrier [4]. The average diameter of GT1b-liposomes was 120 nm and the suspension resulted monodispersed (P.I. = 0,104). ζ-Potential was –66 mV due to the negative charge of sialic acid residues.

The ability of GT1b-liposomes to interact with Aβ fibrils was then investigated by SPR. As expected, a good interaction of liposomes with Aβ fibrils was observed and binding was concentration-dependent. The separate analysis of the three sensorgrams shown in Fig. 1B, according to the simplest equation modeling a Langmuir 1:1 interaction, resulted in Kd values in the micromolar range (5–6 μM total lipids). Assuming that the lipid components are equally distributed between the two leaflets of the NPs bilayer and that the interaction with the peptide is occurring only on the outer layer, the Kd value referred to exposed GT1b is 125–150 nM. This value is not far from the values previously obtained by NAD Consortium for acidic phospholipids and curcumin-analogue liposomes (5–50 nM) [6–7]. As mentioned before, each curve was fitted separately since, due to the complexity of the interaction, the global fitting could not be used. Thus, Kd values obtained should be considered as indicative of an apparent high affinity.

Finally, the capability of GT1b-liposomes to interfere with Aβ peptide aggregation process was evaluated using Congo Red (CR) or Thioflavin T (ThT) binding assays, that have been extensively used to characterize the presence of amyloid fibrils and their rates of formation [15–16]. The results of CR binding assay demonstrated that in the presence of GT1b-liposomes the aggregation process is attenuated. In particular, the aggregation of Aβ was reduced of about 12% and 38% (using 50 μM total lipids) and of 34% and 52% (250 μM total lipids), after 4 and 14 days, respectively (Fig. 1C). Similar results were obtained utilizing ThT binding assay. GT1b-liposomes showed to reduce fibril formation of about 27% (50 uM lipids) and 52% (250 uM lipids) after 14 days, compared to the peptide alone (Fig. 1D). The inhibitory effect of GT1b-liposomes on fibril formation is likely due to their affinity for Aβ peptide, as for other functionalized NPs [9].

Further experiments will be carried out to investigate the GT1b-liposomes binding affinity to the other Aβ aggregation forms, monomers and oligomers. Moreover, in-vitro assays will be performed to assess if they induce any modification in the cellular viability. Successively, they could be multi-functionalized withmolecules to facilitate the passage through the blood brain barrier. In conclusion, GT1b-liposomes resulting from this study, together with other NPs prepared among the NAD Consortium, display interesting

features as possible future diagnostic and therapeutic tools for the treatment of AD.

Acknowledgments This research has received funding from the European Community's Seventh Framework Programme (FP7/2007–2013) under grant agreement no 212043.

REFERENCES

[1] Palmer AM (2002) Pharmacotherapy for Alzheimer's disease: Progress and prospects. Trends Pharmacol Sci 23, 426-433.

[2] Hardy J, Selkoe DJ (2002) The amyloid hypothesis of Alzheimer'sdisease: Progress and problems on the road to therapeutics. Science 297, 353-356.

[3] Di Stefano A, Iannitelli A, Laserra S, Sozio P (2011) Drug delivery strategies for Alzheimer's disease treatment. Review.Expert Opin Drug Deliv 8, 581-603.

[4] Al-Jamal WT, Kostarelos K (2011) Liposomes: From a clinically established drug delivery system to a nanoparticle platform for theranostic nanomedicine. Acc Chem Res 44, 1094-1104.

[5] Williams TL, Serpell LC (2011) Membrane and surface interactions of Alzheimer's Aβ peptide – insights into the mechanism of cytotoxicity, FEBS Journal 278, 3905-3917.

[6] Gobbi M, Re F, Canovi M, Beeg M, Gregori M, Sesana S, Sonnino S, Brogioli D, Musicanti C, Gasco P, Salmona M, Masserini ME (2010) Lipid-based nanoparticles with high binding affi nity for amyloid-beta1-42 peptide. Biomaterials 31, 6519-6529.

7] Mourtas S, Canovi M, Zona C, Aurilia D, Niarakis A, La Ferla B, Salmona M, Nicotra F, Gobbi M, Antimisiaris SG (2011) Curcumin-decorated nanoliposomes with very high affinity for amyloid-β1-42 peptide. Biomaterials 32, 1635-1645.

[8] Tassa C, Duffner JL, Lewis TA, Weissleder R, Schreiber SL, Koehler AN, et al. (2010) Binding affi nity and kinetic analysis of targeted small molecule-modifi ed nanoparticles. Bioconjugate Chem 21, 14-19.

[9] Taylor M, Moore S, Mourtas S, Niarakis A, Re F, Zona C, La Ferla B, Nicotra F, Masserini M, Antimisiaris SG, Gregori M, Allsop D (2011) Effect of curcumin-associated and lipid ligand-functionalized nanoliposomes on aggregation of the Alzheimer's Aβ peptide. Nanomedicine 7, 541-550.

[10] Bereczki E, Re F, Masserini ME, Winblad B, Pei JJ (2011) Liposomes functionalized with acidic lipids rescue Aβ- induced toxicity in murine neuroblastoma cells. NanomedDNanotechnol 7, 560-571.

[11] Re F, Cambianica I, Zona C, Sesana S, Gregori M, Rigolio R, La Ferla B, Nicotra F, Forloni G, Cagnotto A, Salmona M, Masserini M, Sancini G (2011) Functionalization of liposomes with ApoE-derived peptides at different density affects cellular uptake and drug transport across a blood-brain barrier model. Nanomedicine 7, 551-559.

[12] Re F, Cambianica I, Sesana S, Salvati E, Cagnotto A, Salmona M, Couraud PO, Moghimi SM, Masserini M, Sancini G (2010) Functionalization with ApoE-derived peptides enhances the interaction with brain capillary endothelial cells of nanoliposomes binding amyloid-beta peptide. J Biotechnol 156, 341-346.

[13] Gazzotti G, Sonnino S, Ghidoni R, Kirschner G, Tettamanti G (1984) Analytical and preparative high-performance liquid chromatography of gangliosides. J Neurosci Res 12, 179-192.

[14] Airoldi C, Zona C, Sironi E, Colombo L, Messa M, Aurilia D, Gregori M, Masserini M, Salmona M, Nicotra F, La Ferla B (2010) Curcumin derivatives as new ligands of Aβ peptides. J Biotechnol 156, 317-324.

[15] Klunk WE, Jacob RF, Mason RP (1999) Analytical Biochemistry 266, 66-76.

[16] Le vine III H (1993) Protein Sci 2, 404-410.

CHAPTER 3

Functionalization with ApoE-derived peptides enhances the interaction with brain capillary endothelial cells of nanoliposomes binding amyloid-beta peptide

Journal of Biotechnology, 2011, 156, pp. 341– 346

Francesca Re, Ilaria Cambianica, Silvia Sesana, Elisa Salvati, Alfredo Cagnotto, Mario Salmona, Pierre-Olivier Couraud, S. Moein Moghimi, Massimo Masserini, Giulio Sancini

ABSTRACT

Nanoliposomes containing phosphatidic acid or cardiolipin are able to target in vitro with very high affinity amyloid-β (Aβ), a peptide whose overproduction and progressive aggregation in the brain play a central role in the pathogenesis of Alzheimer's disease. However, the presence of the blood–brain barrier (BBB) severely limits the penetration of either drugs or drug vehicles (nanoparticles) to the brain. Therefore, there is a need to develop and design approaches specifically driving nanoparticles to brain in a better and effective way. The aim of the present investigation is the search of a strategy promoting the interaction of liposomes containing acidic phospholipids with brain capillary endothelial cells, as a first step toward their passage across the BBB. We describe the preparation and physical characterization of nanosized liposomes decorated with peptides derived from apolipoprotein E and characterize their interaction with human immortalized brain capillary cells cultured in vitro (hCMEC/D3). For this purpose, we synthesized two ApoE-derived peptides (the fragment 141–150 or its tandem dimer) containing a cysteine residue at the C-terminus and decorated NL by exploiting the cysteine reaction with a maleimide-group on the nanoparticle surface. NL without ApoE functionalization did not show either relevant membrane accumulation or cellular uptake, as monitored by confocal microscopy using fluorescently labeled nanoliposomes or quantifying the cell-associated radioactivity of isotopically labeled nanoliposomes. The uptake of nanoliposomes by cell monolayers was enhanced by ApoE-peptide-functionalization, and was higher with the fragment 141–150 than with its tandem dimer. The best performance was displayed by nanoliposomes containing phosphatidic acid and decorated with the ApoE fragment 141–150. Moreover, we show that the functionalization of liposomes containing acidic phospholipids with the ApoE fragment 141–150 scarcely affects their reported ability to bind Apeptide in vitro. These are important and promising features for the possibility to use these nanoliposomes for the targeting of Ain the brain districts.

INTRODUCTION

Alzheimer's disease (AD) is the most common cause of dementia in the elderly population, and the fourth most common cause of death in Western countries after heart disease, cancer and stroke. Therefore, strategies for early detection as well as for therapy of AD are perhaps among one of the most challenging and timely areas in modern medicine. The pathogenic mechanisms underlying AD are not yet completely clear, however, in recent years, it has been clarified that the overproduction and progressive aggregation of amyloid-β peptide (Aβ) in the brain play a central role (Jeynes and Provias, 2011; Lui et al., 2010) Aβ is the major component of senile plaque (and cerebrovascular) amyloid in AD brains, and data from molecular genetics, together with biochemical and animal model studies, all suggest that the self-association and aggregation of Aβ is a seminal event in the early stages of AD. Moreover, it has been reported that brain and blood Aβ are in equilibrium through the blood–brain-barrier (BBB), and that peripheral sequestration of Aβ may shift this equilibrium toward the blood, eventually drawing out the excess from the brain ("sink" effect) (Matsuoka et al., 2003). Not surprisingly, therefore, there has been a considerable effort to try and develop new drugs, targeting either central or systemic Aβ. However, the major problem in drug delivery to the brain is the presence of the BBB which limits their penetration. Among non-invasive techniques to overcome this barrier, the use of nanoparticles (NPs) has been proposed, since they are either suitable vehicles for imaging probes or therapeutic agents, or for the possibility to functionalize their surface with target-specific ligands (Bhaskar et al., 2010). Moreover, multivalent interactions may strikingly increase the affinity of functionalized NPs for their targets. Among all the different nanoparticles, liposomes have many advantages for drug delivery, due to their non-toxic and non-immunogenic, fully biodegradable and structurally versatile nature. Within this frame, we have recently designed nanoliposomes (NL) containing phosphatidic acid (PA) or cardiolipin (CL), and able to target with very high affinity Aβ 1–42 peptide in vitro (Gobbi et al., 2010). In the present investigation we are approaching the problem of promoting the interaction of such liposomes with brain capillary endothelial cells, as a first step toward their passage across the BBB. We describe the preparation and physical characterization of PA- or CL-containing liposomes decorated with peptides derived from apolipoprotein E (ApoE) and characterize their interaction with human immortalized brain capillary cells cultured in vitro (hCMEC/D3).

METERIALS AND METHODS

Materials. All chemical reagents were from Sigma–Aldrich, Milano, Italy. Bovine brain sphingomyelin (Sm), cholesterol (Chol) and 1,2-stearoyl-sn-glycero-3-phosphoethanolamine-N-[maleimide(poly(ethylene glycol)-2000)] (mal-PEG-PE) were purchased from Avanti Polar Lipids (Inc., U.S.A.). N-(4,4-Difluoro-5,7-dimethyl-4-bora-3a, 4a-diaza-s-indacene-3-dodecanoyl) sphingosyl phosphocholine (fluorescently labeled sphingomyelin, BODIPY-Sm) was from Molecular Probes, Invitrogen Srl, Milano. Dimyristoylphosphatidic acid (PA), cardiolipin (CL) and Aβ1–42 peptide were purchased from Sigma–Aldrich, Milano, Italy. Polycarbonate filters for extrusion procedure were purchased from Millipore Corp., Bedford, MA. Extruder was from Lipex Biomembranes, Vancouver, Canada. PD-10 columns were purchased from GE Healthcare, Uppsala, Sweden. All the media and supplements for cell cultures and Phalloydin were supplied by Invitrogen Srl, Milano, Italy. Triton X-100 was from Sigma–Aldrich, Milano, Italy. [3H]-Dipalmitoyl-phosphatidylcholine ([3H]-DPPC) was from Amersham (Castle Hill, NSW, Australia). The hCMEC/D3 cell line was obtained under license from Institut National de la Sante et de la Recherche Medicale (INSERM, Paris, France). Rat type I collagen, 1/100 chemically defined lipid concentrated, Phalloydin and all the media and supplements for cell cultures were from Invitrogen Srl (Milano). LAMP-1 was from Abcam (Science Park, Cambridge, UK).

Synthesis and characterization of ApoE peptides. The sequence corresponding to a.a. residues 141–150 of human ApoE peptide and its tandem dimer repeat (141–150)2 were synthesized on an automated Applied Biosystems synthesizer model 433A at 0.1 mM scale with NOVASYN-TGA resin (Novabiochem, Darmstadt, Germany), using Fmoc-protected l-amino acid4s (Flamma, Bergamo, Italy). The peptides were bearing at the C-terminal a tryptophan residue for fluorescence monitoring and ended with cysteine residue for covalent coupling with mal-PEG-PE. Amino acids were activated by reaction with O- (Benzotriazol-1-yl)-N,N,N,N-tetramethyluronium tetrafluoroborate and N,N-diisopropylethylamine. A capping step with acetic anhydride after the last coupling cycle of each amino acid was included. Peptides were cleaved from the resin with trifluoroacetic acid:thioanisole:water:phenol:ethanedithiol (82.5:5:5:2.5, v/v), precipitated and washed with diethyl ether. The precipitate was then purified by reverse

phase HPLC on a semi-preparative C4 column (Symmetry 300, Waters) and peaks collected were characterized by matrix-assisted laser desorption/ionization (MALDI) mass spectrometry. To the sequence CWG-(LRKLRKRLLR)-NH2 (M = 1698.18 g/mol), corresponding to a.a. residues 141–150, it will be referred as ApoE monomer (mApoE). The sequence CWG-(LRKLRKRLLR)-(LRKLRKRLLR)-NH2 (M = 3030.94 g/mol), corresponding to the tandem sequence (141–150) that is referred to ApoE dimer (dApoE). The purity for both peptides assessed by HPLC and MALDI was higher than 95%. The fractions containing the purified peptides were finally lyophilized and stored at −20°C.

Preparation and characterization of NL. NL were composed of Sm/Chol (1:1 molar ratio) mixed with 2.5 molar% of mal-PEG-PE (Sauer et al., 2005), and containing either 5 molar% of PA or CL (Gobbi et al., 2010). BODIPY-Sm (0.5 molar%) was also present in the case of confocal microscopy experiments (Section 2.8). A tritiated lipid tracer ([3H]-DPPC, less than 0.0001% of total lipids) was present for quantification of cellular uptake (Section 2.9) and binding experiments (Section 2.6). Briefly, lipids were mixed in chloroform/methanol (2:1, v/v) and dried under a gentle stream of nitrogen followed by a vacuum pump for 3 h to remove traces of organic solvent. The resulting lipid film was rehydrated in phosphate-buffered saline (PBS), vortexed and then extruded 10 times at 55 ◦C through a stack of two polycarbonate filters (100- nm pore size diameter) under 20 bar nitrogen pressure with an extruder. NL were separated from possible unincorporated material by size-exclusion chromatography using PD-10 column and PBS as the eluent. Lipid recovery after PD-10 column was assessed by assaying the individual components or by measuring the radioactivity associated (Gobbi et al., 2010). BODIPY-Sm recovery was assessed measuring the fluorescence emission intensity before and after PD-10 column. Size, stability and Z-potential were determined by Dynamic Light Scattering (DLS), as described below (Section 2.5).

Preparation and characterization of NL functionalized with ApoE peptides (ApoE-NL). mApoE or dApoE peptide was added to NL in PBS to give a final peptide:mal-PEG-PE molar ratio of 1.2:1, and incubated over night at room temperature to form a thioether bond with mal-PEG-PE. NL decorated with the peptide (ApoE-NL) were separated from unbound peptide using PD-10 column (Sauer et al., 2005). The yield of coupling of the peptide to NL was assessed by measuring the tryptophan fluorescence intensity (ex =

280 nm) of the incubation mixture and of ApoE-NL recovered from the PD-10 column. Spectra were recorded between 300 and 450 nm using a Cary Eclipse spectrofluorometer (Varian). The amount of peptide bound to NL was calculated from the fluorescence intensity of a known amount of the peptide dissolved in PBS, taken as the standard.

Dynamic Light Scattering. NL and ApoE-NL size, polydispersity index and Z-potential were obtained using a ZetaPlus particle sizer and Z-potential analyzer (Brookhaven Instruments Corporation, Holtsville, NY, U.S.A.) at 25 ◦C in PBS by DLS with a 652 nm laser beam. NL size and polydispersity were obtained from the intensity autocorrelation function of the light scattered at a fixed angle of 90°. The correlation function was analyzed by means of a two cumulant expansion. Z-potential measurement was performed under an electrical field of 29.7 V/cm (Gobbi et al., 2010). NL size and polydispersity index were measured in buffer by DLS for 2 days. Standard deviations were calculated from at least three measurements.

Culture of hCMEC/D3 cells. Human brain endothelial cells (hCMEC/D3) were obtained from Institut National de la Santé et de la Recherche Médicale (INSERM, Paris, France). hCMEC/D3 cells cultured between passage 25 and 35 were used. For culturing, the cells were seeded at a concentration of 27,000 cells/cm2 and grown in tissue culture flasks coated with 0.1 mg/mL rat tail collagen type 1, in the following medium: EBM-2 medium (Lonza, Basel, Switzerland) supplemented with 5% fetal bovine serum (FBS), 1% Penicillin–Streptomycin, 1.4 µM hydrocortisone, 5 µg/mL ascorbic acid, 1/100 chemically defined lipid concentrate (Invitrogen), 10 mM HEPES and 1 ng/mL basic FGF (bFGF). The cells were cultured at 37 ◦C, 5%CO2/saturated humidity. Under these culture conditions, hCMEC/D3 cells can be considered polarized (Tai et al., 2009; Vu et al., 2009). NL were added to the apical membrane, exposed to the medium, and corresponding to the luminal side of capillary vessels. Cells culture medium was changed every 2–3 days. For fluorescent studies cells were cultured for two days on rat type I collagen-coated cover slips (diameter 25 mm) positioned in culture dishes; for uptake studies cells were grown in 12-well plates and used when confluent.

Liposome uptake studies carried out by confocal-laser-scanning microscopy. Confocal-laser-scanning microscopy (CLSM) was employed in order to study the uptake of fluorescently labeled NL or ApoE-NL. CLSM pictures were taken using an LSM710 inverted confocal laser scanning microscope equipped with a Plan-Neofluar 63×/1.4 oil objective (Carl Zeiss, Oberkochen, Germany). Excitation was performed using two V/VIS-laser diode 25 mV (405–488) and Ar-laser (540 nm) at 10% intensity. The pinhole was set to 1 A. Image acquisition was done sequentially to minimize cross-talk between the fluorophores. Cells were cultured for two days on rat type I collagen-coated cover slips (diameter 25 mm) positioned in culture dishes, and incubated at 37 ◦C with NL or with ApoE-NL containing BODIPY-Sm for 3 h, rinsed three times with PBS and fixed with a 10% formalin solution. After three washes with PBS, cells were permeabilized with 0.2% Triton X-100 in PBS for 15 min, then rinsed twice and incubated with a solution of 1% Phalloydin (actin filaments staining) in PBS for 1 h, then with 20 µM DAPI (nuclear staining) in PBS for 10 min and finally with LAMP-1 (1:200) for 4 h at room temperature. After three washes, the samples were mounted using polyvinyl alcohol mounting medium (Sigma–Aldrich). All washes were done with PBS.

Liposome uptake studies carried out by radiochemical techniques. Liposomes containing [3H]-DPPC as a tracer were diluted to 100 nmol/mL of total lipid (corresponding to 3000 dpm/mL) in serum free culture medium (SFM), 400 µL was added to the cells grown in 12-well plates, and incubated for 3 h at 37°C. The liposome dispersion was withdrawn and cells were washed 1× with 1 mL culture medium containing 0.5% serum 1× with 1 mL PBS and 1× with 400 µL trypsin 0.1% for 3 min, followed by PBS washing. Finally the cells were detached with 400 µL trypsin 0.25%/EDTA (v/v) and the suspensions were mixed with 5.0 mL scintillation cocktail (Ultima Gold, Perkin Elmer) and counted with a Tri-Carb 2200 CA Liquid Scintillation Analyzer (Packard) to quantify the amount of radioactivity associated with cells.

Preparation of Aβ1–42 fibrils. Fibrils of Aβ1–42 peptide were obtained as described (Gobbi et al., 2010). The commercial Aβ1–42 peptide was dissolved in HFIP at 1 mg/mL concentration to monomerize pre-existing aggregates; HFIP was then allowed to evaporate and the resulting peptide film was stored at −20°C. The peptide was resuspended before use in DMSO at a concentration of 5 mM, bath sonicated for 10 min and to obtain fibrils the

peptide solution was diluted with water to 100 μM, acidified to pH 2.0 with HCl and left for 24 h at 37°C. The presence of fibrils in this preparation has been previously confirmed and characterized (Gobbi et al., 2010).

Binding of NL or mApoE-NL to Aβ1–42 peptide by ultracentrifugation on sucrose density gradient. NL or mApoE-NL, containing either 5 molar% of PA or CL and [3H]-DPPC as a tracer, were incubated with Aβ1–42 peptide in PBS (1:5 = peptide:total lipids molar ratio) at 37°C for 15 min, as already described (Gobbi et al., 2010). After incubation, the peptide bound to NL was separated from free peptide by ultracentrifugation on a discontinuous sucrose density gradient; 10 fractions were collected from the gradient and analyzed for the peptide content by dot-blot procedure, using mAb6E10 (Signet, Dedham, MA), and for the lipid content by measuring the NL-associated radioactivity. Fractions of the gradient carrying both lipids and peptide (usually fractions 1–5) were considered as "NL-bound peptide" and fractions containing the peptide alone (usually fractions 6–10) were considered as "unbound peptide". The proportion of peptide bound to NL was determined from the chemiluminescent spots on PVDF membrane, that were digitally semi-quantitatively estimated by a KodakvImage station 2000R using Kodak Molecular Imaging Software Version 4.0, and was expressed as the % ratio between the amount of peptide amount in the fractions 1–5 over the total peptide (sum of bound and unbound).

Statistical analysis. Each experiment was performed at least in triplicate. The differences were evaluated for statistical significance using Student's t-test.

RESULTS

NL characterization. The total lipid recovery of NL, with or without anionic phospholipids, was about 90%. The different lipid components of the mixtures were recovered with equal efficiency and always reflected the proportion in the starting mixture (data not shown). Final preparations of NL had a size below 200 nm diameter and low PDI value (Table 1). The Z-potential is a value related to the stability of dispersion: the high negative zeta potential of NL (reported in Table 1) indicates that the dispersion is electrically stabilized.

ApoE-NL characterization. The tryptophan fluorescence spectrum of mApoE, displaying an emission maximum at 354 nm, showed a blue shift to 350 nm in the ApoE-NL fraction recovered from the PD-10 column (Fig. 1), suggesting the coupling of the peptide with the mal-PEG-PE lipid, as previously reported (Sauer et al., 2005). The yield of coupling was between 50 and 60%. After coupling with ApoE peptide, the size of NL slightly increased (Table 1). The high negative zeta potential and the low PDI of ApoE-NL indicate that the NL are stable after functionalization with ApoE peptide. The size of the ApoE-NL remained unchanged for at least 48 h (data not shown).

Cellular uptake studied by CLSM. Cellular uptake by hCMEC/D3 cells of fluorescent-labeled NL was qualitatively evaluated by CLSM (Fig. 2). NL containing PA or CL and functionalized with mApoE or dApoE were studied. Non-functionalized NL displayed neither membrane accumulation nor cellular uptake of the fluorescent marker. On the contrary, the coupling with either dApoE or mApoE peptide, increased the association to hCMEC/D3 cells. This was substantially higher in case of mApoE-PA-NL. Indeed after 3 h incubation with mApoE-NL, we found the highest amount of green (BODIPY-Sm) fluorescence associated with cells. The images showed the presence of hot green spots below the plasma membrane and near the perinuclear recycling regions. With dApoE-NL, a lower amount of fluorescence was associated to hCMEC/D3 cells, compared with mApoE-NL. A lesser number of green spots was visible near the nucleus although a clearly green signal was present just below the plasma membrane. CL-NL mApoE resulted in few high density aggregates mainly located on the outer plasma-membrane and a low amount of intracellular fluorescence was detectable (Fig. 2A). To support the hypothesis that the NL were taken up by the cells, we performed staining of late-endosomes and early-lysosomes using LAMP-1. Our results show that, mApoE-PA-NL and mApoECL- NL do not co-localize with late-endosomes and early-lysosomes, their fluorescence is present in the same optical section (Fig. 2B), indicating their cellular uptake.

Cellular uptake studied by radiochemical techniques. CLSM studies qualitatively confirmed mApoE as the best ligand in targeting NL to brain capillary endothelial cells. Thus, we decided to evaluate the association with hCMEC/D3 cells of the 3H-labeled NL containing PA or CL and functionalized with mApoE (Fig. 3). After incubation with radiolabeled NL, the radioactivity stably associated with cells was counted after washings with PBS and mild trypsin treatment to remove membrane surface-adsorbed radioactivity. The radioactivity stably associated with cells was about 5% of the total incubated dose. The cellular uptake of NL (without PA or CL) strongly increased after functionalization with mApoE peptide. When NL containing PA and functionalized with mApoE were used, a significant increasing in the amount of the cell-associated radioactivity (+60%, $p < 0.05$), than compared with the same NL without mApoE. In the case of NL containing CL, and functionalized with mApoE, an increase in the uptake was noted (+10%).

Binding of Aβ1–42 peptide to mApoE-NL. The ability of NL containing PA or CL to bind Aβ1–42 peptide was compared with the same NL functionalized with mApoE peptide, using ultracentrifugation on a discontinuous sucrose density gradient to separate the bound from the unbound peptide. Each gradient fractions was analyzed for the lipid (Fig. 4A) and peptide (Fig. 4B) content. Our results show that amount of Aβ1–42 bound to NL and the amount bound to mApoE-NL was comparable; only a small decrease in the amount of peptide bound was recorded after functionalization of NL containing PA with mApoE peptide (Fig. 4C).

	Av. diameter (nm)	PDI	Z-pot ± SD (mV)
Non-functionalized NL			
Chol/Sm/5 mol% PA	114	0.318	−28.38 ± 0.059
Chol/Sm/5 mol% CL	119	0.183	−25.69 ± 0.027
ApoE-NL			
Chol/Sm/5 mol% PA	136	0.198	−27.74 ± 0.018
Chol/Sm/5 mol% CL	146	0.281	−21.40 ± 0.029

SD = standard deviation; Z-pot = Z-potential; PDI = polydispersion index.

Table 1 Physicochemical properties of NL and ApoE-NL. Nanoliposomes, composed of Chol/Sm/mal-PEG-PE added or not with 5 molar% of PA or CL, were functionalized with mApoE or dApoE peptide and characterized by Dynamic Light Scattering (see text for details) in order to determine the size distribution and Z-potential.

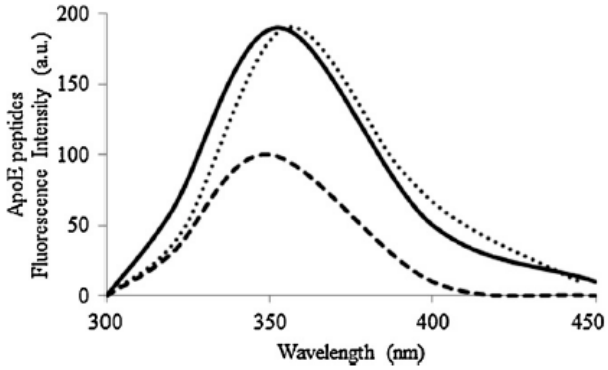

Fig. 1. Characterization of NL and ApoE-NL. NL, composed of Sm/Chol/mal-PEG-PE added or not with 5 molar% of PA or CL and added with BODIPY-Sm were functionalized with mApoE or dApoE peptide and purified as described in the text. Fluorescence spectra of ApoE peptides in solution (•••), after overnight incubation with NL (—) and after ApoE-NL purification by column chromatography (---). NL = nanoliposomes.

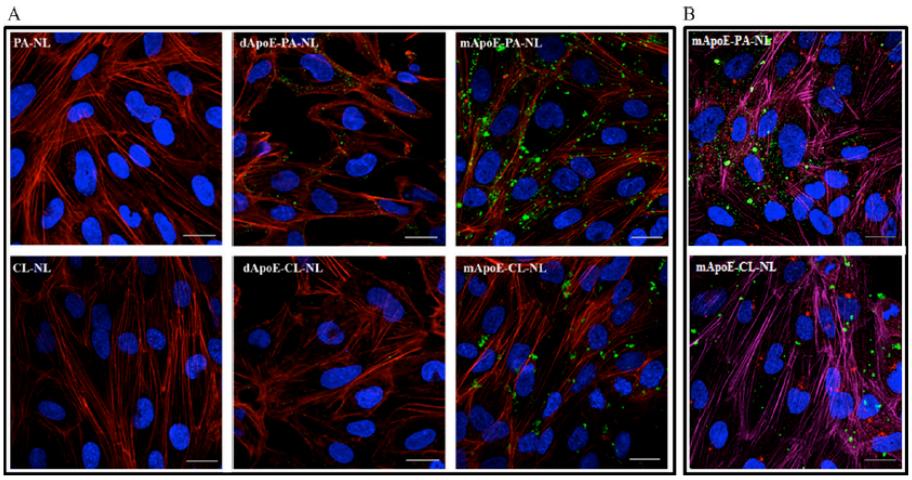

Fig. 2. Confocal laser scanning microscopy of hCMEC/D3 cells after incubation with fluorescent ApoE-NL. NL containing PA or CL and BODIPY-Sm (green fluorescence), without surface-located ApoE peptides displayed neither membrane nor intracellular uptake (PA-NL and CL-NL panels). The intracellular fluorescence uptake was the greatest in case of liposomes containing PA and functionalized with mApoE peptide (mApoE-PA-NL panel) and progressively decreased in case of liposomes containing CL and mApoE (mApoE-CL-NL panel), liposomes containing PA and dApoE (dApoE-PA-NL panel) and liposomes containing CL and dApoE (dApoE-PA-NL panel). (A) Cells were incubated with Phalloydin in order to visualize the actin filaments (red fluorescence) and nuclear staining was performed by DAPI (blue staining). (B) Cells were incubated with Phalloydin

in order to visualize the actin filaments (magenta fluorescence), nuclear staining was performed by DAPI (blue staining) and LAMP-1 to mark late-endosomes and early-lysosomes (red staining). Scale bar = 20 μm. PA-NL = nanoliposomes composed of Sm/Chol/malPEG-PE/PA; mApoE-PA-NL = PA-NL functionalized with mApoE peptide; CL-NL = nanoliposomes composed of Sm/Chol/malPEG-PE/CL; mApoE-CL-NL = CL-NL functionalized with mApoE peptide; dApoE-PA-NL = PA-NL functionalized with dApoE peptide; dApoE-CL-NL = CL-NL functionalized with dApoE peptide.

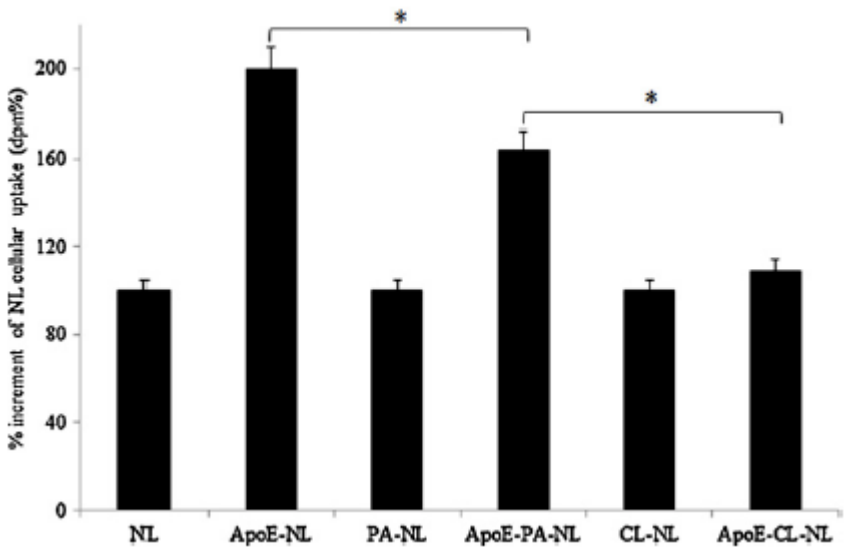

Fig. 3. Quantification of NL and mApoE-NL binding to hCMEC/D3 cells by radiochemical technique. NL, composed of Sm/Chol/mal-PEG-PE added or not with 5 molar% of PA or CL and containing [3H]-DPPC as a tracer, were functionalized or not with mApoE peptide and purified as described in the text. NL and mApoE-NL were incubated with hCMEC/D3 cells at 37 ◦C for 3 h. After incubation, the radioactivity uptaken from the cells was measured by liquid scintillation counting. The radioactivity uptake of mApoE-functionalized NL was expressed as % increment with respect to non-functionalized NL. *Statistical significance (t test; $p < 0.05$). NL = nanoliposomes composed of Sm/Chol/malPEG-PE; ApoE-NL = NL functionalized with mApoE peptide; PA-NL = nanoliposomes composed of Sm/Chol/malPEG-PE/PA; mApoE-PA-NL = PA-NL functionalized with mApoE peptide; CL-NL = nanoliposomes composed of Sm/Chol/malPEG-PE/CL; mApoE-CL-NL = CL-NL functionalized with mApoE peptide.

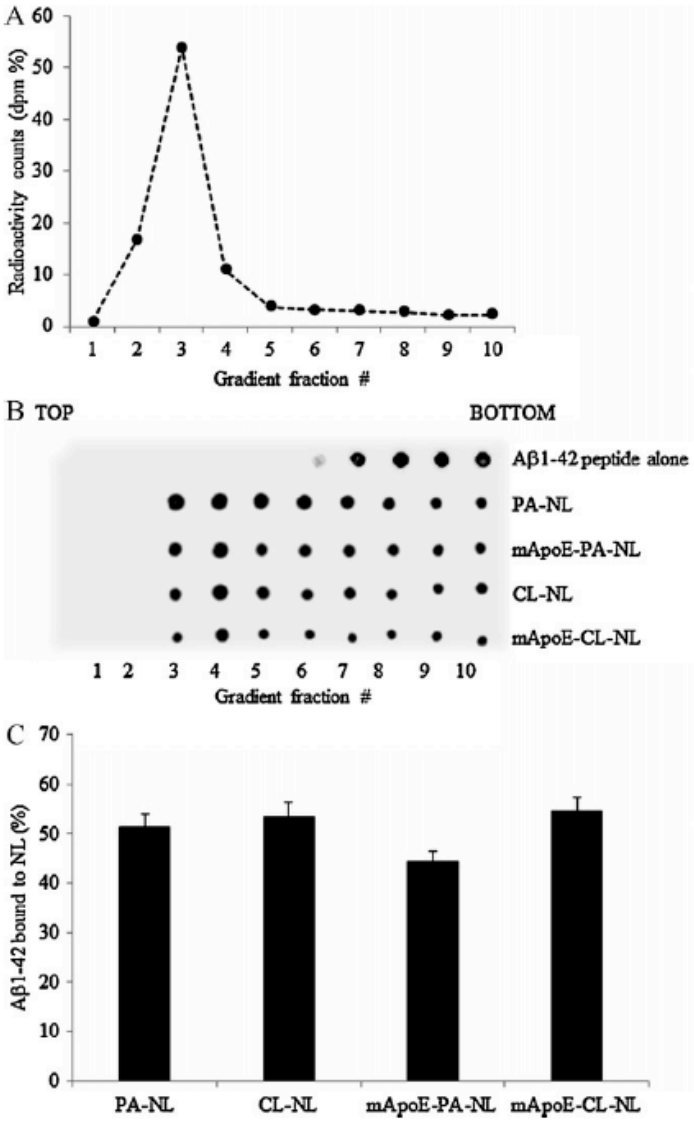

Fig. 4. Assessment Aβ1–42 binding features of mApoE-NL. NL, composed of Sm/Chol/mal-PEG-PE added with 5 molar% of PA or CL and added with [3H]-DPPC, were functionalized with mApoE peptide and purified as described in the text. mApoE-NL were incubated with Aβ1–42 peptide and the Aβ bound to NL was separated from the unbound peptide by ultracentrifugation on a density gradient. 10 fractions collected from the top of the gradient and analyzed for the radioactivity and Aβ content. (A) Radioactivity distribution (dpm%) along the gradient fractions was determined by counting the radioactivity of each gradient fraction. (B) Aβ1–42 peptide distribution along the gradient fractions was determined by dot-blot procedure. See text for details. (C) The amount of peptide bound to NL or mApoE-NL was determined by densitometric measurement of the intensity of Aβ peptide spots on PVDF membrane and expressed as % of peptide bound to NL over the total peptide amount. NL = nanoliposomes; dpm = disintegration per minute; Aβ1–42 peptide alone: Aβ1–42 peptide

loaded alone on sucrose density gradient, without NL; PA-NL = nanoliposomes composed of Sm/Chol/malPEG-PE/PA; mApoE-PA-NL = PA-NL functionalized with mApoE peptide; CL-NL = nanoliposomes composed of Sm/Chol/malPEG-PE/CL; mApoE-CL-NL = CL-NL functionalized with mApoE peptide.

DISCUSSION

AD is one of the most common neurodegenerative diseases that affects millions of people worldwide and, due to its graveness and social and economic costs, the effectiveness of a targeted and effective therapy remains a huge problem to solve (Dartigues, 2009). The strategies for the therapy and diagnosis of AD, as such as for many other neurological diseases, are severely limited by the presence of the blood–brain-barrier (BBB). To overcome this barrier, many delivery strategies have been attempted, such as local injection, induction of enhanced permeability and targeted delivery (de Boer and Gaillard, 2007). Currently, nanoparticles seem to provide an important non-invasive contribution to overcome this problem, arising from the possible strategies of multi-functionalization. Within this context and starting from the recent report that NL incorporating phosphatidic acid or cardiolipin (PA or CL) showing high binding affinity toward Apeptide (Gobbi et al., 2010), we started to design NL with improved interaction with the BBB endothelium, as a first step toward their passage across the barrier, by decorating their surface with ligands exploiting the transcellular route of transport of macromolecules (Cerletti et al., 2000; Markoutsa et al., 2011). A well-established pathway is the one triggered by low-density lipoprotein-receptor (LDLr) (Bu, 2009; Laskowitz et al., 2001), through the recognition of apolipoprotein E (ApoE). A first theoretical support to take advantage of LDLr pathway comes from the observation that these receptors are present on capillary endothelial cells of several species and that their expression is up-regulated in the BBB with respect to other endothelia (Dehouck et al., 1994). A further theoretical support comes from the observation that, in analogy with LDL, NPs functionalized with ApoE-derived peptides (corresponding to the binding domain of the ApoE) are able to interact with the LDLr and could be transported across the BBB by transcytosis, bypassing the lysosomal degradation (Michaelis et al., 2006; Hulsermann et al., 2009; Zensi et al., 2009). The NL containing 5 molar% of anionic phospholipids (PA or CL), since at this low proportion, they do not induce complement activation in vitro (Moghimi et al., unpublished data). Cellular uptake of NL, that was

scarce for non-decorated NL, increased with mApoE peptide. These NL containing PA and decorated with the 141–150 sequence of ApoE displayed the most efficient uptake in hCMEC/D3 cells. These formulation did not co-localize with late-endosomes and early-lysosomes; thus indicating a possible cellular uptake based on caveolae-mediated mechanisms. These data were obtained by confocal-laser-scanning microscopy, giving a qualitative evaluation of the uptake, and quantitatively confirmed using radiochemical techniques. It should be remarked that a significantly higher binding to the hCMEC/D3 was displayed by NL functionalized with mApoE and containing PA but not by those containing CL. We can speculate that the higher number of negative charges carried by CL, in comparison with PA, modify the surface properties of NL and partially masking the receptor binding site of mApoE peptide. This speculation is supported by the high cellular uptake obtained with ApoE-NL without PA or CL lipids. Moreover, we asked whether the presence of the polycationic chains of mApoE peptide on the liposome surface, could alter the binding capacity of acidic phospholipids with Aβ peptide. Very importantly, the results obtained with ultracentrifugation experiments showed that the functionalization of NL containing PA or CL, retain their ability to bind the Aβ1–42 peptide in vitro. This result is an important and promising feature for the possibility to use these NL for the targeting of the peptide in the brain districts. Moreover, our NL could be able to carry out peripheral sequestration of A, eventually drawing out the excess from the brain ("sink" effect) (Matsuoka et al., 2003). Of course these are intriguing hypotheses that will deserve further experimental investigation.

CONCLUSION

In conclusion, herein we show that NL composed of Sm/Chol (1:1, M:M) and containing 5 molar% PA or CL, after functionalization with ApoE-derived peptide (fragment 141–150) display enhanced targeting of human microvascular brain capillary endothelial cells in vitro. The uptake in the brain capillary cells was up to 60% higher compared to the non-functionalized NL. The functionalization with ApoE-derived peptide does not affect their previously reported ability to bind amyloid-β, whose overproduction and progressive aggregation in the brain play a central role in AD pathogenesis.

Acknowledgements The research leading to these results has received funding from the European Community's Seventh Framework Programme

(FP7/2007-2013) under grant agreement n◦ 212043 (NAD).

REFERENCES

Bhaskar, S., Tian, F., Stoeger, T., Kreyling, W., de la Fuente, J.M., Grazú, V., Borm, P., Estrada, G., Ntziachristos, V., Razansky, D., 2010. Multifunctional nanocarriers for diagnostics, drug delivery and targeted treatment across blood–brain barrier: perspectives on tracking and neuroimaging. Particle Fibre Toxicol. 7, 3.

Bu, G., 2009. Apolipoprotein, E and its receptors in Alzheimer's disease: pathways, pathogenesis and therapy. Nat. Rev. Neurosci. 10, 333–344.

Cerletti, A., Drewe, J., Fricker, G., Eberle, A.N., Huwyler, J., 2000. Endocytosis and transcytosis of an immunoliposome-based brain drug delivery system. J. Drug Target. 8, 435–446.

Dartigues, J.F., 2009. Alzheimer's disease: a global challenge for the 21st century. Lancet Neurol. 8, 1082–1083.

de Boer, A.G., Gaillard, P.J., 2007. Drug targeting to the brain. Ann. Rev. Pharmacol. Toxicol. 47, 323–355.

Dehouck, B., Dehouck, M.P., Fruchart, J.C., Cecchelli, R., 1994. Upregulation of the low-density lipoprotein receptor at the blood–brain barrier: intercommunications between brain capillary endothelial cells and astrocytes. J. Cell Biol. 126,465–473.

Gobbi, M., Re, F., Canovi, M., Beeg, M., Gregori, M., Sesana, S., Sonnino, S., Brogioli, D., Musicanti, C., Gasco, P., Salmona, M., Masserini, M., 2010. Lipid-based nanoparticles with high binding affinity for amyloid-beta-1–42 peptide. Biomaterials 31, 6519–6529.

Hulsermann, U., Hoffmann, M.M., Massing, U., Fricker, G., 2009. Uptake of apolipoprotein E fragment coupled liposomes by cultured brain microvessel endothelial cells and intact brain capillaries. J. Drug Target. 17, 610–618.

Jeynes, B., Provias, J., 2011. The case for blood–brain barrier dysfunction in the pathogenesis of Alzheimer's disease. J. Neurosci. Res. 89, 22–28.

Laskowitz, D.T., Thekdi, A.D., Thekdi, S.D., Han, S.K., Myers, J.K., Pizzo, S.V., 2001. Downregulation of microglial activation by apolipoprotein E and apoE-mimetic peptides. Exp. Neurol. 167, 74–85.

Lui, J.K., Laws, S.M., Li, Q.X., Villemagne, V.L., Ames, D., Brown, B., Bush, A.I., De Ruyck, K., Dromey, J., Ellis, K.A., Faux, N.G., Foster, J., Fowler, C., Gupta, V., Hudson, P., Laughton, K., Masters, C.L., Pertile, K., Rembach, A., Rimajova, M., Rodrigues, M., Rowe, C.C., Rumble, R., Szoeke, C., Taddei, K., Taddei, T., Trounson, B., Ward, V., Martins, R.N., 2010. Plasma amyloid-beta as a biomarker in Alzheimer's disease: the AIBL study of aging. J. Alzheimers Dis. 20, 1233–1242.

Markoutsa, E., Pampalakis, G., Niarakis, A., Romero, I.A., Weksler, B., Couraud, P.O., Antimisiaris, S.G., 2011. Uptake and permeability studies of BBB-targeting immunoliposomes using the hCMEC/D3 cell line. Eur. J. Pharm. Biopharm. 77, 265–274.

Matsuoka, Y., Saito, M., LaFrancois, J., Saito, M., Gaynor, K., Olm, V., Wang, L., Casey, E., Lu, Y., Shiratori, C., Lemere, C., Duff, K., 2003. Novel therapeutic approach for the treatment of Alzheimer's disease by peripheral administration of agents with an affinity to beta-amyloid. J. Neurosci. 23, 29–33.

Michaelis, K., Hoffmann, M.M., Dreis, S., Herbert, E., Alyautdin, R.N., Michaelis, M., 2006. Covalent linkage of apolipoprotein e to albumin nanoparticles strongly enhances drug transport into the brain. J. Pharmacol. Exp. Ther. 317, 1246–1253.

Sauer, I., Dunay, I.R., Weisgraber, K., Bienert, M., Dathe, M., 2005. An apolipoprotein E-derived peptide mediates uptake of sterically stabilized liposomes into brain capillary endothelial cells. Biochemistry 44, 2021–2029.
Tai, L.M., Reddy, P.S., Lopez-Ramirez, M.A., Davies, H.A., Male, D.K., Loughlin, A.J., Romero, I.A., 2009. Polarized P-glycoprotein expression by the immortalized human brain endothelial cell line, hCMEC/D3, restricts apical-to-basolateral permeability to rhodamine 123. Brain Res. 1292, 14–24.
Vu, K., Weksler, B., Romero, I., Couraud, P.O., Gelli, A., 2009.

Immortalized human brain endothelial cell line hCMEC/D3 as a model of the

blood–brain barrier facilitates in vitro studies of central nervous system infection by Cryptococcus neoformans. Eukaryot. Cell 8 (11), 1803–1807.

Zensi, A., Begley, D., Pontikis, C., Legros, C., Mihoreanu, L., Wagner, S., 2009. Albumin nanoparticles targeted with ApoE enter the CNS by transcytosis and are delivered to neurons. J. Control. Release 137, 78–86.

CHAPTER 4

Nanoliposomes functionalized to overcome the blood-brain barrier and to target amyloid-βpeptide: the chemical design affects the permeability across a model barrier

Submitted

Elisa Salvati, Francesca Re, Silvia Sesana, Ilaria Cambianica, Giulio Sancini, Massimo Masserini, Maria Gregori.

Abstract

In the search of new strategies for therapy and diagnosis of Alzheimer disease, nanoparticles functionalized to bind amyloid-β aggregates, hallmarks of the pathology, and to cross the blood-brain barrier, main obstacle for treating brain diseases, are promising tools. Herein, we functionalized nanoliposomes composed of sphingomyelin and cholesterol and containing phosphatidic acid, as amyloid-βligand, with anti-transferrin receptor antibody RI7217, as blood-brain barrier ligand. RI7217 was attached on nanoliposomes by two different techniques, biotin/streptavidin ligation or thiol-maleimide covalent coupling, in order to investigate how the biological activity might be affected by chemical design. Double-functionalized nanoliposomes displayed high affinity either towards transferrin receptor (K_D=2.5-11 nM) or amyloid-βpeptide (K_D=37-48.5 nM), as assessed by Surface Plasmon Resonance and immunoblotting techniques. Successively, we investigated the uptake and permeability of nanoliposomes functionalized or nor with RI7217 and labeled with fluorescent (sphingomyelin-BODIPY) or radioactive ([^{3}H]-sphingomyelin/[^{14}C]-phosphatidic acid) probes utilizing an in vitr o blood-brain barrier cellular (hCMEC/D3) model. Confocal microscopy experiments showed that functionalization with RI7217 enhances cell uptake with no co-localization

with early or late endosomes or early lysosomes. The best performing immuno-liposomes were those with covalently coupled antibody that, noteworthy, displayed also the highest permeability across the barrier model ($7.24\pm0.39x10^{-6}$ cm/min), with no alterations in cells viability and monolayer integrity. The ratio between the two radiotracers, identical in the two compartments of the transwell system, suggests that immuno-liposomes were transported intact across the monolayer. Overall, our results provide evidence of the superiority of covalent coupling versus biotin-streptavidin βligation, in promoting in vitr o barrier crossing of immuno-liposomes containing phosphatidic acid.

INTRODUCTION

Approximately 24 million people worldwide suffer from dementia, of which 60% is due to Alzheimer disease (AD). AD incidence is 0.4% for individuals aged 65-69 and increases to 10% for those over 90 years [1]. AD is characterized clinically by learning and memory impairment, and pathologically by neuronal loss, primarily due to intracellular neurofibrillary tangles and extracellular amyloid plaques, mainly composed of aggregates of amyloid-β peptides (Aβ)[2]. The delivery of drugs to the central nervous system (CNS) is troubled by the existence of the blood-brain barrier (BBB) and this poses limitations for the treatment and diagnosis of brain disorders [3]. The use of properly designed nanoparticles represents a promising strategy to successfully enhance the CNS penetration of therapeutics [4-6]. The main advantage of nanoparticles is based on the possibility of surface multi-functionalization, potentially allowing both targeting of Aβ and BBB crossing, thus making them suitable for therapy and/or diagnosis of AD [7-9].

Within this framework, we have recently designed nanoliposomes (NL) functionalized with phosphatidic acid (PA-NL) that demonstrated very high

affinity for A [10] and that were able to rescue cells from A toxicity in vitr o [11]. In the present investigation we functionalized NL with a possible promoter of BBB crossing, the antibody RI7217 against transferrin receptor (TfR). TfR targeting has been suggested as possible strategy to reach the brain [12], given its expression on BBB endothelial cells for the regulation of brain uptake of iron [13].

Among the various strategies that have been proposed to couple antibodies on nanoparticles [14], we employed biotin/streptavidin ligation and thiol-maleimide covalent coupling to attach RI7217 on NL surface, to investigate how the chemical design may influence their biological performance [15,16]. For this purpose we examined their uptake by cultured human immortalized

brain capillary cells hCMEC/D3 and their permeability across an in vitro BBB model made with the same cells. At the best of our knowledge how NL design affects these features has not yet been studied.

MATERIALS AND METHODS

Materials

All chemical reagents were from Sigma-Aldrich (Milano, Italy). Bovine brain sphingomyelin (Sm), cholesterol (Chol), 1,2-Dimyristoyl-sn-glycero-3-phosphatidic acid (PA), 1,2-distearoyl-sn-glycero-3-phospho-ethanolamine-N-[maleimide(polyethyleneglycol)-2000] (PE-PEG-mal), 1,2-distearoyl-sn-glycerol-3-phosphoethanolamine-N-[biotinyl(polyethyleneglycol)-2000] (PE-PEG-biotin), were purchased from Avanti Polar Lipids Inc. (Alabaster, USA). N-(4,4-difluoro-5,7-dimethyl-4-bora-3a,4a-diaza-s-indacene-3-dodecanoyl)sphingosyl-phosphocholine (BODIPY-Sm) was from Molecular Probes, Invitrogen Srl (Milano, Italy). Aβ1-42 peptide (Aβ), N-acetyl-L-cysteine, streptavidin, Sepharose CL-4B, Triton X-100 were purchased from Sigma-Aldrich (Milano, Italy). [^{3}H]-Sm and [^{14}C]-PA were from Perkin Elmer (Waltham, USA). Amicon Ultra-15 centrifugal 10K filter devices and polycarbonate filters for extrusion procedure were purchased from Millipore Corp (Bedford, USA). Extruder was from Lipex Biomembranes (Vancouver, Canada). Purified rat anti-mouse RI7217 and the biotinylated one were from Biolegend (San Diego, USA). Non specific mouse IgG2a was from Serotec (Oxford, UK). Recombinant mouse TfR was from Sino Biological Inc. (Segrate, Italia). All the media and supplements for cell cultures and phalloidin were supplied by Invitrogen Srl (Milano, Italy).

Preparation of NL

NL were composed of a matrix of Sm/Chol/PA (PA-NL) (47.5:47.5:5 molar ratio) as previously described [10], and mixed or not with PE-PEG-biotin

(for biotin/streptavidin ligation, b/s) or PE-PEG-mal (for covalent coupling). For preparation of fluorescently labeled NL, 0.5 molar % of total Sm was substituted with BODIPY-Sm. For in vitro studies of cellular uptake and permeability, 0.001 molar % of [^{3}H]-Sm (100 μCu/ml) and 0.002 molar % of [^{14}C]-PA (50 μCu/ml), were added as tracers to follow lipid distribution by radioactivity counting. NL were prepared in 10 mM PBS, pH 7.4 by extrusion procedure through a 100-nm pores polycarbonate filters, as previously described [10]. Phospholipid recovery after extrusion was determined by phosphorous assay using the method of Stewart [17].

Functionalization of PA-NL with RI7217 by b/s ligation technique

Biotinylated PA-NL were incubated with 2.5-fold molar excess of streptavidin, with respect to total biotin, for 1h at 25°C and then overnight at 4°C. Free streptavidin was removed by gel filtration (Sepharose 4B-CL column, 25x1 cm) [18]. Streptavidin-labeled NL were then incubated with biotinylated RI7217 at 25°C for 2h and then overnight at 4°C. Unbound antibody was removed again by gel filtration, collected and quantified for the indirect measurement of antibody attachment yield by ELISA technique, as already reported for similar antibodies [18]. These NL will be called b/s-Ab-NL.

Functionalization of PA-NL with RI7217 by covalent coupling

To covalently bind RI7217 to maleimide-containg NL, free thiol groups were generated by reacting the antibody with Traut's reagent in 0.15 M Na-borate buffer with 0.1 mM EDTA, pH 8.5 as described [19]. After incubation for 90 min at 25°C under N_2, RI7217 solution was concentrated and the buffer exchanged with PBS (pH 7.4) using an Amicon filter device. Ellmann's reagent was used to determine the number of sulfhydryl groups on RI7217, using acetyl-cysteine for the calibration curve [20]. Using a RI7217/2-iminothiolane (Traut's reagent) molar ratio of 1:10, an average of 3 primary amines per antibody were thiolated. Thiolated RI7217 was then incubated with NL containing PE-PEG-mal overnight at 25°C. To remove the unbound RI7217, the NL suspension was passed through a Sepharose

4B-CL column (25x1 cm). The amount of RI7217 bound to NL was quantified by Bradford assay [21]. Phospholipids recovery after column was determined as above described [17]. These NL will be called cov-Ab-NL.

Characterization of NL

All NL preparations were characterized in terms of size, ζ-potential, polydispersity index and stability by Dynamic Light Scattering (DLS), as described [10].

Assessment of RI7217 binding to TfR by dot-blot procedure

The binding of chemically modified RI7217 and immuno-NL to TfR was assessed by dot-blot procedure, modified from the previously described protocol [22]. 20 ng of TfR were spotted on PVDF membranes, left to dry and then incubated at 37°C for 30 min in 5% non-fat milk PBS solution. Membranes were incubated for 90 min at 25°C with 60 nM of non specific mouse IgG2a or RI7217 or biotinylated RI7217 or thiolated RI7217 or b/s-Ab-NL or cov-Ab-NL diluted in non-fat milk PBS solution. After washing, the membranes were incubated with HRP-conjugated secondary antibody for 2h at 25°C (anti-mouse 1:20000 dilution in non-fat milk PBS solution), followed by enhanced chemiluminescence (ECL) detection (KODAK image station 2000R).

Assessment of NL binding properties by Surface Plasmon Resonance (SPR)

The binding properties of immuno-NL for TfR and Aβwere assessed by SPR. A SensiQ semi-automatic instrument (ICX Technologies) with two flow channels was employed. A COOH5 sensor chip (ICX Technologies) was installed in the system and TfR was immobilized on one channel using amine-coupling chemistry, while the other one was used as reference surface. The sensor surface was activated by injecting 0.4 M EDC and 0.1 M NHS (1:1, v/v) into the flow channels. TfR was diluted to 10 μg/mL in

acetate buffer (pH 4.0) and injected for 2 min at a flow rate of 10μL/min. The unoccupied sites were blocked with 1 M ethanolamine (pH 8.0). The final immobilization level was ~ 6000 RU. NL were injected at concentrations of exposed RI7217 of 10, 30, 100, 300, 600 nM, at a flow rate of 30 μl/min.

Aβaggregates were prepared as already described [10] and immobilized on a second COOH5 sensor chip by the same procedure described in [23]. The final immobilization level was ~ 5000 RU. NL were injected at a flow rate of 30 μl/min at two concentration of total lipids (100 μM and 300 μM, corresponding to 2.5 μM and 7.5 μM of exposed PA). All the procedures were performed at 25°C. Non-specific binding of NL on the reference channel were automatically subtracted from the total signal. The observed data were fitted to the 1:1 association model and the dissociation constant (K_D) was automatically obtained from the ratio between dissociation and association rate (K_d/K_a). The data analysis was carried out with Qdat Software (ICX Technologies) provided by the manufacturer.

Cellular uptake of NL by confocal microscopy

Immortalized human brain endothelial cells (hCMEC/D3) were provided by Institut National de la Santé et de la Recherche Médicale (INSERM, Paris, France) and cultured as previously described [24]. 65000 cells/cm^2 were cultured for 2 days on rat type I collagen-coated cover slips (diameter 22 mm) positioned in culture dishes and incubated at 37°C with fluorescent NL for 2h, rinsed three times with PBS and fixed with a 10% formalin solution. Cells were permeabilized with 0.2% Triton-X100 in PBS for 15 min then rinsed twice and incubated with a solution of 1% phalloydin (staining actin filaments) in PBS for one hour, then with 20 μM DAPI (nuclear staining) in PBS for 10 min and finally with antibodies against LAMP-1 (late endosomes and early lysosomes staining) (1:200) or EAA1(early endosomes staining) (1:200) for 4h at 25°C, as previously described [24]. LSM710 inverted confocal laser scanning microscope equipped with a Plan-Neofluar 63×/1.4 oil objective (Carl Zeiss, Oberkochen, Germany) was employed to assess the cellular uptake of NL.

Cellular uptake and permeability of NL by radiochemical techniques

hCMEC/D3 cells (passages 25-35) were seeded on 12-well transwell inserts coated with type I collagen in a density of $5x10^4$ cells/cm^2 and cultured with 0.5 mL and 1 mL of culture medium in the upper and in the lower chamber, respectively. Cells were treated with NL when the trans-endothelial-electrical resistance (TEER) value (measured by EVOMX meter, STX2 electrode, World Precision Instruments, Sarasota, Florida) was found to be highest. The functional properties of monolayers were assessed by measuring the endothelial permeability (PE) of [^{14}C]-sucrose and [^{3}H]-propranolol (between 0-120 min) as described [25]. 0.5 mL of radiolabelled NL (from 100 to 400 nmols of total lipids/well) were added to the upper chamber and incubated between 10 and 120 min. After these periods of incubation, the radioactivity in the upper and lower chambers was measured by liquid scintillation counting to calculate the PE of NL across the cell monolayers, taking account of the passage of them through the filter without cells [25]. After 2h, hCMEC/D3 cells were washes with PBS and detached from the transwell inserts with trypsin/EDTA for 15 min at 37°C. Cell-associated radioactivity was measured and the total lipids uptake calculated. Each experiment was performed at least in triplicate. The differences were evaluated for statistical significance using Student's t-test.

Assessment of NL cytotoxicity on hCMEC/D3 cells

hCMEC/D3 cells were grown on 12-well plates until confluence. Medium was replaced and NL (400 nmols of total lipids) suspended in cell culture medium were incubated at 37°C with the cells for 24h. After treatment, the cell viability was assessed by MTT ([3-(4,5-dimetiltiazol-2-yl)-2,5-diphenyltetrazolium bromide]) assay, as described in [26]. Each sample was analyzed at least in triplicate. Moreover, TEER and permeability of [^{14}C]-sucrose were also determined in presence of NL to assess the effect of NL on monolayers integrity.

RESULTS

Preparation and characterization of NL

PA-NL were functionalized with RI7217 by biotin/streptavidin ligation (Figure 1A) or by covalent coupling (Figure 1B); for both techniques the RI7217 binding occurred at the PEG terminus of PE-PEG lipid inserted in NL. Preparation conditions have been optimized to couple 40-45 antibody molecules on the surface of each NL, for both ligation methods used. To achieve this goal, different concentrations of PE-PEG-biotin (for b/s ligation) or PE-PEG-mal (for covalent coupling) were incorporated into NL. As showed in Table 1, optimal conditions were achieved with 0.1% (mol/mol of total lipids) of PE-PEG-biotin and with 1% of PE-PEG-mal, and using a molar ratio of RI7217/lipids from 1:2000 to 1:500. Immuno-NL resulted monodispersed (P.I. ≤ 0.1), negatively charged (~ -35 mV) with a size of 129.3±1.7 nm and 121.3±2.3 nm for b/s-Ab-NL and cov-Ab-NL, respectively. All the preparations were stable in size up to 7 days (data not shown).

Binding of immuno-NL to TfR

The ability of RI7217 to bind its receptor, after modifications and after coupling to NL, was verified by immunoblotting and SPR techniques. Immunoblotting results showed that the thiolated or biotinylated RI7217, as well as RI7217 bound to PA-NL in either way, retain the ability of native antibody to bind TfR (Figure 2A). The binding affinity of immuno-NL towards TfR was investigated by SPR. Representative sensorgrams are shown in Figure 2B and 2C. The dissociation constants (K_D), calculated by fitting the experimental data with a single binding site isotherm by Qdat Software analysis, were 2.5 nM for cov-Ab-NL and 11 nM for b/s-Ab-NL, calculated with respect to RI7217 exposed on NL surface.

Binding of NL to Aβ aggregates

The evaluation of binding affinity of NL towards Aβwas carried out by using SPR. The dissociation constants (K_D) were obtained by fitting the experimental data with a single binding site isotherm by Qdat Software analysis and were 48.5 nM for PA-NL, 37.0 nM for cov-Ab-NL and 43.3 nM for b/s-Ab-NL, calculated with respect to PA exposed on NL surface (Figure 3).

Cellular uptake of NL investigated by confocal microscopy

Confocal microscopy images illustrate that the uptake of PA-NL was higher after functionalization with RI7217 (Figure 4). In particular, the uptake was higher for cov-Ab-NL compared to b/s-Ab-NL. Experiments devoted to evaluate the intracellular localization of NL showed that there was no co-localization with early endosomes or late endosomes and early lysosomes, for both NL tested (Figure 5). NL did not induce changes in actin organization of hCMEC/D3 cells.

Cellular uptake and permeability of immuno-NL investigated by radiochemical techniques

hCMEC/D3 cells, grown on transwell membrane inserts, were incubated with NL on day 12, when the maximal TEER value was registered (123±6 $\Omega \cdot cm^2$). Transport of [^{14}C]-sucrose and [^{3}H]-propranolol was measured, with PE values of 1.48×10^{-3} cm/min and 3.51×10^{-3} cm/min, respectively, in agreement with the values reported in literature [27]. Different amounts of NL were added in the upper compartment and the radioactivity uptaken from the cells after 2h of incubation was measured. As shown in Figure 6A, the amount of radioactivity uptaken increased by increasing the administered dose. The highest cellular uptake was detected with cov-Ab-NL (Figure 6A). The PE across the cell monolayers was higher for cov-Ab-NL ($7.24 \pm 0.39 \times 10^{-6}$ cm/min), compared to b/s-Ab-NL ($4.97 \pm 0.51 \times 10^{-6}$ cm/min) (Figure 6B).

For both types of NL, the ratio of the two radio-tracers uptaken from the cells and recovered from the bottom compartment of the transwell system was maintained constant with respect to the initial ratio.

Assessment of NL cytotoxicity on hCMEC/D3 cells

Cell viability after incubation with NL was assessed by MTT assay. All the NL preparations tested were non-toxic, since the cell viability did not decrease below 96% (data not shown). Moreover, the TEER value and the permeability of [^{14}C]-sucrose (119±8 $\Omega \cdot cm^2$ and 1.62×10^{-3} cm/min, respectively) did not change, within the experimental error (< 3%) after hCMEC/D3 incubation with NL.

DISCUSSION

Among all the different nanoparticles available, NL have many advantages for drug delivery, due to their non-toxic and non-immunogenic, fully biodegradable and structurally versatile nature [28]. In this study, we functionalized PA-NL, that already demonstrated high affinity for Aβ[10], with the antibody RI7217 against TfR, as candidate ligand for enhancing BBB crossing. We utilized the human brain endothelial cell line hCMEC/D3, expressing TfR [27], cultured on a transwell system, as in vitro model of BBB.

Among the possible ligands for TfR [19,29,30], anti-TfR RI7217 monoclonal antibody was employed for NL decoration, for different reasons. First, the use of transferrin for decoration was discarded, because it would compete with the endogenous ligand in-vivo [31]. Secondly, RI7217, in spite of being an anti-mouse antibody and probably due to the 86% homology between mouse and human TfR [32], has been reported to associate in vitro with human TfR. Moreover, it was shown to significantly enhance the brain uptake of liposomes in-vivo [33].

We decorated PA-NL with RI7217 using two techniques, biotin/streptavidin ligation and thiol-maleimide covalent coupling and then we examined NL performances in terms of ability to bind Aβor TfR, to be uptaken by and to cross a monolayer of hCMEC/D3 cells, taken as BBB model. Preparation conditions have been optimized to obtain a given number of RI7217 molecules exposed on NL surface (40-45 antibodies/NL), with both techniques. This density was previously suggested to be optimal for brain targeting using liposomes functionalized with another anti-TfR antibody [33]. Since the chemical modifications on RI7217 occur randomly on primary amino groups, also the antigen-binding regions could be affected, thus causing the antibody to lose activity [34,35]. We checked by immunoblotting that the modifications on RI7217 (either biotinylation or thiolation) did not alter its binding properties toward the receptor.

We also disclosed, either by immunoblotting or by SPR techniques, that both cov-Ab-NL and b/s-Ab-NL efficiently bind TfR, proving the efficacy of both coupling methods. In particular, SPR registered higher affinity values for cov-Ab-NL, in comparison to b/s-Ab-NL.

Successively, SPR indicated that RI7217 functionalization, for both types of NL, did not modify the binding properties of PA, that maintains the affinity towards Aβpeptide in the nanomolar range, in close agreement with data previously reported [10].

We demonstrated that the presence of RI7217 on the surface enhanced cellular uptake and permeability of PA-NL on hCMEC/D3 BBB model, with no alterations in cells viability and monolayer integrity.Comparing the two coupling procedures utilized, either cellular uptake or permeability of cov-Ab-NL were higher than those of b/s-Ab-NL. Moreover, the results proved that double radio-labeled immuno-NL are likely transported intact across the hCMEC/D3 monolayer, as the ratio between the two radiotracers does not change in the upper and lower compartments of the transwell system. Confocal microscopy experiments illustrated that immuno-NL are not

transported via the endosome-lysosome pathway, suggesting transcytosis as possible transport mechanism across the hCMEC/D3 monolayer [36]. No cytotoxicity towards hCMEC/D3 cells of all NL tested was found, indicating their potential biocompatible features.

Taken all together, our results demonstrate that the chemical design affects the biological properties of immuno-NL. In particular, PA-NL functionalized with the RI7217 by covalent coupling are the best performing in terms of cellular uptake and permeability across our BBB model. These effects could depend on the higher affinity for TfR of cov-Ab-NL with respect to b/s-Ab-NL, but also on other factors such as the biotin/streptavidin bond, weaker than the covalent, or the steric hindrance of the protein streptavidin affecting the interaction. If one takes also into account the potential immunogenicity of streptavidin in-vivo [37], our results, obtained in vitr o, suggest that the covalent bond could be more adequate for the design of nanosystems for AD treatment in-vivo. Of course this hypothesis should be confirmed.

CONCLUSIONS

The present in vitro study shows that immuno-NL containing PA and RI7217 could be interesting nanosystems for further studies in-vivo for AD therapy and diagnosis. Moreover, our results provide evidences that the covalent coupling strategy could be preferably used rather than biotin/streptavidin method, at least under the experimental conditions adopted, for the construction and design of immuno-NL.

Acknowledgements
The research leading to these results has received funding from the European Community's Seventh Framework Program (FP7/2007-2013) under grant agreement n° 212043 (NAD). We thank Pierre-Olivier Couraud for providing the hCMEC/D3 cells.

References

1. H. Hampel, D. Prvulovic, S. Teipel, F. Jessen, C. Luckhaus, L. Frölich, M. W. Riepe, R. Dodel, T. Leyhe, L. Bertram, W. Hoffmann, F. Faltraco, The future of Alzheimer's disease: the next 10 years, Prog. Neurobiol. 95, 718-728 **(2011)**.

2. A. Serrano-Pozo, M. P. Frosch, E. Masliah, B. T. Hyman, Neuropathological Alterations in Alzheimer Disease, Cold Spring Harb. Perspect. Med. 1, a006189 **(2011)**.

3. A. M. Palmer, The role of the blood brain barrier in neurodegenerative disorders and their treatment, J. Alzheimers Dis. 24, 643-656 **(2011)**.

4. M. M. Patel, B. R. Goyal, S. V. Bhadada, J. S. Bhatt, A. F. Amin, Getting into the brain: approaches to enhance brain drug delivery, CNS Drugs 23, 35-58 **(2009)**.

5. E. F. Craparo, M. L. Bondì, G. Pitarresi, G. Cavallaro, Nanoparticulate systems for drug delivery and targeting to the central nervous system, CNS Neurosci. Ther. 17, 670-677 **(2011)**.

6. L. Costantino, Drug delivery to the CNS and polymeric nanoparticulate carriers, Future Med. Chem. 2, 1681-1701 (2010).

7. D. Brambilla, B. Le Droumaguet, J. Nicolas, S. H. Hashemi, L. P. Wu, S. M. Moghimi, P. Couvreur, K. Andrieux, Nanotechnologies for Alzheimer's disease: diagnosis, therapy, and safety issues, Nanomedicine 7, 521-40 **(2011).**

8. F. Re, M. Gregori, M. Masserini, Nanotechnology for neurodegenerative disorders, Maturitas 73, 45-51 **(2012)**.

9. F. Re, M. Moresco, M. Masserini, Nanoparticles for neuroimaging, J. Phys. D: Appl. Phys. 45, 3001-3012 **(2012)**.

10.M. Gobbi, F. Re, M. Canovi, M. Beeg, M. Gregori, S. Sesana, S. Sonnino, D. Brogioli, C. Musicanti, P. Gasco, M. Salmona, M. E. Masserini, Lipid-based nanoparticles with high binding affinity for amyloid-β1-42 peptide, Biomaterials 31, 6519-6529 **(2010)**.

11.E. Bereczki, F. Re, M. E. Masserini, B. , Winblad, J. J. Pei, Liposomes functionalized with acidic lipids rescue Aù-induced toxicity in murine neuroblastoma cells, Nanomed-Nanotechnol. 7, 560-571 **(2011)**.

12.Z. M. Qian, H. Y. Li, H. Z. Sun, K. Ho, Targeted drug delivery via the transferrin receptor-mediated endocytosis pathway, Pharmacol. Rev 54, 561-587 **(2002)**.

13.T. Moos, N. T. Rosengren, T. Skjørringe, E. H. Morgan, Iron trafficking inside the brain, J. Neurochem.103, 1730-1740 **(2007)**.

14.A. S. Manjappa, K. R. Chaudhari, M. P. Venkataraju, P. Dantuluri, B. Nanda, C. Sidda, K. K. Sawant, R. S. Ramachandra Murthy, Antibody derivatization and conjugation strategies: Application in preparation of stealth immunoliposome to target chemotherapeutics to tumor, J. Control. Rel. 150, 2-22 **(2011)**.

15.Y. Liu, D. Cheng, X. Liu, G. Liu, S. Dou, N. Xiao, L. Chen, M. Rusckowski, D. J. Hnatowich, Comparing the intracellular fate of components within a noncovalent streptavidin nanoparticle with covalent conjugation, Nucl. Med. Biol. 39, 101-107 **(2012)**.

16.C. B. Hansen, G. Y. Kao, E. H. Moase, S. Zalipsky, T. M. Allen, Attachment of antibodies to sterically stabilized liposomes: evaluation, comparison and optimization of coupling procedures, Biochim. Biophys. Acta. 1239, 133-144 **(1995)**.

17.J. C. M Stewart, Colorimetric determination of phospholipids with ammonium ferrothiocyanate, Anal. Biochem. 104, 10-14 **(1980)**.

18.E. Markoutsa, G. Pampalakis, A. Niarakis, I. A. Romero, B. Weksler, P. O. Couraud, S. G. Antimisiaris, Uptake and permeability studies of BBB-targeting immunoNL using the hCMEC/D3 cell line, Eur. J. Pharm. Biopharm. 77, 265-274 **(2011)**.

19.J. Huwyler, D. Wu, W. M. Pardridge, Brain drug delivery of small molecules using immunoliposomes, Proc. Natl Acad. Sci. USA 93, 14164-14169 **(1996)**.

20.G. L. Ellman, Tissue sulfhydryl groups, Arch. Biochem. Biophys. 82, 70-77 **(1959)**.

21.M. M. Bradford, A rapid and sensitive method for the quantitation of microgram quantities of protein utilizing the principle of protein-dye binding, Anal. Biochem. 72, 248-254 **(1976)**.

22.F. Re, S. Sesana, A. Barbiroli, F. Bonomi, E. Cazzaniga, E. Lonati, A. Bulbarelli, M. Masserini, Prion protein structure is affected by pH-dependent interaction with membranes: a study in a model system, FEBS Lett. 582, 215-220 **(2008)**.

23.E. Salvati, M. Masserini, S. Sesana, S. Sonnino, F. Re, M. Gregori, Liposomes Functionalized with GT1b Ganglioside with High Affinity for Amyloid beta-peptide, Journal of Alzheimer Disease 29, 33-36 **(2012)**.

24.F. Re, I. Cambianica, S. Sesana, E. Salvati, A. Cagnotto, M. Salmona, P. O. Couraud, S. M. Moghimi, M. Masserini, G. Sancini, Functionalization with ApoE-derived peptides enhances the interaction with brain capillary endothelial cells of nanoliposomes binding amyloid-beta peptide, J. Biotechnol. 156, 341-346 **(2010)**.

25.R. Cecchelli, B. Dehouck, L. Descamps, L. Fenart, V. Buée-Scherrer, C. Duhem, S. Lundquist, M. Rentfel, G. Torpier, M. P. Dehouck, In vitro model for evaluating drug transport across the blood–brain barrier, Adv. Drug Deliver Rev. 36, 165-178 **(1999)**.

26.F. Re, I. Cambianica , C. Zona, S. Sesana, M. Gregori, R. Rigolio, B. La Ferla, F. Nicotra, G. Forloni, A. Cagnotto, M. Salmona, M.Masserini, G. Sancini, Functionalization of liposomes with ApoE-derived peptides at different density affects cellular uptake and drug transport across a blood-brain barrier model. Nanomedicine 7, 551-559 **(2011)**.

27.B. Poller, H. Gutmann, S. Krähenbühl, B. Weksler, I. Romero, P. O. Couraud, G. Tuffin, J. Drewe, J. Huwyler, The human brain endothelial cell line hCMEC/D3 as a human blood-brain barrier model for drug transport studies, J. Neurochem. 107, 1358-1368 **(2008)**.

28.V. P. Torchilin, Recent advances with liposomes as pharmaceutical carriers, Nat. Rev. 4, 145-160 **(2005)**.

29.U. Bickel, T. Yoshikawa, W. M. Pardridge, Delivery of peptides and proteins through the blood-brain barrier, Adv. Drug Deliver Rev. 46, 247-279 **(2001)**.

30.K. Kissel, S. Hamm, M. Schulz, A. Vecchi, C. Garlanda, B. Engelhardt, Immunohistochemical localization of the murine transferrin receptor (TfR) on blood-tissue barriers using a novel anti-TfR monoclonal antibody, Histochem. Cell. Biol. 110, 63-72 **(1998)**.

31.H. J. Lee, B. Engelhardt, J. Lesley, U. Bickel, W. M. Pardridge, Targeting rat antimouse transferrin receptor monoclonal antibodies through blood-brain barrier in mouse, J. Pharmacol. Exp. Ther. 292, 1048-1052 **(2000)**.

32.E. Wang, N. Obeng-Adjei, Q. Ying, L. Meertens, T. Dragic, R. A Davey, S. R. Ross, Mouse mammary tumor virus uses mouse but not human transferrin receptor 1 to reach a low pH compartment and infect cells, Virology 381, 230-240 **(2008)**.

33.I. van Rooy, E. Mastrobattista, G. Storm, W. E. Hennink, R. M. Schiffelers, Comparison of five different targeting ligands to enhance accumulation of liposomes into the brain, J. Control. Release 150, 30-36 **(2011)**.

34.A. Béduneau, P. Saulnier, F. Hindré, A. Clavreul, J. C. Leroux, J. P. Benoit, Design of targeted lipid nanocapsules by conjugation of whole antibodies and antibody Fab' fragments, Biomaterials 28, 4978-90 **(2007)**.

35.T. Ji, M. C. Muenker, R. V. L. Papineni, J. W. Harder, D. L. Vizard, W. E. McLaughlin, Increased Sensitivity in Antigen Detection with Fluorescent Latex Nanosphere-IgG Antibody Conjugates, Bioconjugate Chem. 21, 427-435 **(2010)**.

36.J. Wang, S. Tian, R. A. Petros, M. E. Napier, J. M. DeSimone, The Complex Role of Multivalency in Nanoparticles Targeting the Transferrin

Receptor for Cancer Therapies, J. Am. Chem. Soc. 132, 11306-11313 **(2010)**.

37.G. Paganelli, M. Chinol, M. Maggiolo, A. Sidoli, A. Corti, S. Baroni, A. G. Siccardi, The three-step pretargeting approach reduces the human anti-mouse antibody response in patients submitted to radioimmunoscintigraphy and radioimmunotherapy, Eur. J. Nucl. Med. 24, 350-351 **(1997)**.

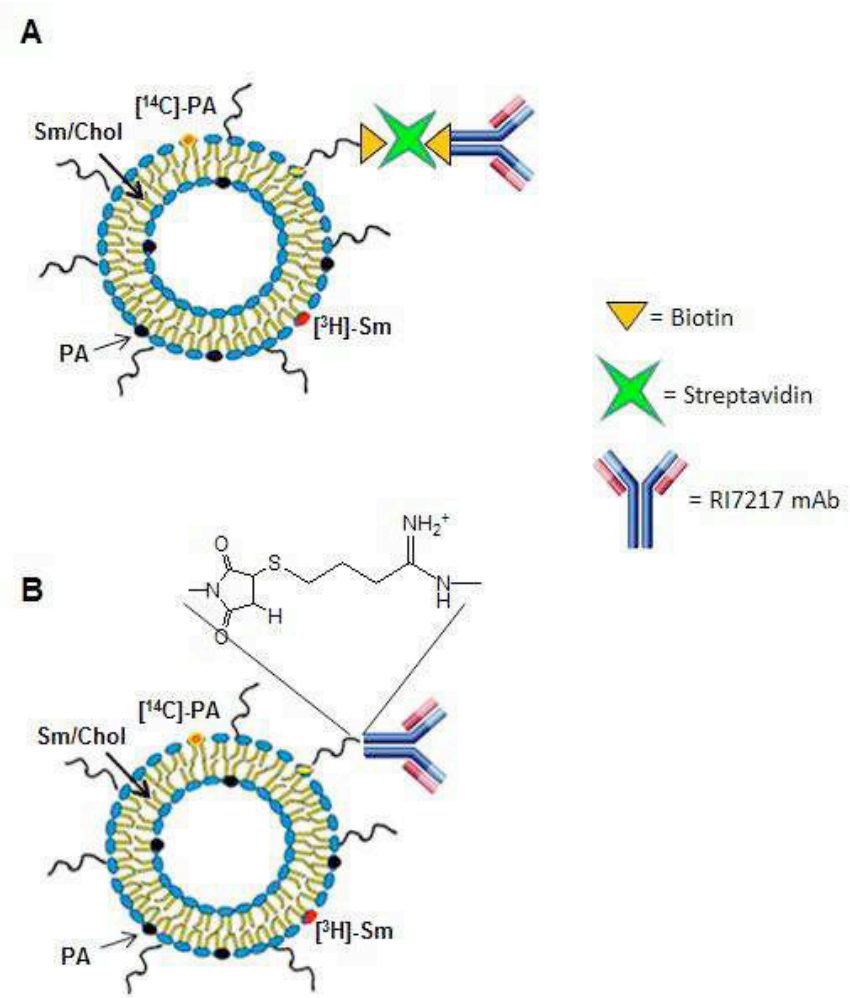

Figure 1.

Theoretical structure of immuno-NL. RI7217 antibody was linked to NL by (A) biotin/streptavidin ligation technique or (B) covalent coupling via thiol-maleimide reaction.

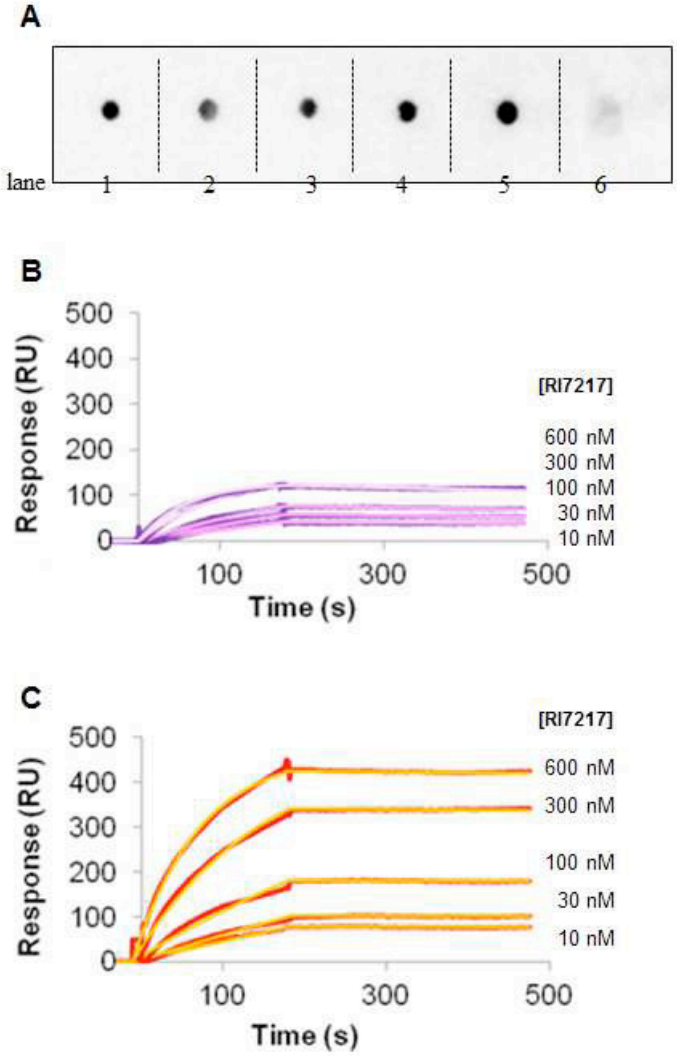

Figure 2.

Binding of NL to TfR. A) Dot-blots of 20 ng of TfR spotted in a PVDF membrane, incubated with cov-Ab-NL (lane 1), or b/s-Ab-NL (lane 2), or biotinylated RI7217 (lane 3), or thiolated RI7217 (lane 4), or native RI7217 (lane 5) or control IgG (lane 6). Spots were detected with HRP-conjugated IgG anti-mouse, followed by ECL detection (A). SPR sensorgrams resulting from the binding of B) b/s-Ab-NL or C) cov-Ab-NL on TfR covalently immobilized on the gold sensor surface. NL were injected at concentrations of exposed RI7217 of 10 to 600 nM.

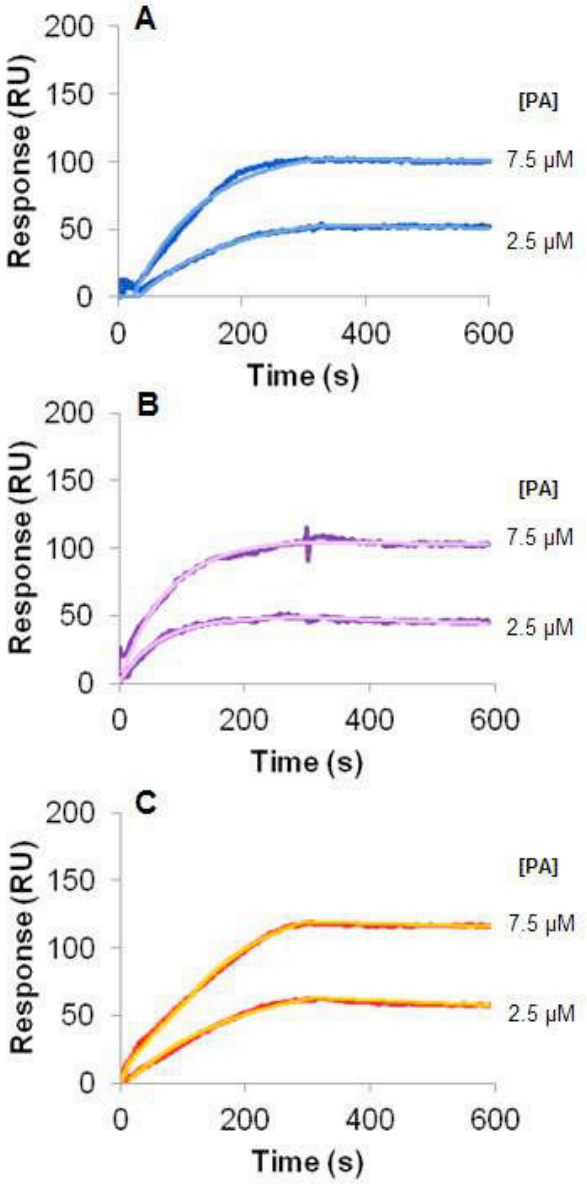

Figure 3.

Binding of NL to Aβfibrils. SPR sensorgrams resulting from the binding of (A) PA-NL or (B) b/s-Ab-NL or (C) cov-Ab-NL on Aβfibrils covalently immobilized on the gold sensor surface. NL were injected at two concentration of total lipids of 100 µM and 300 µM, corresponding to 2.5 µM and 7.5 µM of exposed PA.

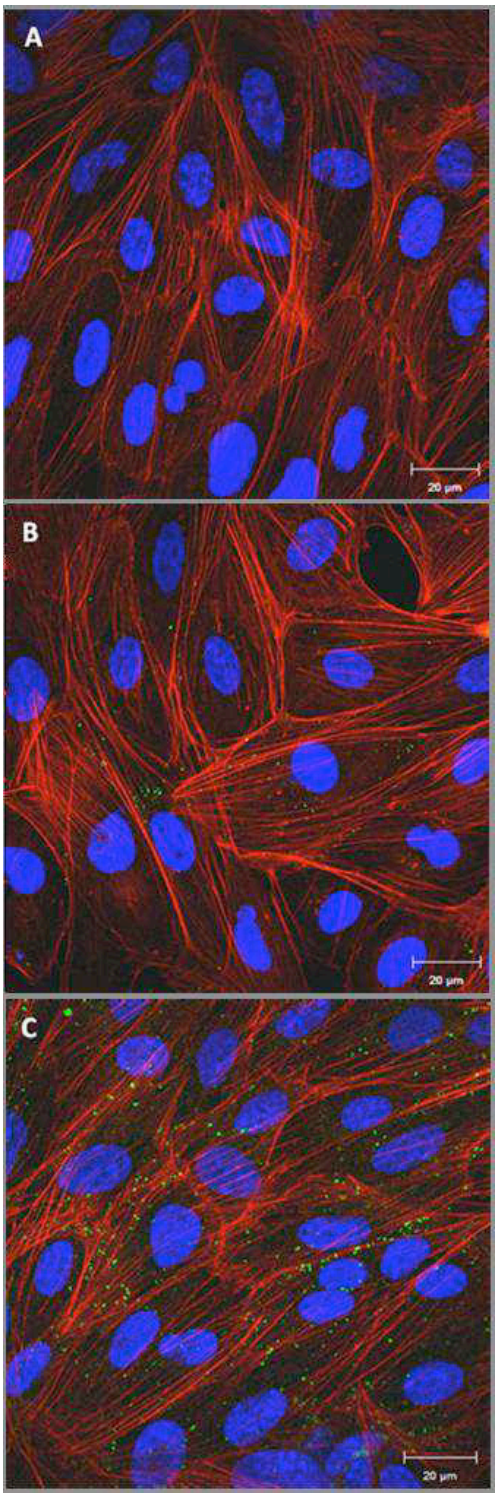

Figure 4.
CLSM of hCMEC/D3 cells after incubation with NL. hCMEC/D3 cells were incubated with fluorescent labeled NL (200 nmols of total lipids) for 2h at 37°C, 5%CO2 saturation. hCMEC/D3 cells after incubation with A) PA-NL; B) NL b/s-Ab-NL; C) cov-Ab-NL. Cells were incubated with phalloydin in order to visualize the actin filaments (magenta fluorescence); nuclear staining was performed by DAPI (blue staining) and BODIPY-Sm to mark NL (green staining). Scale bar=20 µm.

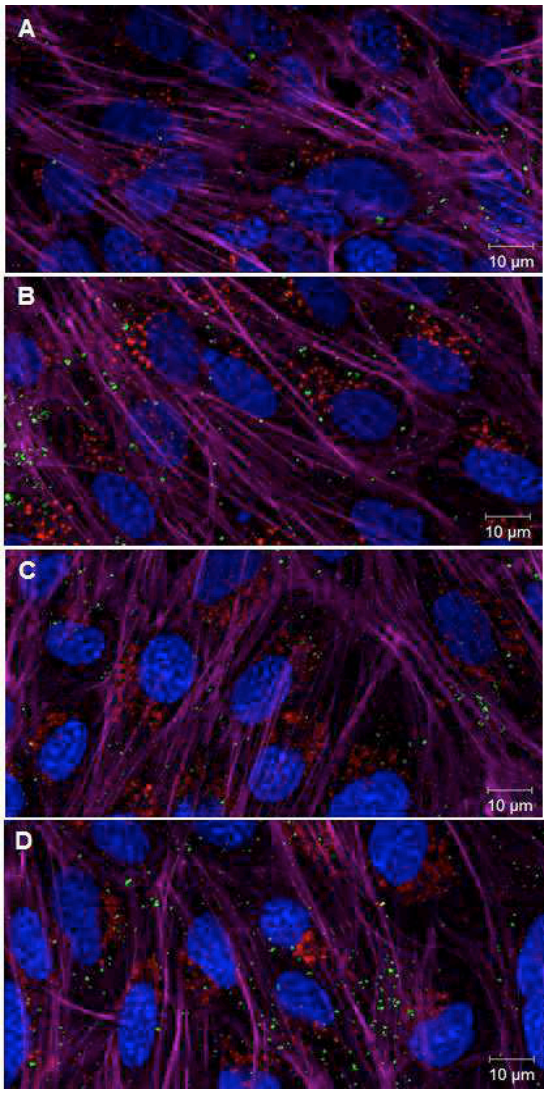

Figure 5. CLSM of hCMEC/D3 cells after incubation with immuno-NL. hCMEC/D3 cells were incubated with fluorescent labeled cov-Ab-NL (200 nmols of total lipids) at 37°C, 5%CO_2 saturation. hCMEC/D3 cells after (A) 2h or (B) O.N. incubation with NL and EAA1; hCMEC/D3 cells after (C) 2h or (D) O.N. incubation with NL and LAMP1. Cells were incubated with phalloydin in order to visualize the actin filaments (magenta fluorescence); nuclear staining was performed by DAPI (blue staining); early endosomes staining was performed by EAA1 (red fluorescence, panels A and B); late endosomes/early lisosomes staining was performed by LAMP1 (red fluorescence, panels C and D) and BODIPY-Sm to mark NL (green staining). Scale bar=10 µm.

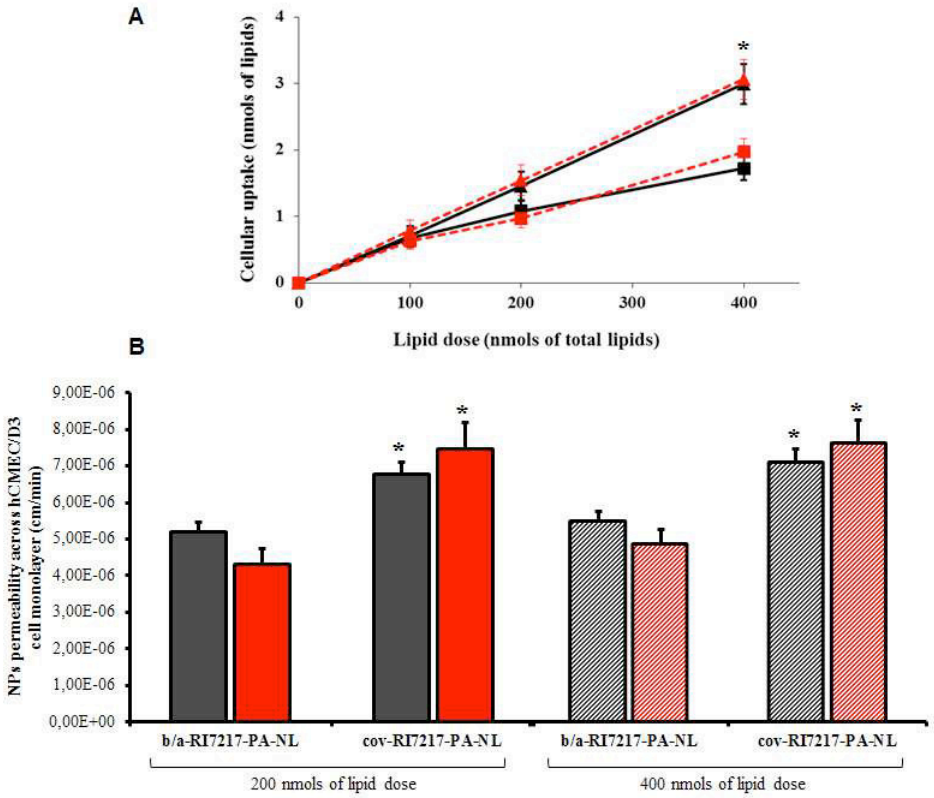

Figure 6. Cellular uptake and permeability of NL by hCMEC/D3 cell monolayers. 10^6 cells were incubated with dual-radiolabeled immuno-NL for 2h at 37°C, 5%CO_2. (A) Cellular uptake of immuno-NL. After incubation, the amount of radioactivity incorporated into the cells was measured and the nmols of total lipids uptaken from the cells calculated for b/s-Ab-NL (squares) or cov-Ab-NL (triangles), for both radiotracers used ([^{3}H]-Sm, black; [^{14}C]-PA, red). (B) Transcytosis of immuno-NL through hCMEC/D3 cell monolayers. Dual-radiolabeled NL were added to the upper chamber of the transwell monolayers and incubated until 120 min at 37°C, 5%CO_2. The permeability of NL across the cell monolayer was calculated for both radiotracers used, [^{3}H]-Sm (dark bars) and [^{14}C]-PA (red bars). Each value is the mean of at least three independent experiments and the SDs of means are presented as bars. *=p<0,05.

Table 1.

Effect of linker lipid content on RI7217 coupling. NL were incubated with various amounts of linker lipids at a constant phospholipids concentration (4mM) and a molar ratio RI7217/phospholipids of 1:1000.

Mol% of linker lipid		Approx. No. Ab per NL[a]
PE-PEG-Biotin	0.05	20±2
	0.1	43±5
PE-PEG-mal	0.1	7±1
	0.2	16±2
	0.5	35±5
	1	46±3

[a]The number of Ab conjugated per NL was based on the assumption that a 100-nm liposome contains ~100000 molecules of phospholipids [16].

CHAPTER 5

Versatile and Efficient Targeting Using a Single Nanoparticulate Platform: Application to Cancer and Alzheimer's Disease

ACS Nano, 2012, 6 (7), 5866–5879

Benjamin Le Droumaguet, Julien Nicolas, Davide Brambilla, Simona Mura, Andrei Maksimenko, Line De Kimpe, Elisa Salvati, Cristiano Zona, Cristina Airoldi, Mara Canovi, Marco Gobbi, Noiray Magali, Barbara La Ferla, Francesco Nicotra, Wiep Scheper, Orfeu Flores, Massimo Masserini, Karine Andrieux, and Patrick Couvreur

ABSTRACT

A versatile and efficient functionalization strategy for polymeric nanoparticles (NPs) has been reported and successfully applied to PEGylated, biodegradable poly(alkyl cyanoacrylate) (PACA) nanocarriers. The relevance of this platform was demonstrated in both the fields of cancer and Alzheimer's disease (AD). Prepared by copper-catalyzed azide-alkyne cycloaddition (CuAAC) and subsequent self-assembly in aqueous solution of amphiphilic copolymers, the resulting functionalized polymeric NPs exhibited requisite characteristics for drug delivery purposes: (i) a biodegradable core made of poly(alkyl cyanoacrylate), (ii) a hydrophilic poly(ethylene glycol) (PEG) outer shell leading to colloidal stabilization, (iii) fluorescent properties provided by the covalent linkage of a rhodamine B-based dye to the polymer backbone, and (iv) surface functionalization with biologically active ligands that enabled specific targeting. The construction method is very versatile and was illustrated by the coupling of a small library of ligands (e.g., biotin, curcumin derivatives, and antibody), resulting in high affinity toward (i)murine lung carcinoma (M109) and human breast cancer (MCF7) cell lines, even in a coculture environment with healthy cells and (ii) the β-amyloid peptide 1-42 (Aβ1-42), believed to be the most representative and toxic species in AD, both under its monomeric and fibrillar forms. In the case of AD, the ligand-functionalized NPs exhibited higher affinity toward Aβ1-42 species comparatively to other kinds of colloidal systems and led to significant aggregation inhibition and toxicity rescue of Aβ1-42 at low molar ratios.

INTRODUCTION

In the past decade, significant achievements have been witnessed in the field of nanotechnology, especially in material science, electronics, photonics, supramolecular assemblies and drug delivery. In particular, the medical

application of nanotechnologies, usually termed nanomedicine,1-7 has given a crucial impulse to the development of various types of drug-loaded nanocarriers. A great deal of effort is now focused on the engineering of nanoparticulate systems able to serve as efficient diagnostic and/or therapeutic tools against severe diseases, such as cancer or infectious or neurodegenerative disorders. 1,8-19 Among the different classes of materials suitable for drug delivery purposes, nanoparticles (NPs) based on biodegradable polymers have attracted much attention 1,8 due to the flexibility offered by macromolecular synthesis methods, the almost infinite diversity of polymer compositions and their ease of functionalization. However, polymeric nanocarriers designed for drug delivery purposes need to fulfill various criteria that are rarely met in a single colloidal system. Thus, the conception of flexible nanomedicine platforms represents an urgent need in the field. Ideally, they should (i) be biocompatible/biodegradable to allow safe administration; (ii) exhibit stealth properties to escape the immune response; (iii) be functionalized with fluorescent or radioactive probes for traceability/localization purposes and, above all, (iv) display at their periphery suitable ligands in order to achieve the "active targeting" to specific cells or tissues. In addition, the versatility of the envisaged nanoconstructs toward different pathologies, simply by changing the nature of the exposed ligand, may be a highly desirable advantage to engineer a universal nanocarrier. In this context, biodegradable poly(alkyl cyanoacrylate) (PACA) nanoparticles hold great promise as they have demonstrated significant preclinical results in multiple pathologies such as cancer20 and severe infections (viral, bacteriologic, and parasitic) 21 as well as in several metabolic and autoimmune diseases.22 Currently in phase III clinical trials, doxorubicin-loaded PACA NPs (i.e., Transdrug) have shown improved survival and safety, comparatively to the standard treatment in patients with multidrug resistance (MDR) hepatocarcinoma.23 Their additional coating with poly(ethylene glycol) (PEG) via the use of poly[hexadecyl cyanoacrylateco-methoxypoly(ethylene glycol) cyanoacrylate] (P(HDCA-co-MePEGCA)) amphiphilic random copolymer that can self-assemble into well-defined NPs,24 not only turns them into

long-circulating nanocarriers, but also enables them to cross the blood-brain barrier (BBB).25,26 The latter feature makes them potential drug transporters to the central nervous system (CNS) for the therapy of CNS-related diseases. However, despite these numerous benefits, the functionalization of PACA NPs in order to achieve cell/tissue targeting has been challenging because of the high reactivity of cyanoacrylate monomers and the marked tendency of the resulting polymers to hydrolyse and biodegrade.27 Herein is reported the design of a versatile and multifunctional targeted PACA nanoparticulate platform and its successful in vitro application in two diseases, namely cancer and Alzheimer's disease (AD), the most common elderly dementia, affecting 35 million people worldwide. While cancer therapy is still an active challenge due to the difficulty of targeting cancer cells, the mechanism involved for AD is still under debate, which hampers any clear and effective therapeutic response. With this in mind, we designed a common colloidal system for which the flexibility of the synthetic strategy allowed ready adaptation of the targeting to the desired pathology simply by choosing the appropriate ligand. In this system, all the required features for drug delivery purposes and cell targeting are gathered: (i) a biodegradable poly(alkyl cyanoacrylate) core,28 (ii) a PEG outer shell leading to stealth/stabilization features, (iii) fluorescent properties provided by the covalent linkage of a rhodamine B-based dye to the polymer backbone, and (iv) biologically active ligands displayed at their surface for active targeting (Figure 1). To accomplish specific disease targeting, we developed two original routes. For cancer, whereas folic acid has been extensively employed as cancer cell homing device,29-31 we used here biotin as a ligand32 to selectively target different cancer cell lines (i.e., human breast carcinoma MCF7 and murine lung cancer M109) via a biotin receptor-mediated uptake, which has scarcely been studied and may open new therapeutic avenues toward cancer therapy. Regarding AD, we functionalized the NPs with either curcumin derivatives, known for their potential role in the prevention and treatment of AD,29-31 or with a novel specific antibody, via the biotin/streptavidin binding strategy, in order to bind not only the β-amyloid peptide 1-42 (Aβ1-42) monomer, a biomarker of AD, but also Aβ1-42 fibrillar aggregates, usually located in AD

brains. Beyond the report of a new methodology for multifunctional NPs construction, this also represents the first example of targeted polymeric NPs for therapeutic application in AD.

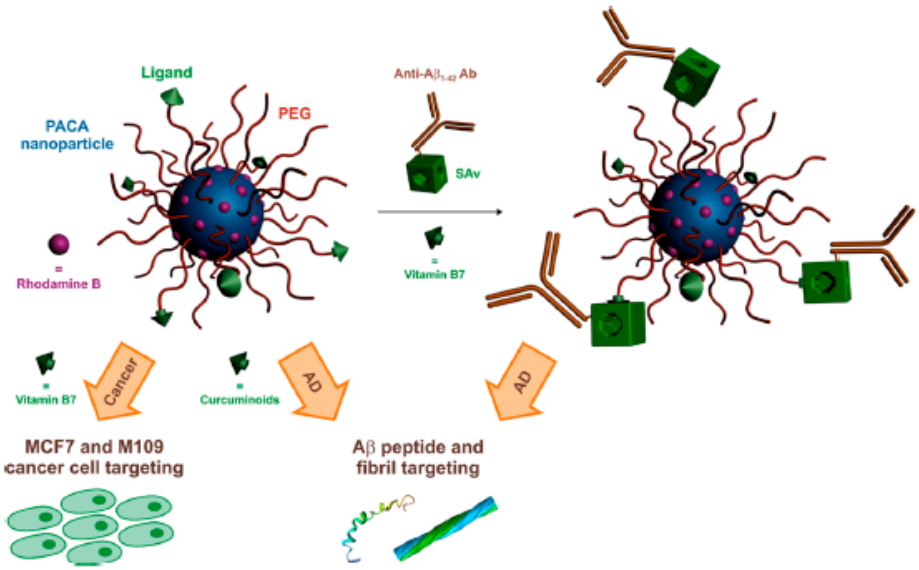

Figure 1. Design of functionalized, PEGylated and biodegradable poly(alkyl cyanoacrylate) (PACA) nanoparticles for specific targeting in the fields of cancer and Alzheimer's disease (AD).

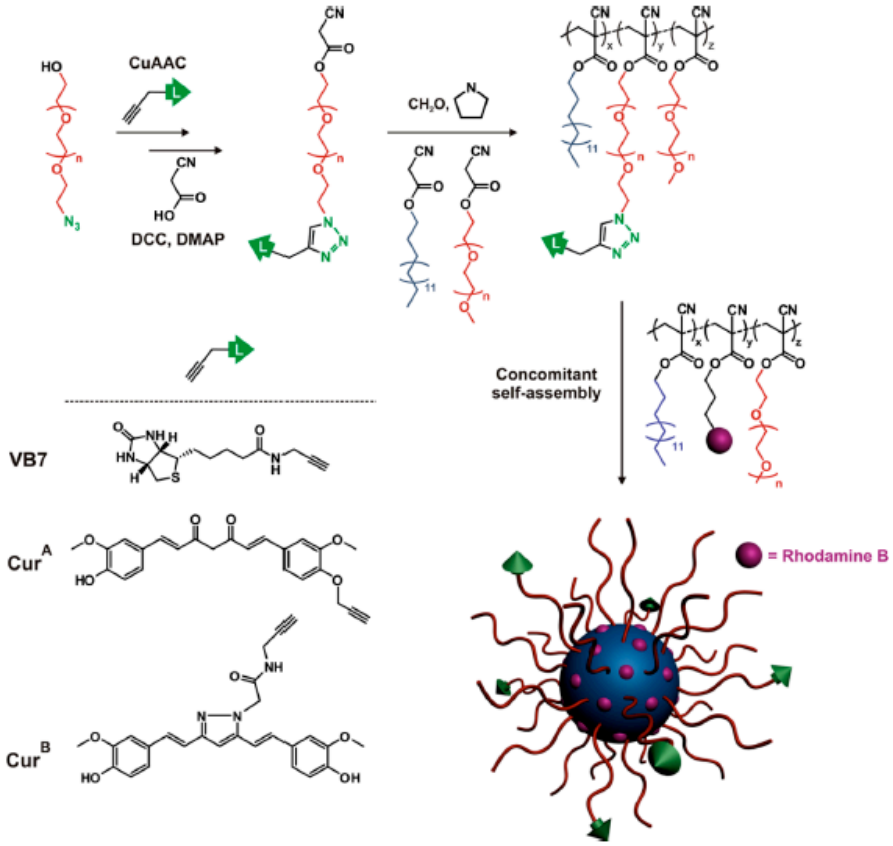

Figure 2. Synthetic pathway to prepare fluorescent, PEGylated and biodegradable poly(alkyl cyanoacrylate) nanoparticles functionalized with biotin (VB7) or curcumin derivatives (CurA and CurB).

TABLE 1. Compositions and Colloidal Properties of Functionalized and Nonfunctionalized PEGylated Poly(alkyl cyanoacrylate) Nanoparticles

expt.	nanoparticle composition[a]	average diameter (nm)[b]	partide size distribution[b]	ζ-potential (mV)
N0	P(HDCA-*co*-MePEGCA) + P(HDCA-*co*-RCA-*co*-MePEGCA)	106 ± 3.0	0.160	−40.2 ± 10.9
N1	P(HDCA-*co*-**VB7**PEGCA-*co*-MePEGCA) + P(HDCA-*co*-RCA-*co*-MePEGCA)	101 ± 1.8	0.116	−7.9 ± 3.6
N2	P(HDCA-*co*-**Cur^A**PEGCA-*co*-MePEGCA) + P(HDCA-*co*-RCA-*co*-MePEGCA)	85 ± 1.6	0.241	−16.2 ± 3.6
N3	P(HDCA-*co*-**Cur^B**PEGCA-*co*-MePEGCA) + P(HDCA-*co*-RCA-*co*-MePEGCA)	103 ± 2.8	0.177	−11.7 ± 3.7

[a] Copolymer blends were 50/50 and concentrations of the nanoparticle suspensions were 2.5 mg · mL^{-1} after self-assembly by the nanoprecipitation technique. [b] Determined by dynamic light scattering.

TABLE 1. Compositions and Colloidal Properties of Functionalized and Nonfunctionalized PEGylated Poly(alkyl cyanoacrylate) Nanoparticles

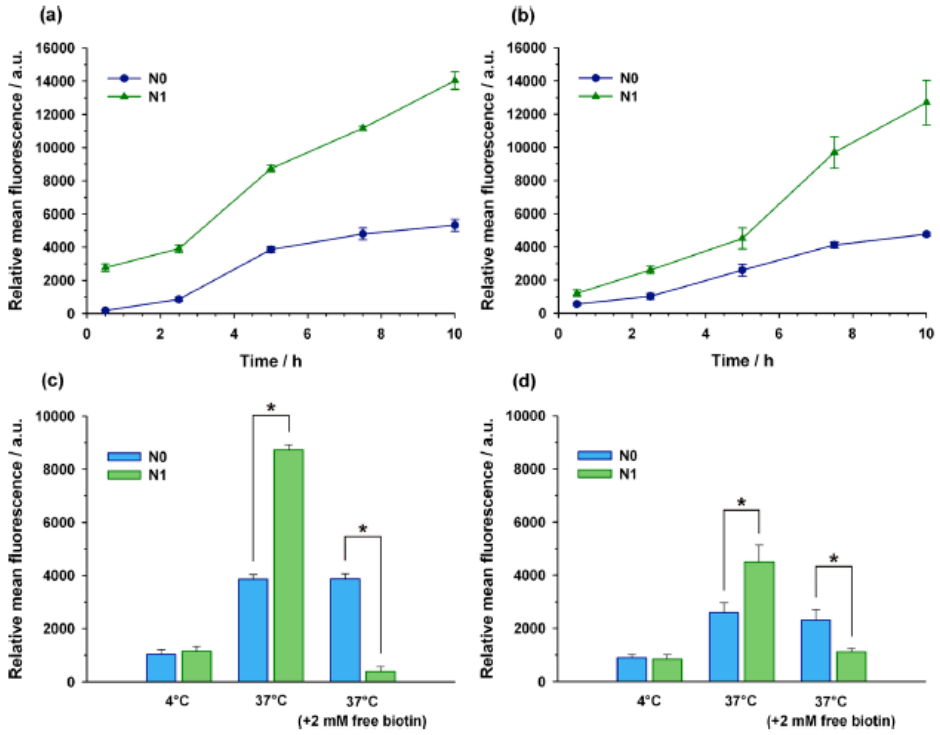

Figure 3. Kinetics of cellular uptake of nonfunctionalized (N0) and biotin-functionalized (N1) NPs in MCF7 (a) and M109 (b) cancer cells exposed to 100 µg 3 mL-1 of NPs. Internal rhodamine B fluorescence in cells after 5 h of MCF7 (c) or M109 (d) exposure to 100 µg 3mL-1 of NPs at 4 and 37°C in the presence or in the absence of 2mMof free biotin. Statistical differences are expressed by an asterisk (*) ($p < 0.01$).

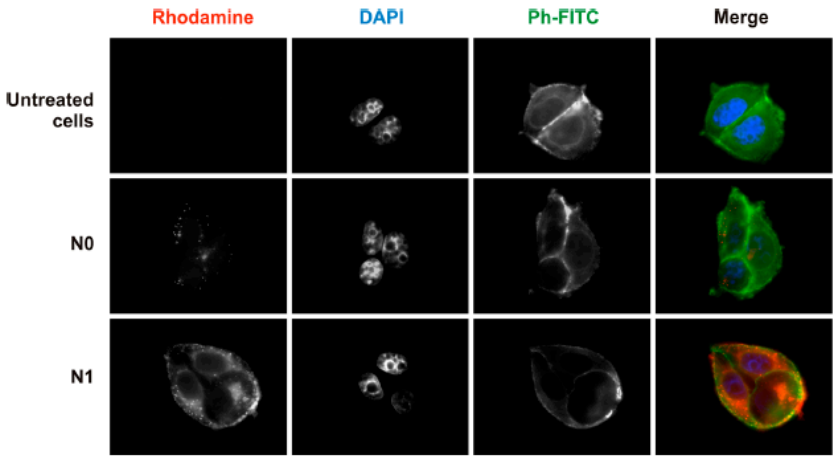

Figure 4. Internalization of rhodamine B-labeled NPs. Fluorescence

microscopy images of MCF7 cells showing the cellular uptake of nonfunctionalized (N0) and biotin-functionalized (N1) NPs (red) after 5 h of incubation. The nuclei were stained with DAPI (blue), phalloidin-fluorescein isothiocyanate (Ph-FITC, green) was used to label F-actin, and the last column represents the overlay of all types of staining.

RESULTS AND DISCUSSION

Design of a Versatile Nanoparticulate Platform. Multifunctional and biodegradable PACA NPs exhibiting stealth, fluorescent, and targeting abilities were synthesized by a combination of (i) copper-catalyzed azide-alkyne cycloaddition (CuAAC)33 to covalently attach the ligand of interest; (ii) copolymerization of different monomer species to introduce the desired features (fluorescence, targeting moiety, hydrophobicity/ hydrophilicity), and (iii) self-assembly in aqueous solution of the resulting amphiphilic copolymers (Figure 2). Practically, a heterobifunctional azidopoly(ethylene glycol) (N3PEG) was first derivatized with the selected ligand by CuAAC using CuSO4/sodium ascorbate as the catalytic system and turned into its cyanoacetate derivative (Ligand-PEGCA) under DCC-assisted chemistry. This functionalized building block was then terpolymerized with varying amounts of MePEGCA and HDCA by tandem Knoevenagel condensation-Michael addition 24 to afford the corresponding ligand containing P(MePEGCA-co-Ligand-PEGCA-co-HDCA) amphiphilic copolymer. Its concomitant self-assembly in aqueous solution with a rhodamine B-tagged P(HDCA-co-RCA-co-MePEGCA) copolymer34 allowed the production of the desired colloidal nanocarrier. The versatility of this methodology was illustrated by the synthesis of a small library of biologically active ligands in order to target cancer and Alzheimer's disease. The use of biotin as a biologically active ligand recently appeared as an elegant way to target cancer cells, 32,35 and represents an original alternative to the extensive use of folic acid toward tumor overexpressed folate receptors. In this view, we prepared PACA NPs functionalized with biotin (VB7) via the synthesis of a P(HDCA-co-VB7PEGCA-co-MePEGCA) copolymer following the synthetic pathway described in Figure 2. The stoichiometry was chosen so as to

achieve a copolymer with 20% of biotinylated PEG chain-ends. A 50/50 P(HDCA-co-VB7PEGCA-co-MePEGCA)/P(HDCAco- RCA-co-MePEGCA) copolymer blend was then coselfassembled in aqueous solution to yield a stable suspension of fluorescent NPs exhibiting 10% of biotin at the extremity of the PEG chains (N1, Table 1). This amount was selected in order to display a sufficient amount of biotin while not altering stealth/stabilizing properties. A similar strategy was followed with curcumin derivatives in order to target Aβ1-42 peptide and the corresponding fibrils. It has recently been shown that curcumin, a major component of the yellow curry spice turmeric, presents potent antioxidant and anti-inflammatory activities,36 but is also able to bind Aβ and to disaggregate Aβ plaques, as well as to prevent fibril and oligomer formation.37-39 Structure-activity relationships of Aβ-aggregation using curcumin derivatives also revealed that subtle changes in the structure led to severe variations of activity.40 Therefore, two curcumin derivatives (CurA and CurB) were equipped with an alkyne moiety and employed in the synthetic pathway depicted in Figure 2 to achieve the corresponding curcumin-functionalized NPs (N2 and N3, respectively, Table 1). Whereas the alkyne group was positioned on one aromatic ring for CurA, allowing conformation mobility, the conformation of CurB was blocked via the formation of a N-heteronuclear pyrazole ring bearing the alkyne moiety. The initial stoichiometry of the reactant was chosen so as to give NPs with 5 mol%of PEG chain functionalized with curcumin. NPs were characterized by dynamic light scattering (DLS) and transmission electron microscopy (TEM). In all cases, NPs N0-N3 were obtained with average diameters in the 85-106 nm range together with rather arrow particle size distributions (Table 1 and Supporting Information, Figures S1-S4). Long-term stability was also assessed over a period of three days in water and in cell culture medium (endothelial cell basal medium supplemented with fetal bovine serum 5%, hydrocortisone 1.4 μM, basic fibroblast growth factor 1 ng 3 mL-1, pen-strep 1%, and HEPES 10 mM),the later being a relevant medium since biomedical applications are envisioned (see Supporting Information, Figure S5). ζ-potential measurements for NPs N1-N3 showed negative values from -7.9 to -16.2 mV (Table 1). The

presence of ligand at the surface of the NPs only slightly affected the colloidal characteristics but led to a decrease of the absolute surface charge as compared to nonfunctionalized NPs (N0), which is a strong indication regarding the effectiveness of the surface modification and the ligand exposure.41 TEM images, with or without negative staining, revealed spherical-shaped nanoparticle suspensions with average diameters and particle size distributions in good agreement with DLS data (Supporting Information, Figure S6).

Biotin Receptor-Mediated Cancer Cell Targeting. Targeting of Cancer Cells. Two cancer cell lines (MCF7 human breast adenocarcinoma cells and M109 murine lung cancer cells), which both overexpress biotin receptors on their surfaces,32,35 were chosen to evaluate the tumor targeting ability of the biotin-functionalized NPs N1. The NPs were added to cells cultured on 6-well plates to target a final nanoparticle concentration of 100 μg 3 mL-1. It is shown in Figure S7 (Supporting Information) the absence of any cytotoxic effect of both nonfunctionalized (N0) and biotinylated (N1) NPs for both cell lines at concentrations up to 250μg 3 mL-1. After incubation at different time intervals, the cells were collected for analysis of rhodamine B fluorescence by flow cytometry. The internalization of biotinylated NPs N1 in both cancer cell lines appeared to be about 3-fold higher after 10 h of incubation comparatively to the nonbiotinylated NPs N0 (Figure 3a and 3b). This result clearly indicated the efficient internalization of targeted NPs in MCF7 and M109 cancer cells. When cells were incubated with NPs N1 for 5 h at 4 °C instead of 37 C, the cell fluorescence intensity dramatically decreased (Figure 3c,d), suggesting that the biotin-functionalized NPs were internalized via endocytosis. Moreover, when cells were preincubated with free biotin (2 mM, 1 h) to saturate the biotin receptors on the cancer cell surface before the addition of NPs N1 (100 μg 3 mL-1, 37°C, 5 h), a substantial decrease in fluorescence (by factors of 5 and 8, respectively, for M109 and MCF7 cell lines) was observed (Figure 3c,d), which confirmed a specific receptor mediated endocytic pathway. Interestingly, when uptake experiments were perfomed with murine leukemia (L1210) cells for which biotin receptors are not overexpressed, it resulted in a poor internalization, thus highlighting the

robustness of the targeting pathway (Supporting Information, Figure S10a,b). The cell uptake and internalization of targeted fluorescent NPs suggested by flow cytometry experiments was confirmed by fluorescence microscopy. As shown in Figure 4, after 5 h incubation, biotinylated NPs N1 (rhodamine B red staining) significantly accumulated into the MCF7 cell cytoplasm (Ph-FITC green staining) contrary to nonfunctionalized NPs N0 which barely entered the cells. In addition, the covalent attachment of the rhodamine moiety to the copolymer conducted to a fine fluorescent signal, as opposed to a typical diffuse signal when hydrophobic dyes are encapsulated.34 Not only this confirmed the formation of mixed NPs (i.e., biotinylated and fluorescent nanocomposites) rather than two independent sets of NPs, but it also allowed to support an endocytic mechanism as fluorescence was mainly localized into vesicles surrounding the nuclei.

Cytotoxicity against Cancer Cells. The biotin-functionalized (N1) nanoparticles were further tested in vitro for their therapeutic efficacy against MCF7 cancer cells using encapsulated paclitaxel (Ptx), one of the most important anticancer agents in clinical use. The reduction of cell viability caused by nanoparticles N0 and N1, either empty (Ptx-) or loaded with paclitaxel (Ptxþ) at a concentration of 1.2 μM (see the Experimental Section and Supporting Information, Figures S8,S9) is reported in Figure 5. Ptx-loaded, nonbiotinylated NPs N0 led to a slight reduction of cell viability, but constant over time, comparatively to empty nanoparticles, probably due to some burst release of Ptx in the cell culture medium (the so-called burst effect). In contrast, biotin-labeled NPs N1 loaded with Ptx conducted to a significantly higher cytotoxicity at 5 h incubation compared to their nonbiotinylated counterparts N0, which was even more pronounced at 10 h (<40% cell viability). It is worth mentioning that the half maximal inhibitory concentration (IC50) was already reached at 10 h with 1.2 μM of Ptx, thus demonstrating the high anticancer activity of Ptx loaded into biotinfunctionalized nanoparticles.

Selectivity of the Targeting. Because anticancer treatments usually lack cell specificity and do not discriminate healthy cells from cancerous ones, causing some severe adverse effects, we first performed uptake experiments

using NPs N0 and N1 with noncancer human endothelial umbilical vein cells (HUVEC) not overexpressing biotin receptors (Supporting Information, Figures S10c,d). In this case, a poor uptake was obtained without any noticeable influence of the temperature or the addition of 2 mM of free biotin, showing the absence of targeting via the biotinreceptor-mediated pathway. The high selectivity of the targeting was further consolidated by a coculture experiment in which healthy NIH/3T3 cells (stained in green) were cocultured with cancer MCF7 cells (unstained), and subsequently incubated with NPs N1 (rhodamine B-labeled, red). The aim was to determine whether healthy cells can be saved fromnanoparticle recognition and if a specific targeting toward cancer MCF7 cells can occur. Remarkably, after 2 h, biotin-functionalized, rhodamine-labeled NPs N1 showed a strong internalization in MCF7 cells, whereas no internalization was noticeable in NIH/3T3 cells (Figure 6). This high targeting selectivity toward cancer cells was even observed up to 10 h incubation. In summary, the presence of overexpressed biotin receptor at the surface of the human breast adenocarcinoma MCF7 and murine lung cancer M109 cell lines was used to demonstrate the efficient and highly selective targeting ability of our PACA nanoparticulate platform, using biotin as the cell-targeting moiety and rhodamine B as the fluorescent marker.

Targeting Aβ1-42 Monomers and Fibrils. Interaction with Curcumin-Functionalized NPs. Several studies have reported the functionalization of curcumin on various monomers or polymer templates by means of the CuAAC reaction.42,43 So far for colloidal systems, only functionalization at the surface of liposomes has been achieved, leading to increased binding affinity toward Aβ1-42 monomer/fibrils.44 Prior to interaction studies, cell viability assays were performed by the MTT test in order to determine the cytotoxicity of curcumin-functionalized NPs N2-N3 on hCMEC/D3 cells. This cell line has been validated as a unique immortalized in vitro model of human BBB and appeared relevant if AD therapy is envisioned. As depicted in Supporting Information, Figure S11, no statistical difference in NPs N2-N3 cytotoxicity was observed up to a copolymer concentration of 50 μg 3 mL-1, which was comparable to the cytotoxicity of their nonfunctionalized

counterparts N0. The ability of these nanoconstructs to interact with the Aβ1-42 peptide was investigated by means of SPR experiments. To this purpose, the curcuminoidfunctionalized NPs N2 and N3, as well as the corresponding nonfunctionalized counterpart N0, used as a control, were made to flow over parallel channels of the same sensor chip immobilizing Aβ1-42 monomers or Aβ1-42 fibrils. Other parallel channels, naked or immobilizing BSA, were used as reference surfaces. As expected with NPs N0 and N2-N3, no binding was detected onto the two reference surfaces (data not shown). However, a clear binding signal was observed for immobilized Aβ1-42, in particular Aβ1-42 fibrils, with all types of NPs (Figure 7), including the nonfunctionalized ones N0, in good agreement with a preliminary study showing that PEGylated PACA NPs could interact to a certain extent with Aβ1-42 monomers.45 Nevertheless, no increase of binding compared to N0 was observed after NP functionalization with CurA (N2), for which the curcuminoid was attached to the PEG chain via an aromatic ring (Figure 7a,b). On the contrary for NPs N3 displaying CurB, a marked increase of binding compared to N0 was observed, indicating that the use of CurB as a ligand conferred additional binding properties to these NPs toward Aβ1-42 monomers and the corresponding fibrils. The equilibrium dissociation constant (KD) values of exposed CurB for Aβ monomers and fibrils were in the submicromolar range, of about 0.8 and 0.3 μM, respectively. The marked discrepancy concerning the binding ability of NPs N2 and N3 toward Aβ1-42 monomers and fibrils was further explained by a difference of stability of the curcumin derivatives in aqueous solution. Nonmodified curcumin is indeed known to be highly unstable, undergoing rapid hydrolytic degradation in neutral or alkaline conditions.46 A stability study was performed with CurA and CurB by means of 1H NMR in PBS (pH 7.4) and revealed that CurA was totally degraded after only 15 min whereas CurB was still intact after 7 days incubation (Supporting Information, Figures S12). In the latter case, the formation of the pyrazole moiety avoids the presence of the chemically labile β-diketone group and, at the same time, locks the keto-enol tautomerism in an enol-type arrangement, crucial for Aβ binding effect.44,47-49 Since curcumin is known to inhibit Aβ1-42 aggregation, the effect of CurB-

functionalized NPs on Aβ1-42 aggregation was analyzed by a Thioflavin T (ThT) binding assay. As shown in Figure 8a,b, CurB-functionalized NPs N3 inhibited the aggregation of Aβ1-42 in a dose-dependent manner, while the nonfunctionalized NPs N0 at the same concentrations only poorly affected the Aβ1-42 aggregation, highlighting the specific effect of the CurB-functionalization. Notably, the aggregation inhibition of Aβ1-42 by NPs N3 was observed at a submolar ratio (1:0.5).

To investigate whether the interference of the CurB functionalized NPs N3 with the aggregation of Aβ1-42 could affect Aβ1-42 cytotoxicity, we performed an MTT assay on differentiated human neuroblastoma cells (SK-N-SH), which is a relevant model to study the targeting of Aβ neurotoxicity. Also in this model, no toxicity of NPs N0 and N3 was observed (Figure 8c). SK-N-SH cells were then treated with aggregated Aβ1--42 peptide in the absence or in the presence of increasing molar ratios of NPs N0 or N3 in order to address whether NPs could interfere with Aβ toxicity. In accordance with ThT data, the samples treated with NPs N3 showed a concentration-dependent protective effect compared to the samples treated with Aβ1-42 alone, whereas control NPs (N0) did not significantly affect cell survival (Figure 8d). This indicated that intervention in aggregation by NPs did not create toxic Aβ species and even conducted to a noticeable toxicity rescue. In conclusion, it was clearly shown that CurB-functionalized NPs significantly inhibited both the aggregation and the toxicity of Aβ1-42 at low molar ratios.

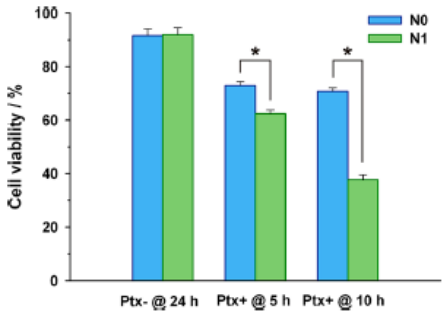

Figure 5. Cell viability of MCF7 cells after exposure to empty (Ptx-) and paclitaxel-loaded (Ptxþ) NPs N0 and N1 at a Ptx concentration of 1.2 μM. Statistical differences are expressed by an asterisk (*) ($p < 0.01$).

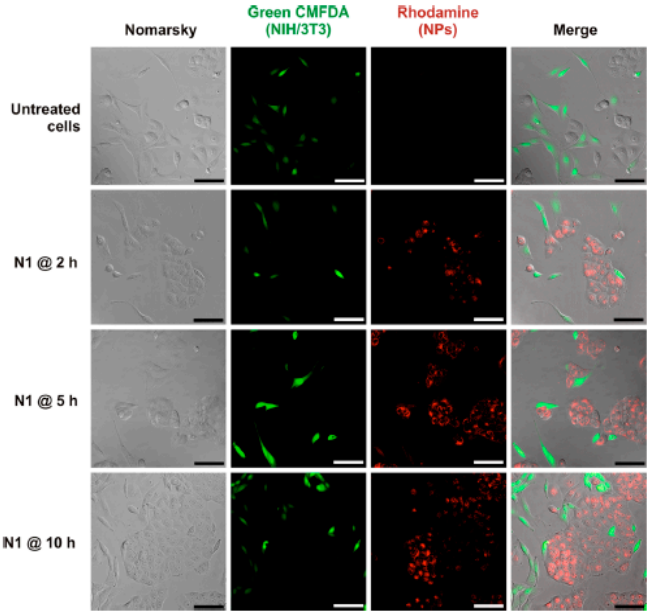

Figure 6. Nomarsky and confocal laser-scanning microscopy images of a coculture of NIH/3T3 (green) and MCF7 cells (unstained) after incubation with biotin-functionalized, rhodamine-labeled (N1) NPs (red) at 40 μg 3 mL-1 at different time intervals (2, 5, and 10 h). The NIH/3T3 cells were stained with Green CMFDA (green). Scale bars = 100 μm.

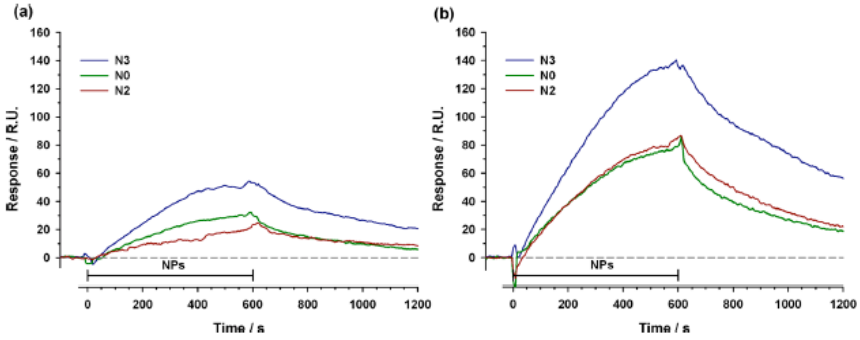

Figure 7. SPR sensorgrams (resonance units, RU, versus time) obtained by simultaneous injections of CurA-functionalized (N2), CurB-functionalized (N3), and nonfunctionalized (N0) NPs for 10 min (bars) over Aβ1-42 monomers (a) or fibrils (b) immobilized on two parallel channels of the same sensor chip. The final concentration of the curcuminoid was 240 nM.

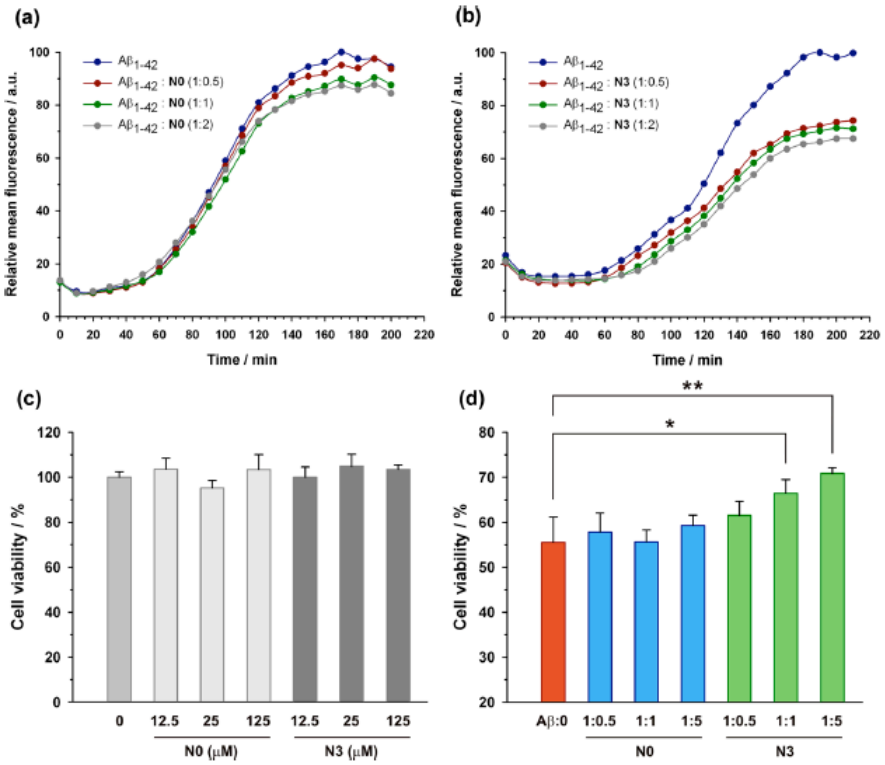

Figure 8. Effects of NPs on the aggregation of Aβ1-42 using the Thioflavin T binding assay (a and b). Aggregation kinetics of 25 μM Aβ1-42 alone or coincubated with increasing molar ratios (1:0.5; 1:1 and 1:2) of nonfunctionalized (N0) (a) or CurB functionalized (N3) (b). NPs. Data are shown as mean (n = 3) from a representative experiment of three independent experiments. Effects of NPs on Aβ1-42 toxicity using an MTT viability assay (c and d). Differentiated SK-N-SH cells were treated for 48 h in the absence or in the presence of different concentrations of NPs N0 or N3 (12.5; 25 or 125 μM) to assess toxicity of the NPs (c); by differentiated SK-N-SH cells were treated for 48 h in the absence or presence of Aβ1-42 (25 μM) preaggregated in PBS for 24 h at 25°C, alone or in combination with three different molar ratios (1:0.5; 1:1 and 1:5) of NPs N0 or N3 (d), to address interference of the NPs with Aβ toxicity. Cell viability was measured using a MTT assay and is depicted as a percentage of the untreated cells (control). The graph represents the mean (SD (n = 4) from one experiment and results shown are representative for three independent experiments. Statistical differences are expressed by asterisks: (*) $p < 0.05$ and (**) $p < 0.01$.

Design of Anti-Aβ142-functionalized Nanoparticles and Interaction with Aβ1-42. Although CurB-functionalized NPs N3 led to an increased interaction with Aβ1-42 monomer/fibrils by means of specific aromatic binding,37 we decided to go a step further by designing a truly specific and even more efficient Aβ-binding nanocarrier. Thanks to the presence of biotin at the surface of NPs N1, previously employed for cancer cell targeting, we took advantage of the versatility of this nanoparticulate platform to decorate the NPs with a novel monoclonal anti-Aβ142 antibody (mAb) by means of the biotin/streptavidin (SAv) ligation strategy. The availability of the exposed biotin to SAv was confirmed by confocal laser scanning microscopy (CLSM) as shown in Figure 9. A fluorescein-tagged streptavidin (SAv-FITC) was incubated with either biotin- functionalized (N1) or nonfunctionalized (N0) NPs. Only in the case of N1 were some NPs-SAv-FITC aggregates observed via the formation of clearly colocalized bigger size aggregates (note that the SAv-FITC concentration was chosen so as to be in the same range as the exposed biotin for N1). This result was further confirmed by SPR experiments showing strong binding of NPs N1 to avidin-immobilized chip (Supporting Information, Figure S13), compared to nonfunctionalized NPs N0 or N1 flowed over noncoated chip (i.e., ethanolamine surface). The amount of surface available biotin on NPs N1 per gramof nanoparticle was quantified by the competitive avidin/HABA binding assay (see the Supporting Information) and gave 5360 nmol 3 g-1. When compared to the theoretical value (i.e., 29 400 nmol 3 g-1), the fraction of surfaceavailable biotin is ∼18%, which is consistent with literature data.50 A streptavidin-anti Aβ142 antibody conjugate was prepared (Supporting Information) and characterized by PAGE electrophoresis (Figure S14). Visualization under UV excitation (λ = 488 nm) revealed the presence of the conjugate characterized by a higher molecular weight when compared to native SAv-FITC, while a SAv-FITC/anti-Aβ1-42 mAb physical mixture did not show any coupling product. A suspension of NPs N1 was then incubated with the SAv-FITC-anti-Aβ1-42 mAb conjugate followed by a centrifugation step that allowed anti-Aβ1-42 mAb-functionalized NPs N4 to be isolated (Dz = 151 nm (24 nm) from unreacted species. A Bradford's assay revealed that 37% of the

SAv-FITC-anti-Aβ1-42 mAb conjugate were bound to the surface of the NPs, whereas this amount was as low as 10% with nonfunctionalized NPs N0 (i.e., due to aspecific adsorption of Aβ1-42 mAb at the surface of N0). The MTT assay showed that NPs N4 were not cytotoxic up to 50 μg 3 mL-1 (Figure S11). The ability of NPs N4 to specifically interact with Aβ1-42 was investigated by SPR experiments on monomeric or fibrillar peptide (Figure 10). As expected, a strong interaction was obtained with NPs N4 (60 μM), whereas no or only a weak signal was observed under identical experimental conditions with either nonfunctionalized NPs N0 or with a physical mixture of N0 and anti-Aβ1-42 mAb, further purified from free mAb (data not shown). Moreover, NPs N4 led to a dose-response behavior, allowing the equilibrium dissociation constants to be determined. The affinity of the mAb functionalized NPs N4 for the peptide was very high and exhibited KD values in the picomolar range (monomers, KD ∼700 pM; fibrils, KD ∼300 pM). KD values for the free mAb were about 150 and 240 pM for monomers and fibrils, respectively (data not shown). These data clearly indicated that the functionalization with the anti-Aβ142mAbconferred to the corresponding NPs a remarkable ability to strongly bind the Aβ142 peptide (as monomer or as aggregated fibrils), and that the procedure used for NP functionalization only slightly altered the affinity for the peptide. It is worth noting that the affinity of the NPs N4 for Aβ1-42 species was higher than any other colloidal systems reported so far.44,48,49,51

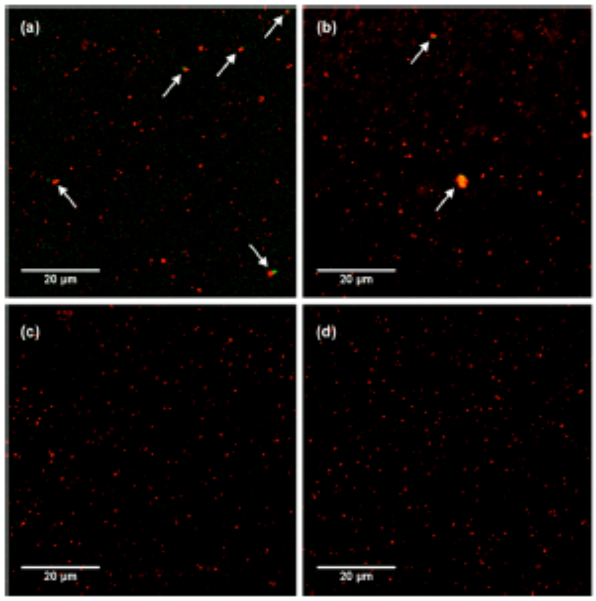

Figure 9. Confocal laser scanning microscopy images of nonfunctionalized (N0) and biotin-functionalized (N1) NP suspensions (20 µM) incubated with fluorescein-labeled streptavidin (FITC-SAv): N1, [FITC-SAv] = 0.2 µM (a); N1, [FITC-SAv] = 0.5 µM (b); N0, [FITC-SAv] = 0.2 µM (c); and N0, [FITC-SAv] = 0.5 µM (d).

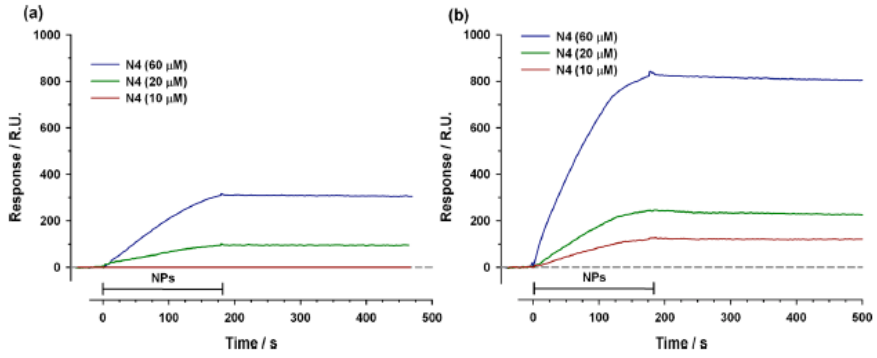

Figure 10. SPR sensorgrams (resonance units, RU, versus time) of anti-Aβ1-42 mAb-functionalized (N4) NPs at various concentrations (10, 20, 60 µM), flowed for 3 min (bars) onto a Aβ1-42 monomer (a) or Aβ1-42 fibrils (b) immobilized on the sensor chip.

CONCLUSIONS

This study described the design of a new versatile and ligand-functionalized

poly(alkyl cyanoacrylate) nanoparticulate platform, gathering together all crucial features required for targeting and drug delivery. Multifunctional NPs arising from this platform were successfully used to target two major pathologies, namely cancer and Alzheimer's disease, via their functionalization by appropriate biologically active ligands.

These nanocarriers exhibited (i) a biodegradable core; (ii) stealth features due to a PEG outer shell; (iii) fluorescent properties provided by the covalent linkage of a fluorescent probe; and (iv) biologically active ligands displayed at their surface to achieve active targeting. Regarding potential cancer therapy, biotin has been used as a ligand for specific recognition of different cancer cell lines, while letting noncancer cells or cancer cells with nonoverexpressed biotin receptors be unaffected, even in a healthy/cancer cells coculture environment. This strategy is now applicable to a variety of anticancer agents by simple encapsulation into the PACA polymeric matrix using the robust methodologies already developed before, and could have important clinical applications for cancer therapy. In this view, the encapsulation of paclitaxel, one of the most important anticancer agents in clinical use, has been achieved and led to a strong toxicity against cancer cells with biotinfunctionalized NPs. Interestingly, because drug-loaded PACA NPs have been shown to overcome cancer MDR, it is expected that the biotin-functionalized PACA NPs described here may open a more specific avenue toward the treatment of solid tumors that are hard to treat by conventional chemotherapy. In the field of AD, both curcumin derivatives as well as a specific anti-Aβ1-42 antibody were positioned at the surface of PACA NPs which exhibited strong affinity toward Aβ1-42 monomers and the corresponding fibrils. In the case of the anti-Aβ1-42 mAb, the biotin/ streptavidin ligation strategy was employed, using biotin-functionalized NPs as the same colloidal system that served to target cancer cells. Dissociation rate constants in the picomolar range were obtained, which represent the highest values ever reported for colloidal systems so far. With curcumin functionalization, the resulting NPs offered a significant aggregation inhibition of Aβ1-42 together with a marked toxicity rescue, both at low molar ratios. The proposed synthetic pathway is therefore very flexible and

adaptable for applications to a broad range of pathologies, simply by adjusting the surface functionalization of the nanocarriers by means of suitable ligands.

EXPERIMENTAL SECTION

Synthesis Methods. Synthesis of CurcuminA-poly(ethylene glycol) (CurAPEG), CurcuminB-poly(ethylene glycol) (CurBPEG), CurcuminA-poly(ethyleneglycol) cyanoacetate (CurAPEGCA), CurcuminB-poly(ethylene glycol) cyanoacetate (CurBPEGCA), biotinpoly(ethylene glycol) (VB7PEG), biotin-poly(ethylene glycol) cyanoacetate (VB7PEGCA), anti-Aβ1-42 antibody and Anti-Aβ1-42 antibody-fluorescein labeled streptavidin bioconjugate (mAb-SAv) are detailed in the Supporting Information. HDCA, MePEGCA,P(MePEGCA-co-HDCA) copolymer C0 (Mn,SEC=2430g3mol-1,Mw/Mn = 1.27) and the fluorescent rhodamine-B-tagged P(MePEGCA-co-RCA-co-HDCA) copolymerC1(Mn,SEC=2270g3 mol-1, Mw/Mn = 1.30) were prepared according to previously published procedures.34,52

General Copolymerization Procedure for the Preparation of Biotin-Functionalized P(MePEGCA-co-VB7PEGCA-co-HDCA) Copolymers C2. In a 25 mL round-bottom flask containing HDCA (170 mg, 550 μmol, 40 equiv), MePEGCA (229 mg, 110 μmol, 8 equiv), and VB7PEGCA (65 mg, 27.5 μmol, 2 equiv or 20 mol % in the initial PEG cyanoacetate mixture) monomers, CH2Cl2 (2.84 mL) and EtOH (1.42 mL) under magnetic stirring, were sequentially introduced formaldehyde (345 μL, 4.63 mmol) and pyrrolidine (14.5 μL, 176 μmol). The mixture was allowed to stir for 24 h at room temperature and was then concentrated under reduced pressure. The residue was taken into CH2Cl2 and washed multiple times with water. The resulting organic layer was dried over MgSO4, filtered, concentrated under reduced pressure and dried under vacuum to give a brown, waxy solid. Quantification of VB7PEGCA in the copolymer was estimated by 1H NMR that confirmed the presence of 20 mol % VB7PEGCA monomer insertion

(when compared to the overall PEGCA content in the polymerization feed). Mn,SEC = 2160 g 3 mol-1, Mw/Mn = 1.34.

General Copolymerization Procedure for the Preparation of Poly-[Hexadecyl Cyanoacrylate-co-CurAPEGcyanoacrylate-co-methoxypoly(ethyleneglycol) Cyanoacrylate] (P(HDCA-co-CurAPEGCA-co-MePEGCA), C3) and Poly-[hexadecyl cyanoacrylate-co-CurBPEGcyanoacrylate-co-methoxypoly(ethylene glycol) Cyanoacrylate] (P(HDCA-co-CurBPEGCA-co-MePEGCA), C4) Copolymers. In a 25mL round-bottomflask containingMePEGCA (258mg, 124 μmol, 9 equiv), HDCA (170 mg, 550 μmol, 40 equiv), CurAPEGCA (34 mg, 13.8 μmol, 10 mol % in the initial PEG cyanoacetate mixture or 1 equiv) or CurBPEGCA (35 mg, 13.8 μmol, 1 equiv) monomers, EtOH (1.42 mL) and CH2Cl2 (2.84mL) under magnetic stirring, were sequentially introduced formaldehyde (345 μL, 4.6 mmol) and pyrrolidine (14.5 μL, 176 μmol). The mixture was allowed to stir for 24 h at room temperature and was then concentrated under reduced pressure. The residue was taken into CH2Cl2 and washed multiple times with water. The resulting organic layer was dried over MgSO4, filtered, concentrated under reduced pressure and dried under vacuum to give the resulting copolymers. Quantification of CurAPEGCA or CurBPEGCA in the copolymer was estimated by 1H NMR that confirmed the presence of about 10 mol % curcumin-functionalized PEGCA (when compared to the overall PEGCA content in the polymerization feed).

Nanoparticle Preparation. Fluorescent NPs N0 were prepared by the nanoprecipitation technique using a 50/50 blend of P(MePEGCA-co-HDCA) (C0) and P(MePEGCA-co-RCA-co-HDCA) (C1) copolymers. Fluorescent and functionalized N1-N3 NPs were prepared by the nanoprecipitation technique using a 50/50 blend of P(MePEGCA-co-RCA-co-HDCA) (C1) and P- (MePEGCA-co-VB7PEGCA-co-HDCA) (C2), P(MePEGCA-co-CurAPEGCA-co-HDCA) (C3), or P(MePEGCA-co-CurBPEGCA-co-HDCA) (C4) copolymers, respectively (see Table 1 for details). Briefly, 5mg of each copolymer was dissolved in acetone (2 mL), and the copolymer

solution was added dropwise to an aqueous solution 0.5% (w/v) of Pluronic F-68 (4 mL) under vigorous mechanical stirring. Acetone was then evaporated under reduced pressure, and NPs were purified by ultracentrifugation (150 000g for N0, N2N3, and 82 000g for N1, 1 h, 4 C, Beckman Coulter, Inc.). The supernatant was discarded and the pellet was resuspended in the appropriate volume of deionized water to yield a 2.5 mg3 mL1 nanoparticle suspension. Paclitaxel-loaded NPs N0 and N1 were prepared by the emulsion/solvent evaporation technique using the same copolymer blends as previously described for nonbiotinylated (C0/C1) or biotinylated (C0/C2) NPs. Briefly, 5 mg of each copolymer was dissolved in 1 mL of 1 mg3 mL1 organic solution of paclitaxel (chloroform/ethanol 90/10 v/v). To this organic phase was added 4 mL of an aqueous solution of PVA (0.25% w/w) presaturated with 1% chloroform. The resulting emulsion was vortexed two times for 1 min at 2400 rpm and ultrasonicated on ice for 3 min at 150 V using a sonicating device (Ultrasons Annemasse, France). The solvent was then removed under reduced pressure to yield a stable suspension of NPs. NPs were purified by filtration on 1 μm glass fiber membrane (Acrodisc, Pall) slide. Paclitaxel-loaded NPs were further purified by centrifugation for 20 min at 17 000g and 20 C. After 24 h, a second centrifugation step was performed. NPs were stored at 20°C until use. To assess the Ptx concentration, NPs were radiolabeled by entrapment of 3H-paclitaxel. A 100 μL aliquot of radioactive drug dissolved in ethanol (10 μCi) was added to 900 μL of chloroform solution in which the blend of polymers and the nonradiolabeled paclitaxel have been previously dissolved. NPs were then prepared according to the same experimental procedure as described before. After the second centrifugation step, 500 μL of NPs were placed in the scintillation counting vials and 10 mL of Ultima Gold scintillant was added. The mixture was vortexed vigorously for 1 min. Then, the radioactivity present in the samples was measured (n = 3) using a liquid scintillation counter (Beckman, LS 6000TA; Beckman Coulter). In both cases, drug encapsulation efficiency was 1.1%. For in vitro cytotoxicity experiments, Ptx-loaded NPs were tested at a concentration of 1.2 μMPtx.

Cell Culture. hCMEC/D3 cells were grown in EBM-2 basal medium (Lonza, Belgium) supplemented with fetal bovine serum 5% (FBS, Lonza, Belgium), hydrocortisone 1.4 μM, basic fibroblast growth factor 1 ng 3 mL1, pen-strep 1%, and HEPES 10 mM. Murine lung carcinoma cell lines M109, human breast cancer cell lines MCF7, human endothelial umbilical vein cells(HUVEC), murine leukemia cells (L1210), and embryonic murine fibroblast (NIH/3T3) were obtained from the American Type Culture Collection and maintained as recommended. Briefly, M109 and L1210 cells were maintained in RPMI 1640 medium (Lonza, Belgium). MCF7, SK-N-SH, HUVEC, NIH/3T3 cells were grown in Dulbecco's modified Eagle's medium (DMEM, Lonza, Belgium) supplemented with 50 U 3 mL1 penicillin, 50 U 3 mL1 streptomycin, and 10% heat-inactivated FBS. Cells were maintained in a humid atmosphere at 37°C with 5% CO2.

Coculture. NIH/3T3 fibroblasts (5x104) were plated onto microscopic glass slides and incubated for 18 h at 37 C and 5% CO2 in cell culture medium. To visualize and distinguish between NIH/3T3 fibroblasts and MCF7 cells in coculture, NIH/3T3 cells were stained with 5 μM CellTracker green 5-chloromethylfluorescein diacetate (CMFDA, Life Technology, Molecular Probes) according to the manufacturer's protocol. After staining, cells were left to rest for 2 h at 37 C and 5% CO2 in cell culture medium, followed by addition of unstained MCF7 cells (15x104). The seeding ratio between MCF7 and NIH/3T3 cells was 1:3 due to the faster doubling time of the latter. After 12 h, the coculture was incubated with NPs (N1) diluted in fresh cell culture medium at 40 μg 3 mL1. At different time points (2, 5, and 10 h) cells were washed with prewarmed culture medium before imaging.

Cytotoxicity Studies. The cytotoxicity of NPs N0N4 was investigated by MTT [3-(4,5-dimethylthiazol-2-yl)-2,5-diphenyl tetrazolium bromide] viability test on hCMEC/D3 human brain endothelial cell line. Briefly, cells were grown on 10 cm diameter plates in EBM-2 basal medium supplemented with fetal bovine serum 5%, hydrocortisone 1.4 μM, basic fibroblast growth factor 1 ng 3mL1, penicillin/streptomycin solution 1%, ascorbic acid 5 μg 3 mL1, Chemically Defined Lipid Concentrate (1/100), and HEPES 10 mM.

Polystyrene 96 wells plates were used and cells were seeded in each well (75 000 cells 3 mL1) with the medium previously described. After a 2 days growth, an aqueous suspension of NPs was incubated at five different concentrations: 10, 20, 30, 50, and 100 μg 3mL1. After 48 h of incubation at 37 C in 5% CO2, the MTT reagent (at a final concentration of 0.05% in Dulbecco's PBS, D-PBS) was added and 3 h later, the percentage of living cells was evaluated with a 96 wells plate absorbance reader at 570 nm. Cells treated with the same volume of water were used as negative controls. A MTT viability test was also performed with N0 and N1 NPs on MCF7 and M109 cell lines. Briefly, 10000 MCF7 or 5000 M109 cells per well were incubated in 200 μL of medium containing 10% FBS in 96-well plates for 24 h. The cells were then exposed to a series of concentrations of N1 NPs for 24 h. After drug exposition, the medium was removed and 100 μL of MTT solution (0.5 mg3 mL1 in DMEM containing 10% FBS) was added to each well. The plates were incubated for 2 h at 37 C, and 100 μL of 20% SDS solution was then added to each well for 24 h at 37 C. Absorbance was measured at 570 nm using a plate reader (Perkin-Elmer). All experiments were set up in quadruplicate to determine means and SDs. We examined the antiproliferative effect of the studied NPs on the growth of a murine lung carcinoma and human breast cancer cell lines (M109 and MCF7). For further studies, the noncytotoxic concentration of NPs (i.e., 100 μg 3 mL1) was used. For toxicity of NPs N0 and N3, SK-N-SH cells were plated in 96-well plates at a density of 20x103 cells per well and differentiated for 5 days in medium supplemented with 10 μM retinoic acid (Sigma). HFIP treated Aβ142 was dissolved in DMSO and subsequently diluted in PBS. A 25 μM aliquot of Aβ142 containing different concentrations of NPs (12.5, 25, or 125 μM) was then incubated for 24 h at 25 C. This mixture was diluted 25 times into DMEM without phenol red and added in quadruplicate to differentiated SK-N-SH. After 48 h of incubation at 37 C in 5% CO2, the MTT reagent (at a final concentration of 0.05% in D-PBS) was incubated for 2 h, and subsequently the insoluble formazan salt generated by the viable cells was solubilized in DMSO. The number of viable cells was directly quantified by measuring the absorbance at 570 nm. Viability was expressed as a percentage

of untreated cells.

Cell-Internalization of Biotin-Labeled Nanoparticles. In this study we used MCF7 human breast adenocarcinoma and M109 murine lung carcinoma cell lines with increased expression of biotin receptors.32,35 MCF7 cancer cells were cultured on a coverslip in a culture dish for 24 h to achieve approximately 40% confluence. Cells were then incubated with NPs N0 and N1 at a concentration of 100 μg 3 mL1 (37 C) for 5 h. After treatment, the cells were washed with D-PBS, fixed in 3% paraformaldehyde (PFA), stained with phalloidinfluorescein isothiocyanate (Ph-FITC, 200 μM) and DAPI (40 μM) (Invitrogen), washed with D-PBS five times, and imaged using a fluorescence microscope (Leica) with a x63 oil-immersion objective. The following wavelengths were used: excitation at 488 nm and detection through a 515 nm filter for FITC, and excitation at 488 nm and detection through a long-pass 560 nm filter for rhodamine B. To quantitatively measure the internalization of biotinfunctionalized NPs N1, MCF7 or M109 cells (2x105) were cultured on 6-well plates for 24 h to achieve 6080% confluence. NPs N1 and control N0 NPs were then added at the noncytotoxic concentration of 100 μg 3 mL1 to each well. After incubation for determined times (0.5, 2.5, 5, 7.5, and 10 h), the cells were collected for measurement of rhodamine B fluorescence. The fluorescence from individual cells was examined using a flow cytometer C6 (Accuri Cytometers Ltd., UK). For fluorescence detection of NPs, excitation was carried out with the 488-nm line of an argon laser, and emission fluorescence between 560 and 606 nm was measured. For all experiments in which the intracellular rhodamine B was quantified using a flow cytometer, 10000 cells were measured from each sample. For low temperature experiments, the cells were incubated in the cold room at 4°C for 5 h. For competition experiments, cells were preincubated at 37°C for 1 h in the presence of free biotin at the concentration of 2 mM. All experiments were set up in triplicate to determine means and SDs.

Interaction Experiments between Curcumin-Functionalized NPs (N2 and N3) and Aβ142 Monomers/Fibrils. Aβ142 monomers or fibrils were obtained from the in-house depsi peptide as previously described.53 They were immobilized in parallel-flow channels of a GLC sensor chip (Biorad)

using amine-coupling chemistry. Briefly, after sensor surface activation, the peptide solutions (10 μM in acetate buffer pH 4.0) were injected for 5 min at a flow rate of 30 μL 3 min1, and the remaining activated groups were blocked with ethanolamine, pH 8.0. The final immobilization levels were about 2000 Resonance Units (1 RU = 1 pg protein 3mm2) for both Aβ142 monomers and fibrils. Bovine serum albumin (BSA) was also immobilized, in a parallel flow channel as a reference protein and another reference surface was prepared in parallel using the same immobilization procedure but without addition of the peptide (naked surface). Preliminary injections were performed in order to check the binding features of the immobilized species. The anti-Aβ antibody 6E10 (Covance) was injected and, as expected, bound to both Aβ fibrils and monomers (not shown) whereas Congo-Red, a dye specifically recognizing β-sheet-containing species, only bound to Aβ fibrils but not monomers (not shown). The suspensions of curcumin-functionalized P(MePEGCA-co-PHDCA) NPs N2 and N3 were diluted and injected onto immobilized Aβ species or the reference surfaces. All the injections were carried out for 5 min at a flow rate of 30 μL 3 min1 at 30°C in PBST (PBS þ 0.005% Tween20, pH 7.4).

Interaction Experiments between Biotin-Functionalized NPs (N1) and Avidin. Avidin (which is a protein having the same activity as streptavidin) was immobilized on a channel of a CM5 sensor chip (Biacore, GE Healthcare) using amine-coupling chemistry. Briefly, after sensor surface activation by EDC/NHS, the avidin solution (50 μg 3 mL1 in acetate buffer pH 5.0) was injected for 7 min at a flow rate of 10 μL 3 min1, and the remaining activated groups were blocked with ethanolamine, pH 8.0. The final immobilization levels were about 8500 Resonance Units (1 RU = 1 pg protein 3mm2), that is, 8.5 ng 3mm2. Another parallel channel, on which ethanolamine blocked the surface (empty surface), using the same immobilization procedure but without addition of avidin (immobilization level about 23 RU), was used as a reference channel. The 10% biotin-functionalized N1 NP suspension was diluted at a 1 mg3 mL1 final concentration and flowed onto both channels for 10 min. The same experiments were performed with rhodamine B-tagged nonfunctionalized

NPs N0 as negative controls. The interaction between streptavidin and biotin-functionalized NPs was also demonstrated using fluorescein-tagged streptavidin (SAv-FITC) and rhodamine B-labeled 10% biotinfunctionalized N1 NPs. Increasing volumes of a 20 mM phosphate buffer saline solution of SAv-FITC (5 mg3 mL1, 94 μM) were incubated for 15 min with a 20 μM suspension of rhodamine B-labeled 10% biotin-functionalized N1 NP suspension to reach final SAv-FITC concentrations of 0.2, 0.5, 1, 2, and 20 μM. A 10 μL deposit of this final incubation sample on glass coverslips was visualized by confocal laser scanning microscopy (CLSM) under both fluorescence channels. The same experiments were performed with rhodamine B-tagged nonfunctionalized N0 NPs as negative controls.

Preparation of Anti-Aβ142 Antibody Functionalized NPs (N4). To 34 μL of a suspension of N1 NPs was added 1 mL of the anti-Aβ142-streptavidin conjugate solution (see the Supporting Information for details). The resulting suspension was gently shaken for 30 min before purification by ultracentrifugation at 150 000g for 1 h at 4 C. The amount of anti-Aβ142-mAb streptavidin conjugate linked to the NPs was determined by Bradford's assay. The anti-Aβ142-mAb functionalized N4 NPs were used without further purification.

Interaction Experiments between Anti-Aβ142-Functionalized NPs (N4) and Aβ142 Monomers/Fibrils. Aβ142 monomeric or fibrillar preparations were obtained from the commercial peptide (Sigma) as previously described, and the presence of monomers or fibrils was checked by atomic force microscopy (AFM) (data not shown).48 SensiQ semiautomatic apparatus with two parallel flow channels was employed (ICX Technologies). A COOH5 sensor chip (ICX Technologies) was installed in the system, and monomers were immobilized using amine-coupling chemistry on one channel, while the other one was used as reference surface. In the same way, a second COOH5 sensor chip was used for the immobilization of fibrils. Briefly, after sensor surface activation, the peptide solution (10 μMin acetate buffer pH 4.0) was flowed for 5 min at a rate of 30 μL 3 min1, and the remaining activated groups were blocked with ethanolamine, pH 8.0. The

final immobilization levels were about 4000 Resonance Units (1 RU = 1 pg protein 3mm2). The reference surface was prepared in parallel using the same immobilization procedure but without the addition of the peptide (naked surface). Preliminary injections with the anti-Aβ antibody 6E10 (Covance) were performed and, as expected, it bound to both Aβ fibrils and monomers. The suspensions of NPs N4 were diluted and injected. The same experiments were performed with nonfunctionalized NPs N0 as well as with a physical mixture of N0 and anti-Aβ142 mAb, (purified from the free mAb) as negative controls. All the injections were carried out for 3 min at a flow rate of 30 μL 3 min1 at 30°C in PBST (PBS þ 0.005% Tween20, pH 7.4). .

Acknowledgment. The authors warmly thank Dr. Claire Boulogne for the TEM analysis, Valérie Nicolas (Plateforme Imagerie Cellulaire, IFR 141) for her help with the CLSM, and Dario Carradori for his help on the HABA assay. This work has used the facilities and the expertises of the (Electron Microscopy Platform) Cell biology unit of the Imagif platform (Centre de Recherche de Gif). The research leading to these results has received funding from the European Community's Seventh Framework Programme (FP7/2007-2013) under agreement no. 212043. The CNRS and the French Ministry of Research are also warmly acknowledged for financial support.

Supporting Information Available: Detailed experimental section [materials, synthesis of CurAPEG, synthesis of CurBPEG, synthesis of CurAPEGCA, synthesis of CurBPEGCA, synthesis of VB7PEG, synthesis of VB7PEGCA, synthesis of anti-Aβ142 antibody, synthesis of anti-Aβ142 antibody-fluorescein-labeled streptavidin bioconjugate, nuclear magnetic resonance (NMR) spectroscopy, size exclusion chromatography (SEC), dynamic light scattering (DLS), transmission electron microscopy (TEM), surface plasmon resonance (SPR), avidin/HABA competitive binding assay, thioflavin T assay, confocal laser scanning microscopy CLSM), NMR evaluation of compound CurA and CurB chemical stability, Anti-Aβ142 antibody-SAv complex quantification at the surface of rhodamine B labeled P(MePEGCA-co- VB7PEGCA-co-HDCA) NPs, DLS and TEM data for NPs N0N3], supporting Figures S1S14.

REFERENCES

1. Brigger, I.; Dubernet, C.; Couvreur, P. Nanoparticles in Cancer Therapy and Diagnosis. Adv. Drug Delivery Rev. 2002, 54, 631–651.

2. Brambilla, D.; Le Droumaguet, B.; Nicolas, J.; Hashemi, S. H.; Wu, L.-P.; Moghimi, S. M.; Couvreur, P.; Andrieux, K. Nanotechnologies for Alzheimer's Disease: Therapy, Diagnosis and Safety Issues. Nanomedicine: NBM 2011, 7, 521–540.

3. Farokhzad, O. C.; Langer, R. Impact of Nanotechnology on Drug Delivery. ACS Nano 2009, 3, 16–20.

4. Sanhai, W. R.; Sakamoto, J. H.; Canady, R.; Ferrari, M. Seven Challenges for Nanomedicine. Nat. Nanotechnol. 2008, 3,242–244.

5. Erb, S. E. Nanotechnology in Drug Delivery. Drug Delivery Syst. 2009, 24, 63–70.

6. Riehemann, K.; Schneider, S. W.; Luger, T. A.; Godin, B.; Ferrari, M.; Fuchs, H. Nanomedicine-Challenge and Perspectives. Angew. Chem., Int. Ed. 2009, 48, 872–897.

7. Arias, J. L.; Reddy, L. H.; Othman, M.; Gillet, B.; Desmaële, D.; Zouhiri, F.; Dosio, F.; Gref, R.; Couvreur, P. Squalene Based Nanocomposites: A New Platform for the Design of Multifunctional Pharmaceutical Theragnostics. ACS Nano 2011, 5, 1513–1521.

8. Hans, M. L.; Lowman, A. M. Biodegradable Nanoparticles for Drug Delivery and Targeting. Curr. Opin. Solid State Mater. Sci. 2002, 6, 319–327.

9. Panyam, J.; Labhasetwar, V. Biodegradable Nanoparticles for Drug and Gene Delivery to Cells and Tissue. Adv. Drug Delivery Rev. 2003, 55, 329–347.

10. Brannon-Peppas, L. Recent Advances on the Use of Biodegradable Microparticles and Nanoparticles in Controlled Drug Delivery. Int. J. Pharm. 1995, 116, 1–9.

11. Sinha, R.; Kim, G. J.; Nie, S.; Shin, D. M. Nanotechnology in Cancer

Therapeutics: Bioconjugated Nanoparticles for Drug Delivery. Mol. Cancer Ther. 2006, 5, 1909–1917.

12. Soppimath, K. S.; Aminabhavi, T. M.; Kulkarni, A. R.; Rudzinski, W. E. Biodegradable Polymeric Nanoparticles as Drug Delivery Devices. J. Controlled Release 2001, 70, 1–20.

13. Cabral, H.; Nishiyama, N.; Kataoka, K. Supramolecular Nanodevices: From Design Validation to Theranostic Nanomedicine. Acc. Chem. Res. 2011, 44, 999–1008.

14. Couvreur, P.; Vauthier, C. Nanotechnology: Intelligent Design to Treat Complex Disease. Pharm. Res. 2006, 23, 1417–1450.

15. Sukhorukov, G. B.; Rogach, A. L.; Zebli, B.; Liedl, T.; Skirtach, A. G.; Köhler, K.; Antipov, A. A.; Gaponik, N.; Susha, A. S.; Winterhalter, M.; et al. Nanoengineered Polymer Capsules: Tools for Detection, Controlled Delivery, and Site-Specific Manipulation. Small 2005, 1, 194–200.

16. Zhang, F.; Lees, E.; Amin, F.; Rivera_Gil, P.; Yang, F.;Mulvaney, P.; Parak, W. J. Polymer-Coated Nanoparticles: A Universal Tool for Biolabelling Experiments. Small 2011, 7, 3113–3127.

17. Sperling, R. A.; Rivera Gil, P.; Zhang, F.; Zanella, M.; Parak,W. J. Biological Applications of Gold Nanoparticles. Chem. Soc. Rev. 2008, 37, 1896–1908.

18. Laurent, S.; Forge, D.; Port, M.; Roch, A.; Robic, C.; Vander Elst, L.; Muller, R. N. Magnetic Iron Oxide Nanoparticles: Synthesis, Stabilization, Vectorization, Physicochemical Characterizations, and Biological Applications. Chem. Rev. 2008, 108, 2064–2110.

19. Kelkar, S. S.; Reineke, T. M. Theranostics: Combining Imaging and Therapy. Bioconjugate Chem. 2011, 22, 1879–1903.

20. Barraud, L.; Merle, P.; Soma, E.; Lefranc-ois, L.; Guerret, S.; Chevallier, M.; Dubernet, C.; Couvreur, P.; Trépo, C.; Vitvitski, L. Increase of Doxorubicin Sensitivity by Doxorubicin-Loading into Nanoparticles for Hepatocellular Carcinoma Cells in Vitro and in Vivo. J. Hepatol. 2005, 42, 736–743.

21. Fattal, E.; Youssef,M.; Couvreur, P.; Andremont, A. Treatment of

Experimental Salmonellosis in Mice with Ampicillin-Bound Nanoparticles. Antimicrob. Agents Chemother. 1989, 33, 1540–1543.

22. Calvo, P.; Gouritin, B.; Villarroya, H.; Eclancher, F.; Giannavola, C.; Klein, C.; Andreux, J. P.; Couvreur, P. Quantification and Localization of Pegylated Polycyanoacrylate Nanoparticles in Brain and Spinal Cord During Experimental Allergic Encephalomyelitis in the Rat. Eur. J. Neurosci. 2002, 15, 1317–1326.

23. Reddy, L. H.; Couvreur, P. Nanotechnology for Therapy and Imaging of Liver Diseases. J. Hepatol. 2011, 55, 1461–1466.

24. Peracchia, M. T.; Desmaële, D.; Couvreur, P.; d'Angelo, J. Synthesis of a Novel Poly(MePEG yanoacrylate-co-alkyl cyanoacrylate) Amphiphilic Copolymer for Nanoparticle Technology. Macromolecules 1997, 30, 846–851.

25. Calvo, P.; Gouritin, B.; Chacun, H.; Desmaele, D.; D'Angelo,J.; Noel, J. P.; Georgin, D.; Fattal, E.; Andreux, J. P.; Couvreur,P. Long-Circulating Pegylated Polycyanoacrylate Nanoparticles as New Drug Carrier for Brain Delivery. Pharm. Res. 2001, 18, 1157–1166.

26. Brigger, I.; Morizet, J.; Aubert, G.; Chacun, H.; Terrier-Lacombe, M. J.; Couvreur, P.; Vassal, G. Poly(ethylene glycol)-Coated Hexadecylcyanoacrylate NanospheresDisplay a Combined Effect for Brain Tumor Targeting. J. Pharmacol. Exp. Ther. 2002, 303, 928–936.

27. Nicolas, J.; Couvreur, P. Synthesis of Poly(alkyl cyanoacrylate)-Based Colloidal Nanomedicines. Wiley Interdiscip. Rev. Nanomed. Nanobiotechnol. 2009, 1, 111–127.

28. Müller, R. H.; Lherm, C.; Herbort, J.; Couvreur, P. In Vitro Model for the Degradation of Alkylcyanoacrylate Nanoparticles. Biomaterials 1990, 11, 590–595.

29. Low, P. S.; Henne, W. A.; Doorneweerd, D. D. Discovery andDevelopment of Folic-Acid-Based Receptor Targeting for Imaging and Therapy of Cancer and Inflammatory Diseases. Acc. Chem. Res. 2008, 41, 120–129.

30. Lu, Y.; Low, P. S. Folate-Mediated Delivery of Macromolecular

Anticancer Therapeutic Agents. Adv. Drug Delivery Rev. 2002, 54, 675–693.

31. Lu, Y.; Sega, E.; Leamon, C. P.; Low, P. S. Folate Receptor- Targeted Immunotherapy of Cancer: Mechanism and Therapeutic Potential. Adv. Drug Delivery Rev. 2004, 56, 1161–1176.

32. Lee, E. S.; Na, K.; Bae, Y. H. Super pH-Sensitive Multifunctional Polymeric Micelle. Nano Lett. 2005, 5, 325–329.

33. Kolb, H. C.; Finn, M. G.; Sharpless, K. B. Click Chemistry: Diverse Chemical Function from a Few Good Reactions. Angew. Chem., Int. Ed. 2001, 40, 2004–2021.

34. Brambilla, D.; Nicolas, J.; Le Droumaguet, B.; Andrieux, K.; Marsaud, V.; Couraud, P.-O.; Couvreur, P. Design of FluorescentlyTagged Poly(alkyl cyanoacrylate) Nanoparticles for Human Brain Endothelial Cell Imaging. Chem. Commun. 2010, 46, 2602–2604.

35. Russell-Jones, G.; McTavish, K.; McEwan, J.; Rice, J.; Nowotnik, D. Vitamin-Mediated Targeting as a Potential Mechanism to Increase Drug Uptake by Tumours. J. Inorg. Biochem. 2004, 98, 1625–1633.

36. Kelloff, G. J.; Crowell, J. A.; Hawk, E. T.; Steele, V. E.; Lubet, R. A.; Boone, C. W.; Covey, J. M.; Doody, L. A.; Omenn, G. S.; Greenwald, P.; et al. Strategy and Planning for Chemopreventive Drug Development: Clinical Development Plans II. J. Cell. Biochem. 1996, 63, 54–71.

37. Porat, Y.; Abramowitz, A.; Gazit, E. Inhibition of Amyloid

Fibril Formation by Polyphenols: Structural Similarity and Aromatic Interactions as a Common Inhibition Mechanism.Chem. Biol. Drug Des. 2006, 67, 27–37.

38. Ono, K.; Hasegawa, K.; Naiki, H.; Yamada, M. Curcumin Has Potent Anti-amyloidogenic Effects for Alzheimer's B-Amyloid Fibrils in Vitro. J. Neurosci. Res. 2004, 75, 742– 750.

39. Yang, F.; Lim, G. P.; Begum, A. N.; Ubeda, O. J.; Simmons, M. R.; Ambegaokar, S. S.; Chen, P. P.; Kayed, R.; Glabe, C. G.;Frautschy, S. A.; et al. Curcumin Inhibits Formation of Amyloid β Oligomers and Fibrils, Binds Plaques, and Reduces Amyloid in Vivo. J. Biol. Chem. 2005, 280, 5892–5901.

40. Reinke, A. A.; Gestwicki, J. E. StructureActivity Relationships of Amyloid Beta-Aggregation Inhibitors Based on Curcumin: Influence of Linker Length and Flexibility. Chem. Biol. Drug Des. 2007, 70, 206–215.

41. Thielbeer, F.; Donaldson, K.; Bradley, M. Zeta Potential Mediated Reaction Monitoring on Nano and Microparticles. Bioconjugate Chem. 2011, 22, 144–150.

42. Ouberai, M.; Dumy, P.; Chierici, S.; Garcia, J. Synthesis and Biological Evaluation of Clicked Curcumin and Clicked Klvffa Conjugates as Inhibitors of B-Amyloid Fibril Formation. Bioconjugate Chem. 2009, 20, 2123–2132.

43. Shi, W.; Dolai, S.; Rizk, S.; Hussain, A.; Tariq, H.; Averick, S.; L'Amoreaux, W.; El Idrissi, A.; Banerjee, P.; Raja, K. Synthesis of Monofunctional Curcumin Derivatives, Clicked Curcumin Dimer, and a Pamam Dendrimer Curcumin Conjugate for Therapeutic Applications. Org. Lett. 2007, 9, 5461–5464.

44. Mourtas, S.; Canovi, M.; Zona, C.; Aurilia, D.; Niarakis, A.; La Ferla, B.; Salmona, M.; Nicotra, F.; Gobbi, M.; Antimisiaris, S. G. Curcumin-Decorated Nanoliposomes with Very High Affinity for Amyloid-B142 Peptide. Biomaterials 2011, 32, 1635–1645.

45. Brambilla, D.; Verpillot, R.; Taverna, M.; De Kimpe, L.; Le Droumaguet, B.; Nicolas, J.; Mantegazza, F.; Canovi, M.; Gobbi, M.; Salmona, M.; et al. Capillary Electrophoresis with Laser-Induced Fluorescence Detection (Ce-Lif) as a New Protocol to Monitor Interaction between Nanoparticles and the Amyloid-B Peptide. Anal. Chem. 2010, 82, 10083–10089.

46. Wang, Y.-J.; Pan, M.-H.; Cheng, A.-L.; Lin, L.-I.; Ho, Y.-S.; Hsieh, C.-Y.; Lin, J.-K. Stability of Curcumin in Buffer Solutions and Characterization of Its Degradation Products. J. Pharm. Biomed. Anal. 1997, 15, 1867–1876.

47. Airoldi, C.; Zona, C.; Sironi, E.; Colombo, L.; Messa, M.; Aurilia, D.; Gregori, M.; Masserini, M.; Salmona, M.; Nicotra, F.; et al . Curcumin Derivatives as New Ligands of Aβ Peptides. J. Biotechnol. 2011, 156, 317–324.

48. Gobbi, M.; Re, F.; Canovi, M.; Beeg, M.; Gregori, M.; Sesana, S.; Sonnino, S.; Brogioli, D.; Musicanti, C.; Gasco, P.; et al Lipid-Based

Nanoparticles with High Binding Affinity for Amyloid-B142 Peptide. Biomaterials 2010, 31, 6519– 6529.

49. Canovi, M.; Markoutsa, E.; Lazar, A. N.; Pampalakis, G.; Clemente, C.; Re, F.; Sesana, S.; Masserini, M.; Salmona, M.; Duyckaerts, C.; et al. The Binding Affinity of Anti- Aβ142 mab-Decorated Nanoliposomes to Aβ142 peptides in Vitro and to Amyloid Deposits in Postmortem Tissue. Biomaterials 2011, 32, 5489–5497.

50. Qi, K.; Ma, Q.; Remsen, E. E.; Clark, C. G., Jr.; Wooley, K. L. Determination of the Bioavailability of Biotin Conjugated onto Shell Crosslinked Nanoparticles. J. Am. Chem. Soc. 2004, 126, 6599–6607.

51. Brambilla, D.; Verpillot, R.; Le Droumaguet, B.; Nicolas, J.; Taverna, M.; Kóna, J.; Lettiero, B.; Hashemi, S. H.; De Kimpe, L.; Canovi, M.; et al. Pegylated Nanoparticles Bind to and Alter Amyloid-Beta Peptide Conformation: Toward Engineering of Functional Nanomedicines for Alzheimer's Disease. ACS Nano 2012, 10.1021/nn300489k.

52. Nicolas, J.; Bensaid, F.; Desmaele, D.; Grogna, M.; Detrembleur, C.; Andrieux, K.; Couvreur, P. Synthesis of Highly Functionalized Poly(alkyl cyanoacrylate) Nanoparticles by Means of Click Chemistry. Macromolecules 2008, 41, 8418–8428.

53. Beeg, M.; Stravalaci, M.; Bastone, A.; Salmona, M.; Gobbi, M. A Modified Protocol to Prepare Seed-Free Starting Solutions of Amyloid-B (Aβ)140 and Aβ142 from the Corresponding Depsipeptides. Anal. Biochem. 2011, 411, 297–299.

CHAPTER 6

Final Discussion

6.1 Summary

Alzheimer Disease (AD) is the most common form of dementia among the older people and, as the population ages, it is estimated to triplicate by 2040. Since an effective therapy and early diagnosis are not available at the date, there is an urgent need to develop new methods and tools to treat this huge disease. The abnormal deposition of amyloid-beta peptides (Aβ) on brain tissues is one of the main neuropathological features of AD. Therefore, targeting of cerebral Aβhas been suggested for therapeutic and/or diagnostic purposes for the pathology. One of the main obstacle in the treatment of CNS diseases is the presence of the Blood-Brain Barrier (BBB) that selectively allows nutrients into the brain, while keeping out harmful components. Thus, the majority of drugs and contrast agents do not cross the BBB. Nanoparticle-mediated delivery represents one promising strategy to successfully treat CNS diseases, thanks to the unique properties of materials at the nanometer scale. Among the different nanoparticles (NPs), liposomes are attractive tools in biomedical applications thanks to their biocompatibility, non-immunogenicity, non-toxicity, biodegradability, high physical stability, versatility in surface functionalization.

In this work of thesis liposomes have been functionalized with ligands able to bind Aβ and eventually inhibit its aggregation, or multi-functionalized with both ligands directed to Aβ and molecules (antibodies or peptides) enhancing the BBB crossing. These last ones have been attached on liposome surface by covalent or non-covalent coupling techniques (i.e. maleimide-thiol coupling chemistry or

biotin-streptavidin conjugation). The ability of these NPs to bind Aβhas been assessed in vitr o by using the Surface Plasmon Resonance (SPR) technology, as principal technique, and the ability to cross the BBB has been studied on a cellular model of barrier (hCMEC/D3). Within this PhD project, functionalized polymeric NPs have been also tested for their binding towards different aggregation forms of Aβ peptide.

6.2 Conclusions and future prospective

This project aimed to design NPs able to interact with Aβ peptide and to cross the BBB, as possible tools for the treatment of AD. It was performed within the frame of the European project NAD – Nanoparticles for Therapy and Diagnosis of Alzheimer's Disease- in which NPs having different nature have been developed as versatile platform to be decorated with targeting ligands, imaging tracers or/and drugs, for diagnosis and therapy of this disease.

Liposomes

In this view, in our lab we managed to develop nanoliposomes able to bind Aβ with high affinity and with enhanced features of crossing an in vitro model of BBB, made with human brain capillary endothelial cells hCMEC/D3, cultured in a transwell system. Aβ, one of the main hallmarks of AD, was chosen as target because the abnormal accumulation in the brain plays a central role in the onset and development of the pathology [Small, 2001; Matsuoka, 2003]. Thus, NPs carrying molecules binding the peptide and acting as inhibitors of Aβ aggregation could promote the clearance of Aβ by forming complexes recognizable by the immune system or the reticulo-endothelial system (microglia in the brain), and employed as novel therapy fo AD. Moreover, the specific targeting of cerebral Aβ could be useful for enabling an early diagnosis of the disease and for developing imaging tools to discriminate AD-related dementia among other forms.

Liposomes were first discovered by Bangham in 1965 and currently there are several liposome-based formulation approved for clinical use and more are in various stages of clinical trials [Chang, 2012]. The pharmacokinetic and pharmacological advantages of liposomal delivery systems are well documented. Nevertheless, significant work continues in the optimization of formulations for increased circulation times, drug release rates, and efficacy.

Liposomes composed of cholesterol (Chol) and sphingomyelin (Sm) have been reported to be promising vehicles for therapeutics and are in various clinical trials [Semple, 2005; Chang, 2012]. Hence, we chose to develop our functionalized liposomes starting from a matrix of Chol and Sm, tagged with radioactive or fluorescent lipids in trace amounts, adding Aβ ligands and lipid PEG-derivatives for further surface-functionalizaton with antibodies or peptides.

Starting from the observation that raft-like membranes containing gangliosides bind Aβin vitro, and polysialogangliosides, like GD1a and GT1b, bind the peptide more than monosialogangliosides [Ariga, 2001; Choo-Smith, 1997], we synthesized Chol:Sm liposomes functionalized with GT1b, with the idea to target Aβexploiting the multivalent effect that leads NPs to bind more efficiently the target with respect to the ligand itself [Tassa, 2010]. We investigated the liposomes affinity for Aβ peptide and their putative role in modifying Aβ aggregation process. Our study gives evidences that the presence of GT1b in the liposomes bilayer improved their interaction with Aβ, with respect to the non-functionalized liposomes (Chol:Sm) indicating that GT1b is a good ligand for Aβ. In our study, GT1b-liposomes were

found to slow down Aβ aggregation in vitro. We suggest that, the inhibitory effect of GT1b-liposomes on fibrils formation is likely due to their strong interaction with Aβ peptide interfering with its aggregation, as for other functionalized NPs [Taylor, 2011]. The role of gangliosides on Aβ and in neurodegenerative diseases is still controversial. It has been reported that they mediate amyloid fibril formation which was found to be accelerated especially in the presence of GM1 [Kakio, 2002]. On the other side, gangliosides may have neuroprotective effects to the cells [Ledneen, 1998; Sokolova, 2007] and beneficial effects in animal models of neurodegeneration and diseases, such as AD, Parkinson and stroke, have been also reported [Lenzi, 1994; Kawaguchi, 2010; Matsuoka, 2003; Schneider, 1998; Svennerholm, 2002].
Anyway, further experiments will be carried out to investigate if GT1b-liposomes interact with other Aβ aggregation forms, such as monomers and oligomers. Moreover, in vitro assays will be performed to assess if they induce any modification in the cellular viability.

A potential improvement for GT1b-liposomes as tools for treating AD, will be the interaction with Aβ deposited into the brain. One way to achieve this goal will be the conjugation of GT1b-liposomes surfaces with molecules that can enhance the BBB crossing. Within this frame, this latter strategy has been exploited for liposomes produced in our laboratories and already reported to target Aβ with a very high affinity in vitro, i.e. PA- or CL-containing liposomes [Gobbi, 2010]. We approached the problem as a first step toward their passage across the BBB, by promoting the interaction of such

liposomes with brain capillary endothelial cells hCMEC/D3 in vitro. The liposome surface was decorated with ligands exploiting the physiological transcellular route of transport of macromolecules across the BBB. In particular, we covalently decorated PA- and CL-liposomes with ApoE-derived peptides (monomeric or dimeric), corresponding to the fragment 141-150, involved in the binding with the LDLr, that is up-regulated in the BBB endothelium with respect to other [Dehouck, 1994]. In a second phase, we decorated PA-liposomes with the anti-transferrin receptor monoclonal antibody RI7217 to target TfR, that is the most widely studied receptor for BBB targeting. RI7217 binds to an epitope on TfR different from the one targeted by transferrin, thus avoiding a possible saturation by the endogenous ligand for in vivo application [Van Rooy, 2010; de Boer, 2007]. RI7217 was also reported to be more selective for the brain in vivo, in contrast to other anti-TfR antibodies used [Lee, 2000].

We demonstrated that liposomes containing PA and decorated with the monomer of ApoE peptide displayed a more efficient uptake in hCMEC/D3 cells compared with CL-liposomes, without co-localization with late-endosomes and early-lysosomes, indicating a possible caveolae-mediated uptake mechanisms. We suggest that the higher number of negative charges carried by CL, in comparison with PA, might modify the surface properties of NL and partially mask the receptor binding site of ApoE peptide. Very importantly, ApoE-peptide functionalization of liposomes containing PA or CL, does not affect their ability to bind the Aβ peptide in vitro. These results are important and promising features for the possibility to use these liposomes in vivo for targeting Aβ in the brain districts.

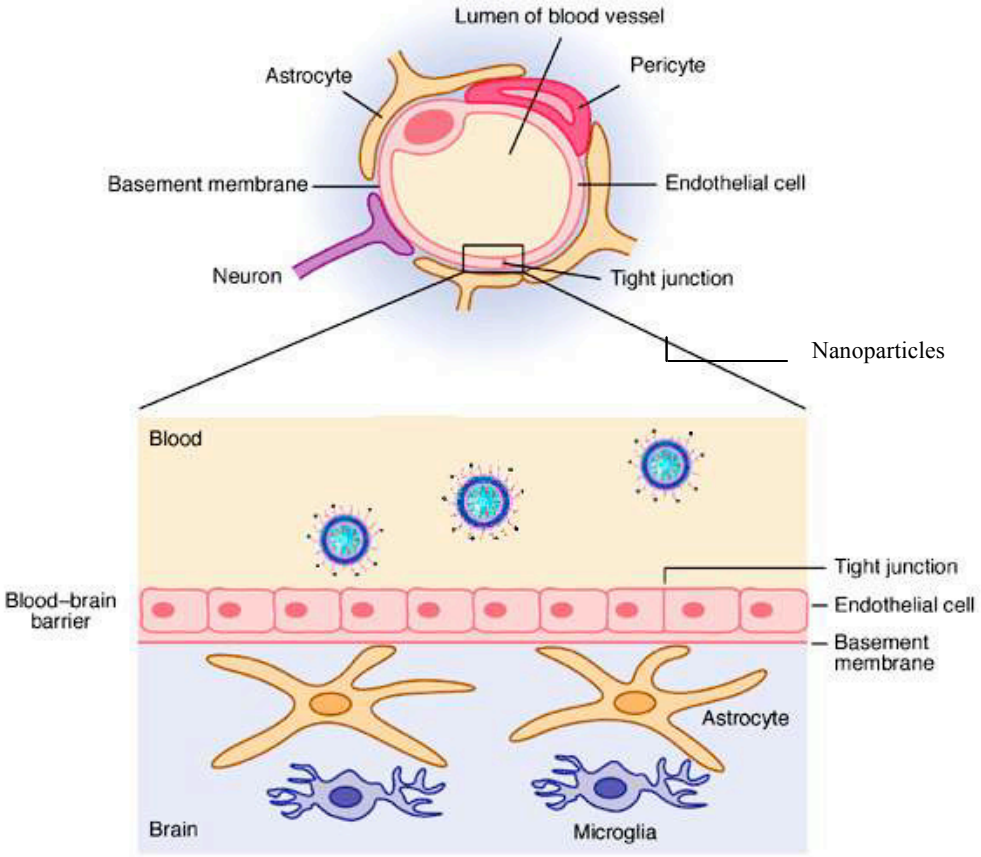

Fig.8 Nanoparticles flowing in the bloodstream interact with the endothelial cells of the blood-brain barrier [Adapted from Expert Reviews in Molecular Medicine, 2003, Cambridge University Press].

In a further investigation we evaluated whether the ligation method used to couple RI7217 on the NPs surface may affect NLs performances in terms of ability to bind Aβ or TfR, to be uptaken by hCMEC/D3 cells and to cross a BBB model made with the same cells. Both covalent and non-covalent techniques were employed and optimized to obtain liposomes decorated with the same surface density of antibodies. As non-covalent technique, the biotin/avidin ligation has been employed, while the thiol-maleimide reaction was chosen as covalent method. An alternative covalent strategy has also been investigated, involving the reaction between the carboxylic groups of a lipid PEG linker and primary amines on RI7217, by using S-NHS/EDC reagents (see Introduction), but a very low coupling efficiency (10-15%) was obtained. Thus, this strategy has been discarded as suitable coupling techniques for RI7217.

Since there are numerous amine functional groups available on the antibodies to be thiolated, it is difficult to control the number of sites modified and this can results in loss of bioactivity.

Herein we proved that RI7217 still bound its receptor either after biotinylation or thiolation and after coupling to liposomes. Nevertheless, we found an higher binding affinity for liposomes covalently modified towards TfR, with respect to the biotinylated ones, meaning that the binding properties of the antibody could be slightly affected by the coupling procedure. On the other hand, the binding affinity of PA towards Aβ was not altered after the addition of RI7217 on the liposome surface.

Liposomes decorated with covalently bound RI7217 were much more uptaken by cells and crossed the BBB much faster than liposomes

decorated with biotin/avidin RI7217. We suggest that these effects could depend i) on the higher binding affinity found for the covalently linked antibody towards TfR with respect to the biotinylated one, ii) on the weaker bond biotin/streptavidin ligation than the covalent, or iii) on the steric hindrance of the protein streptavidin, affecting the interaction. Concluding, we found that the chemical design affects the biological properties of liposomes in terms of uptake and permeability on hCMEC/D3cells, and this should be taken into account in the choice of the functionalization method.

The multi-functionalized liposomes herein described did not display a significant cytotoxicity in vitro towards hCMEC/D3 cells, indicating their potential biocompatible features. Moreover, their size was maintained below 150 nm even after the decoration with peptides or antibodies. This is an important issue to take into account to avoid the possible complement activation after in vivo administration. Of course stability, biocompatibility, non-toxicity, non-immunogenicity of these liposomes, carrying ligands with various nature, should be fully investigated in vitro to predict their behavior in vivo.

Polymeric PACA Nanoparticles

Finally, poly(alkil cyanoacrylate) NPs (PACA) are herein presented as a versatile and efficient tool to treat various pathologies in vitro, i.e. cancer and AD, and could represent an alternative nanosystem to liposomes, applicable in the nanomedicine field.

In regards to AD, two different targeting ligands have been employed to bind Aβ, curcumin-derivatives and a novel specific anti-Aβantibody, synthesized among the NAD Consortium.

Curcumin was chosen for its reported anti-amyloidogenic effects and its potential role in the prevention and treatment of AD [Yang, 2005, Ono, β004]. The ability of curcumin to bind Aβpeptides and inhibit its aggregation has been attributed to three structural features of the curcumin molecule: the presence of two aromatic end groups and their co-planarity, the substitution pattern of these aromatics, and the length and rigidity of the linker region [Reinke, 2007]. Two curcumin-derivatives were synthesized with an additive alkyne moiety to be attached on NPs surfaces via ‘‘click chemistry’’. Only one of the two compounds attached on PACA was found to be stable during time and to retain the ability to bind Aβ. Curcumin-functionalized PACA were found to bind Aβboth in the monomeric and aggregated form, to inhibit Aβ aggregation and to rescue SK-N-SH cells from Aβtoxicity in vitro.

In addition, PACA carrying a new anti-Aβ-antibody have been designed. A very marked binding was found for anti-Aβ-antibody-containing PACA towards both monomeric and fibrillar Aβ. The dissociation constant values in the low picomolar range were indicative of an extremely high affinity, up to 100-fold higher with respect to those found for GT1b, PA or CL [Gobbi, 2010].

This findings demonstrates the high efficiency of the newly synthesized antibody in binding different forms of Aβ, opening the possibility to target the peptide in very specific way. Additional studies on these PACA must be carried out to investigate their

behavior in a cellular environment and their putative role on Aβ aggregation in order to evaluate their future use for diagnosis and therapy of AD.

Taken all together, these studies demonstrate that NPs could be a versatile nanosystem to be used for multiple targeting, simply by linking specific ligands to the outer surface.

Starting from these platform, a future goal within the NAD project will be the creation of NPs carrying both putative therapeutic molecules, such as curcumin-derivative, anionic phospholipids or the anti-Aβantibody, and imaging tracers such as ^{19}F, gadolinium or iron-oxides to be used in MRI, or ^{18}F for PET applications. Finally, the best

multifuntionalized NPs will be selected and tested in vivo against AD models. Such experiments have already started, showing very promising results.

These NPs may represent a novel strategy to treat AD, allowing both an earlier diagnosis of the pathology, by detecting Aβ in the cerebral district, and an effective therapy, based on the specific targeting of Aβleading to modifying the aggregation process with the final result of prevent or slow down neurodegeneration.

References

Ariga T, Kobayashi K, Hasegawa A, Kiso M, Ishida H, Miyatake T. Characterization of high-affinity binding between gangliosides and amyloid beta-protein. Arch Biochem Biophys. 2001. 388(2):225-30.

Chang HI, Yeh MK. Clinical development of liposome-based drugs: formulation, characterization, and therapeutic efficacy. Int J Nanomedicine. 2012. 7:49-60.

Choo-Smith LP, Garzon-Rodriguez W, Glabe CG, Surewicz WK. Acceleration of amyloid fibril formation by specific binding of Abeta-(1-40) peptide to ganglioside-containing membrane vesicles. J Biol Chem. 1997. 272(37):22987-90.

De Boer A.G., Gaillard P.J., Drug targeting to the brain, Annu. Rev. Pharmacol. Toxicol. 2007. 47: 323–355

Dehouck B., Dehouck M.P., Fruchart J.C., Cecchelli R., Upregulation of the low-density lipoprotein receptor at the blood–brain barrier: intercommunications between brain capillary endothelial cells and astrocytes, J. Cell Biol. 1994. 126: 465–473.

Gobbi M, Re F, Canovi M, Beeg M, Gregori M, Sesana S, Sonnino S, Brogioli D, Musicanti C, Gasco P, Salmona M, Masserini ME. Lipid-based nanoparticles with high binding affinity for amyloid-beta1-42 peptide. Biomaterials. 2010.31(25):6519-29.

Kakio A, Nishimoto S, Yanagisawa K, Kozutsumi Y, Matsuzaki K. Interactions of amyloid beta-protein with various gangliosides in raft-like membranes: importance of GM1 ganglioside-bound form as an endogenous seed for Alzheimer amyloid. Biochemistry. 2002. 41(23):7385-90.

Kawaguchi K., Kitaguchi N., Nakai S. Novel therapeutic approach for Alzheimer's disease by removing amyloid βprotein from the brain with an extracorporeal removal system. Journal of Artificial Organs.2010. 13(1): 31–37.

Ledeen R.W., Wu G., Lu Z. H., Kozireskichuback D., Fang Y., The role of GM1 and other gangliosides in neuronal differentiation: overview and new findings, Annals of the New York Academy of Sciences. 1998. 845: 161–175.

Lenzi G. L., Grigoletto F., Gent M. et al., "Early treatment of stroke with monosialoganglioside GM-1: efficacy and safety results of the early stroke trial," Stroke. 1994.β5 (8): 155β–1558.

Lee H.J., Engelhardt B., Lesley J., Bickel U., Pardridge W.M. Targeting rat anti-mouse transferrin receptor monoclonal antibodies through blood-brain barrier in mouse J. Pharmacol. Exp. Ther. 2000. 292: 1048–1052

Matsuoka Y., M. Saito, J. LaFrancois, M. Saito, K. Gaynor, V. Olm, L. Wang, E. Casey, Y. Lu, C. Shiratori, et al. Novel therapeutic approach for the treatment of Alzheimer's disease by peripheral administration of agents with an affinity to ù-amyloid. J. Neurosci. 2003. 23: 29-33.

Ono, K.; Hasegawa, K.; Naiki, H.; Yamada, M.Curcumin Has Potent Anti-amyloidogenic Effects for Alzheimer's B-Amyloid Fibrils in Vitro J. Neurosci. Res. 2004. 75: 742-750.

Reinke AA, Gestwicki JE. Structure-activity relationships of amyloid beta-aggregation inhibitors based on curcumin: influence of linker length and flexibility. Chem Biol Drug Des. 2007. 70(3):206-15.

Schneider J. S., Roeltgen D. P., Mancall E. L., Chapas-Crilly J.,. Rothblat D. S, Tatarian G. T. Parkinson's disease improved function with GM1 ganglioside treatment in a randomized placebo-controlled study. Neurology 1998. 50(6): 1630–1636.

Semple SC, Leone R, Wang J, Leng EC, Klimuk SK, Eisenhardt ML, Yuan ZN, Edwards K, Maurer N, Hope MJ, Cullis PR, Ahkong QF. Optimization and characterization of a sphingomyelin/cholesterol liposome formulation of vinorelbine with promising antitumor activity. J Pharm Sci. 2005.94(5):1024-38.

Small DH, Mok SS, Bornstein JC. (2001) Alzheimer's disease and Aü toxicity: from top to bottom. Nat Rev Neurosci 2:595–598.

Sokolova T.V., Zakharova I.O., Furaev V.V., Rychkova M.P., Avrova N.F. Neuroprotective effect of ganglioside GM1 on the cytotoxic action of hydrogen peroxide and amyloid β-peptide in PC12 cells. Neurochem. Res. 2007. 32:1302—1313.

Svennerholm L., Bråne G., Karlsson I., Lekman A., Ramström I., Wikkelsö C. Alzheimer disease-effect of continuous intracerebroventricular treatment with GM1 ganglioside and a systematic activation programme. Dementia and Geriatric Cognitive Disorders. 2002. 14 (3): 128—136.

Tassa C, Duffner J. L., Lewis T. A. Weissleder R., Schreiber S. L., Koehler A.N., Shaw S. Y., Binding affinity and kinetic analysis of targeted small molecule-modified nanoparticles Bioconjug Chem. Bioconjug Chem. 2010. 21(1):14-9.

Van Rooy I., Mastrobattista E., Storm G., Hennink WE., Schiffelers RM. Comparison of five different targeting ligands to enhance accumulation of liposomes into the brain. J Control Release. 2011. 150(1):30-6.

Yang, F., Lim, G. P., Begum A. N., Ubeda O. J., Simmons M. R., Ambegaokar S. S., Chen, P. P., Kayed R., Glabe C. G., Frautschy S. A. et al. Curcumin Inhibits Formation of Amyloid βOligomers and Fibrils, Binds Plaques, and Reduces Amyloid in Vivo. J. Biol. Chem. 2005. 280: 5892-5901.

Taylor M., Moore S., Mourtas S., Niarakis A., Re F., Zona C., La Ferla B., Nicotra F., Masserini M., Antimisiaris S.G., Gregori M., Allsop D. Effect of curcumin-associated and lipid ligand-functionalized nanoliposomes on aggregation of the Alzheimer's Aβ peptide. Nanomedicine. β011. 7(5):541-50.

Publications

Salvati E., Re F., Sesana S., Cambianica I., Sancini G., Masserini M., Gregori M., *Nanoliposomes Functionalized to Overcome the Blood-Brain Barrier and to Target Amyloid-β peptide: the Chemical Design Affects the Permeability across a Model Barrier*. Submitted

Parthsarathy V., McClean PL, Hölscher C., Taylor M., Tinker C., Jones G., Kolosov O., **Salvati E.,** Gregori M., Masserini M., Allsop D. *A novel retro-inverso peptide inhibitor reduces amyloid deposition, oxidation and inflammation and stimulates neurogenesis in the APPswe/PS1ΔE9 mouse model of Alzheimer's disease.* PlosOne. Accepted (Dec 2012).

Le Droumaguet B., Nicolas J., Brambilla D., Mura S., Maksimenko A., De Kimpe L., **Salvati E.**, Zona C., Airoldi C., Canovi M., Gobbi M., Magali N., La Ferla B., Nicotra F., Scheper W., Flores O., Masserini M., Andrieux K., Couvreur P., *Versatile and efficient targeting using a single nanoparticulate platform: application to cancer and Alzheimer's disease.* ACS Nano. 2012 Jul 24;6(7):5866-79.

Salvati E., Masserini M., Sesana S., Sonnino S., Re F., Gregori M. *Liposomes Functionalized with GT1b Ganglioside with High Affinity for Amyloid beta-peptide.* VII Sindem Congress, J Alzheimers Dis. 2012; 29 (Suppl. 1): 33-36.

Re F., Cambianica I., Sesana S., **Salvati E.**, Cagnotto A., Salmona M., Couraud P.O., Moghimi M., Masserini M., Sancini G. *Functionalization with ApoE-derived peptides enhances the interaction with brain capillary endothelial cells of nanoliposomes binding amyloid-β peptide.* J Biotechnol. 2010 Dec 20;156(4):341-6.